Developing a mouse model of Pulmonary Arterial Hypertension through over-expression of an endothelial-specific fas-inducing apoptosis construct

Heather Anne Margaret Goldthorpe

This thesis is submitted as a partial fulfillment of the M.Sc. program in Cellular and Molecular Medicine

Department of Cellular and Molecular Medicine
Faculty of Medicine, University of Ottawa

Abstract

Pulmonary arterial hypertension (PAH) is a lethal disease, characterized by functional or structural abnormalities involving distal pulmonary arterioles that result in increased pulmonary vascular resistance (PVR) and ultimately right heart failure. Our objective is to establish a conditional transgenic system in mice, to test the hypothesis that lung EC apoptosis at the level of distal pulmonary arterioles is necessary and sufficient to cause a PAH phenotype. In a pilot study, the Fas-Induced Apoptosis (FIA) construct was expressed under the control of endothelial-specific Tie2 promoter in transgenic mice (i.e. EFIA mice). Administration of a small molecule dimerizing agent, AP20187, resulted in lung modest dose-dependent PAH, which was associated with proliferative vascular lesions localized to distal lung arterioles in a small proportion of mice. Due to the low level of transgene expression in preliminary EFIA lines, we re-designed the transgenic vector by incorporating a more robust endothelial promoter (superTie2). The new construct was transfected into HUVEC and BAEC and analyzed by monitoring immunofluorescence (DsRed). Data from the EFIA model suggests that EC apoptosis may be sufficient to induce a PAH phenotype with the characteristic lung vascular lesions. The EFIA model will allow us to better explore the mechanism that links distal lung EC apoptosis with reactive vascular cell proliferation in the pathogenesis of this devastating disease.

Table of Contents

List of Tables and Figures

List of Abbreviations

ALK-1	Activin receptor-like kinase 1
ANOVA	Analysis of variance
APAH	Associated pulmonary arterial hypertension
BMP	Bone morphogenetic protein
BMPR2	Bone morphogenetic protein receptor 2
BSA	Bovine serum albumin
DSRE2	DsRed-Express2
EC	Endothelial cell
EFIA	Endothelial fas-induced apoptosis
ENG	Endoglin
ENOS	Endothelial nitric oxide synthase
HPAH	Hereditary pulmonary arterial hypertension
HE-EFIA	High expressing EFIA
H&E	Hematoxylin & eosin
HRP	Horseradish peroxidase
IF	Immunofluorescence
IHC	Immunohistochemistry
IL	Interleukin
IPAH	Idiopathic pulmonary arterial hypertension
LE-EFIA	Low expressing EFIA
LSAB	Labelled streptavidin biotin
MCS	Multiple cloning site
MCT	Monocrotaline
PAH	Pulmonary arterial hypertension
PAP	Pulmonary arterial pressure
PBS	Phosphate buffered saline
PFA	Paraformaldehyde
PVR	Pulmonary vascular resistance
RHF	Right heart failure
RT-PCR	Reverse transcriptase polymerase chain reaction
RVH	Right ventricular hypertrophy
SMC	Smooth muscle cell
ST2	SuperTie2
T2	Tie2
Tg	Transgenic
TGF-β	Transforming growth factor-beta
TNF	Tumor necrosis factor
TUNEL	Terminal deoxynucleotidyl transferase-mediated dUTP nick end labelling
VEGF	Vascular endothelial growth factor
VEGFR	Vascular endothelial growth factor receptor
WHO	World Health Organization
WT	Wild-type

Acknowledgements

I would like to thank my supervisor, Dr. Duncan J. Stewart, for his mentorship and support throughout my Masters. I have learned so much from you, more than you will ever know. I would also like to thank Dr. Shirley Mei for her guidance and support in and out of my projects in the lab. To Jennifer, my summer student and 4th year honours student who followed me along the way and taught me how to manage time for more than just myself. To all of the lab members who supported me, worked with me, taught me, and stood by me for moral support, thank you. I'd also like to thank my advisory committee members, Dr. Valerie Wallace and Dr. Balwant Tuana for their time, support and guidance throughout my research. And last but not least, I'd like to thank my family, especially my parents, and friends for their support and understanding. To all of you, your encouragement and support has helped me through this challenging experience and educational journey of mine.

1. Introduction

1.1 Pulmonary Arterial Hypertension, a lethal disease of multifactorial origin

Pulmonary arterial hypertension (PAH) is a complex, lethal disease characterized by pulmonary vascular remodeling and increased pulmonary vascular resistance (PVR), This leads to increased pulmonary arterial pressure (PAP), right ventricular hypertrophy (RVH), and ultimately right heart failure (RHF). PAH hemodynamics are characterized by a sustained pulmonary pressure of ≥ 25 mmHg at rest and 30 mmHg during exercise with a pulmonary wedge pressure of ≤ 15 mmHg [1]. The most recent World Health Organization (WHO)-revised classification system includes five categories of Pulmonary Hypertension (PH) in which PAH specifically falls under Group 1 and is subdivided into three categories: 1) sporadic or idiopathic PAH (IPAH); 2) hereditary PAH (HPAH), which can be associated with loss-of-function mutations in the bone morphogenetic protein receptor type 2 (*BMPR2*) gene or less commonly mutations in the activin receptor-like kinase type 1 (*ALK-1*) or Endoglin (*ENG*) genes; and 3) associated PAH (APAH), which is associated with other diseases such as HIV infection, connective tissue disorders (i.e. Scleroderma), congenital heart disease with cardiac shunting, and portal hypertension to mention a few [2-5].

Pathological characteristics of PAH include arteriolar muscularization and medial thickening, concentric intimal hyperplasia, and characteristic plexiform lesions, which are complex obliterative lesions characterized by vascular cell proliferation and inflammation, localized to distal precapillary or intra-acinar pulmonary arteries [6,7]. Constrictive lesions include intimal and adventitial thickening as well as medial hypertrophy of distal pulmonary arteries. Complex (i.e. plexiform) are found in severe stages of IPAH, HPAH, and APAH (Figure 1); however, these lesions are absent in PAH associated with pulmonary occlusive venopathy [7]. The Heath-Edward classification was the first to categorize pathological

"grades'' or characteristics of pulmonary hypertension, those that can still be used to describe the histopathological stages of the disease. According to the Heath-Edward classification, grade 1 is represented by medial thickening, grade 2 includes medial hypertrophy with intimal cellular proliferation, grade 3 includes progressive intimal fibrosis and formation of intimal lesions within arterioles, grade 4 includes progressive arterial dilatation with the development of complex lesions, grade 5 includes chronic arterial dilatation with numerous lesions, and grade 6 is represented by necrotizing arteritis [8]. Overall, pulmonary vasculature remodeling affects all the vascular layers, with hyperproliferation of various cell types, including fibroblasts (mainly in the adventitia), smooth muscle cells (SMC) in the media, and mainly endothelial cells (EC) in the intima [9]. Despite the variety of therapies used to alleviate symptoms associated with PAH, the mean life expectancy upon diagnosis is approximately 3.5 years and the pathogenesis of the disease remains unclear [4]

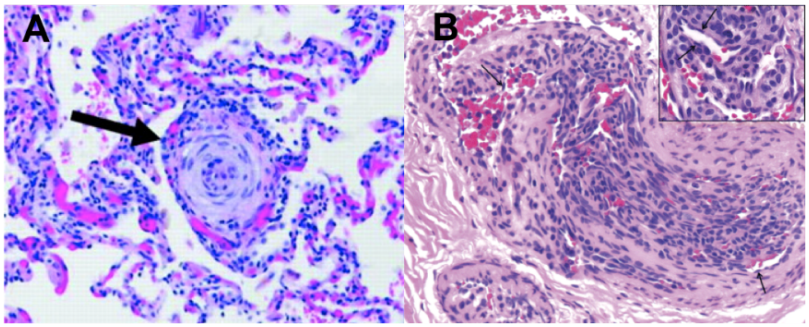

Figure 1. Histopathological Features of PAH; A pulmonary arterial concentric intimal thickening and B formation of plexiform lesions. [10,11]

1.2 The Pulmonary Endothelium: Role in Health and PAH

The endothelium remains an important target in elucidating the pathogenesis of PAH as it is in direct contact with blood, regulates vascular tone and leukocyte trafficking, produces autocrine and paracrine effectors including growth factors and cytokines, and ultimately regulates pulmonary vascular homeostasis. Most importantly, the endothelium lining is characterized by significant regional heterogeneity between the pulmonary and systemic vascular system as well as heterogeneity between different vascular regions within the lung itself [12]. In the pulmonary vascular system, the endothelium controls and maintains a low-pressure vascular bed, at least in part by tightly regulating the production of vasodilators (nitric oxide, NO; prostacyclin) and vasoconstrictors (endothelin-1, ET-1; thromboxane A_2) [13-16]. Upon injury to the endothelium, vascular homeostasis is disrupted, thereby inducing changes in the production of endothelial vasoactive factors, which leads to vasoconstriction, vascular cell proliferation, and coagulation.

Endothelial cell dysfunction is thought to play a role in the structural changes associated with PAH, particularly related to decreased production of vasodilator mediators, favouring a vasoconstrictive environment. This contributes to decreased vascular cross-sectional area, increased pulmonary vascular resistance and ultimately, increased pulmonary vascular pressure; however; the majority of patients presenting with PAH do not show any significant vasomotor component to their disease, and the increase in vascular resistance is thought to be due mainly to arteriolar remodeling. In later stages of PAH, uncontrolled proliferation of intimal cells leads to the formation of plexiform-like lesions, and further contribute to adverse hemodynamic changes in the lung [17]. Furthermore, evidence has demonstrated that pulmonary vascular remodeling involves endothelial cell apoptosis, which may contribute to endothelial dysfunction, endothelial cell dropout, and the emergence of

hyper-proliferative ECs, ultimately leading to the hemodynamic abnormalities associated with PAH, including formation of the characteristic plexiform lesions [6,18]. Most modern day therapies have been developed based on the notion that endothelial cell dysfunction plays an integral role in the development of PAH. These therapies address more of the vasomotor changes rather than the structural remodeling components of this disease such as loss of pulmonary microvasculature and abnormal proliferation of ECs, SMCS, and fibroblasts.

1.2.1 Endothelium Dysfunction and Vasoactive Mediators in PAH

1.2.1.1 Decreased Nitric Oxide production

Nitric oxide (NO) is the most potent endogenous vasodilator produced by the endothelium and is involved in maintaining resting pulmonary vessel tone. The primary functions of NO include regulation of vascular tone and inhibition of SMC proliferation and platelet aggregation. NO is synthesized by NO synthase (NOS) oxidation of L-arginine and serves as a paracrine or autocrine factor, exerting its effects on adjacent ECs and SMCs [19-21]. Endothelial NOS (eNOS) is one of three known NOS isoforms and is constitutively expressed in endothelial cells [21].

The role of eNOS has been previously described in animal models. In particular, mice over-expressing eNOS are protected from developing hypoxia-induced PAH and both homozygous and heterozygous eNOS-deficient mice are susceptible to severe PAH induced by mild hypoxia [22,23]. Human studies, however, are controversial, in such that eNOS expression is elevated in pulmonary plexiform lesions but reduced in the pulmonary vasculature of patients with PAH [24,25]. Furthermore, evidence has shown that NO

provides protection against hypoxia-induced vasoconstriction in the lung and down-regulates ET-1 production, favouring a vasodilated state [26,27]. Despite the controversial role of NO, evidence has suggested that decreased NO levels are associated with pulmonary hypertension and vascular remodeling in the lung. [28-30]

1.2.1.2 Decreased Prostacyclin production

Prostacyclin, a metabolite of arachidonic acid, was one of the original vasoactive mediators identified in PAH. Prostacyclin induces potent vasodilation through activation of the cyclic adenosine monophosphate (cAMP)-dependent pathways and serves as an anti-coagulant and an inhibitor of smooth muscle cell proliferation [13,31]. Evidence from animal models suggests that prostacyclin acts as a protective vasodilator. Over-expression of prostacyclin in mice diminishes the development of chronic hypoxia-induced PAH and prostacyclin receptor-deficient mice develop severe chronic hypoxic-induced PAH [32,33]. In human studies, lower levels of prostacyclin synthase protein are found in small and medium size pulmonary arteries of IPAH patients [34]. Thus, lower levels of prostacyclin production in PAH patients likely favours a pro-coagulant state and contributes to pulmonary vasoconstriction and smooth muscle cell proliferation, which all play a role in the pathological development of PAH.

1.2.1.3 Increased Endothelin-1 production

ET-1 is a vasoactive peptide produced and secreted by endothelial cells and is the most potent endogenous vasoconstrictor known [35,36]. The hemodynamic effects induced by ET-1 are triggered by ligand-receptor binding via the receptors, ET-A and ET-B, which display distinctive expression patterns among different areas of the vascular system [37]. The ET-B receptor mRNA levels are elevated in both the cerebellum and lung in comparison

to other tissues and can be found on various cell types including endothelial cells. ET-B_1, an ET-B receptor subtype, mediates endothelium-dependent vasodilation, whereas ET-B_2 mediates SMC-dependent vasoconstriction. Within the pulmonary vascular system, ET-B receptor mRNA is expressed in the endothelium and adventitia and vasodilatation produced by ET-1 is triggered via the ET-B_1 receptor on endothelial cells, thereby inducing the release of the endothelial-dependent vasodilators, NO and prostacyclin [38-40]. Additionally, ET-1 acts through both ET-A and ET-B receptors on SMCS and ET-A receptors on fibroblasts, thereby inducing vascular SMC contraction and mitogenesis of SMCs and fibroblasts, which may explain the role of ET-1 in vasoconstriction and in the proliferative response accustomed by SMCs and fibroblasts in PAH [38,41]. The first evidence demonstrating elevated circulating levels of ET-1 in PAH patients was identified by our group [42,43]. Additionally, elevated levels of ET-A and ET-B mRNA have been demonstrated in animal models of PAH [44,45]. Collectively, evidence suggests that ET-1 plays a role in the vasoconstrictive status associated with PAH.

1.2.1.4 Increased Thromboxane A_2 production

Thromboxane A_2 is a well-known potent vasoconstrictor, smooth muscle mitogen, and procoagulant produced by endothelial cells and platelets [16,31]. Evidence has demonstrated that thromboxane A_2 levels are elevated in patients with primary and secondary PAH, in which elevated pulmonary arterial pressures are associated with increased level of platelet activation [16]. Unfortunately, a large PAH study in humans using a thromboxane inhibitor, Terbogrel, deemed unsuccessful due to severe leg pain in the treatment group [46]. Considering the imbalance between prostacyclin and thromboxane A_2

in PAH patients, thromboxane A_2 may contribute to the abnormal response of the endothelium in PAH; however, its role in the pathogenesis of PAH remains unclear [16].

1.3 Modern Treatment Strategies for PAH

Current therapies for PAH patients are aimed to decrease alleviate symptoms, increase quality of life, and ultimately reduce the prevalence of death. Most modern day therapies target the imbalance between vasoconstriction and vasodilatation, as described by dysfunctional vasomediators. At diagnosis, IPAH patients who respond to an acute vasodilator challenge may be prescribed calcium-channel blockers, such as Diltiazem, ultimately increasing blood flow and decreasing blood pressure; however, less than 10% of patients with IPAH patients significantly respond to vasodilators [47,48]. Calcium channels blockers are contraindicated in patients without a definite response to inhaled NO or intravenous prostacyclin, and require PAH-specific therapies. Current first-line therapies for low-risk patients include ET-1 receptor antagonists (ERA) such as Bosentan or Ambersentan, which aims to alleviate pulmonary vasoconstriction. ERAs improve functional status of patients and more modestly hemodynamics [47-49]. More recently, phosphodiesterase type V inhibitors such as Slidenafil have been used to enhance the effects of endogenous NO produced by vascular endothelium. NO stimulates soluble guanylate cyclase and the production of its second messenger, cyclic guanosine monophosphate (cGMP), which is selectively degraded by phosphodiesterase type V. Thus, phosphodiesterase type V inhibitors increase cyclic guanosine monophosphate (cGMP) levels by blocking its degradation, and thus amplify pulmonary vasorelaxation in response to NO. Increased cGMP levels also induce antiproliferative effects in SMCs [47,50].

In high-risk patients with WHO functional classes III and IV functional status (Appendix I), most physicians would recommend initial treatment with a prostacyclin analogue, which is the most effective PAH-specific therapy. Intravenous Epoprostenol improves exercise capacity and hemodynamics, and was the first medication to improve survival in IPAH patients [47,48,51]. Again, prostacyclins induce vasodilation and promote antiproliferation and anti-coagulant effects [13]. If patients do not improve to functional Class I or Class II (Appendix I), additional or alternative therapy is implemented. Despite the introduction of many new therapies over the course of the last two decades, the prognosis remains poor, with only a 3 to 5 year survival after initial diagnosis, and lung transplantation remains as the only "cure" for PAH, despite poor postoperative status and a high rate of mortality [47]. Collectively, this data demonstrates the need for more effective PAH treatment strategies.

1.4 The Genetic Basis of PAH

Recently, both hereditary and sporadic cases of PAH have been linked to heterozygous, loss-of-function mutations in the bone morphogenetic protein receptor 2 gene (*BMPR2*), a member of the transforming growth factor-β (TGF-β) receptor family and an important receptor involved in cell growth and survival. The heritance pattern of *BMPR2* mutations is autosomal dominant and approximately 20% of *BMPR2* mutation carriers will go on to develop clinical PAH. Based on the low penetrance of *BMPR2* mutant alleles, a 'multiple-hit' hypothesis was introduced, suggesting that in the presence of other modifier genes or exogenous stimuli such as exposure to toxins (Toxic oil syndrome, anorexogens), and thus mutant *BMPR2* carriers are more susceptible to developing PAH [52,53].

BMPR2 is a ubiquitously expressed protein; however, within the pulmonary vascular system, the *BMPR2* receptor is predominantly expressed in endothelial cells and to a lesser extent in smooth muscle cells [54,55]. In the presence of a BMP ligand, the *BMPR2* forms a heterodimer with a type I receptor at the cell surface, phosphorylating the type 1 receptor, which transduces a signal cascade involving phosphorylation of Smads, a family of signaling proteins. Type 1 receptors within the TGF-B signaling pathway activate receptor-regulated Smads (R-Smads), Smad 2/3 or Smad 1/5/8, which associate with Co-Smad (Smad 4). The R-Smad/Co-Smad complexes move into the nucleus to regulate target gene expression [56,57].

Hypothetically, the link between *BMPR2* mutations and PAH may involve altered Smad signaling; however, both Smad-dependent and Smad-independent signaling pathways can be activated by *BMPR2*. The nature of Smad signaling depends on whether preformed Type2/Type1 *BMPR* heterodimers are ligand-activated, or whether the ligand induces Type2 and Type1 receptors to form heterodimeric complexes [57,58]. *BMPR2* expression has been found within the plexiform lesions and the presence of *BMPR2* has been suggested as a potential contributor to the proliferative state of these complex lesions [59]. Furthermore, the loss of BMP signaling has been found to lead to increased apoptosis in cultured pulmonary artery endothelial cells; whereas in smooth muscle cells it has the opposite effect and increases proliferation [6]. Thus, reduced *BMPR2* signaling promotes two processes that may be central to the pathogenesis of PAH, endothelial injury and reactive vascular cell proliferation.

In addition to *BMPR2* mutant alleles, mutations in a Type 1, endothelial-restricted member of the TGF-β receptor family, the activin-like kinase-1 (*ALK-1*) receptor, have been recently described in association with PAH. However, these mutations more commonly

cause hereditary hemorrhagic telangeictasia (HHT), an autosomal dominant vascular disorder, characterized by remodeling changes that in many ways are opposite to those seen in PAH. Rather than increased PVR, HHT usually presents with decreased PVR, increased cardiac output (CO), and decreased PAP due to the formation in arterio-venous malformations in the lung and other organs. Although the two disease states are distinct in clinical manifestations, analysis of PAH patients from five families with hemorrhagic telangeictasia demonstrated that *ALK-1* mutations might contribute to pulmonary arteriole occlusion together with vasodilation manifested as telangeictasia [60].

The TGF-β signaling pathway can best explain the association between *ALK-1* in the development of PAH. Upon activation, the *ALK-1* receptor forms heterodimeric complexes with type 2 receptors similar to *BMPR2*, resulting in activation of the *ALK-1* kinase domain, which subsequently activates the Smad 1/5/8 pathway [56,60]. *ENG* acts as an accessory receptor predominantly in endothelial cells, including *ALK-1* heterodimeric complex formation [61]. The role of mutant *ALK-1* and *ENG* alleles in PAH has yet to be elucidated; however, *ALK-1* is present in diseased pulmonary vascular endothelium and *ALK-1* mutant carriers are predisposed to the development of PAH [60]. Furthermore, the mutation of *ENG* in HHT supports an essential role for *ENG* in the vasculature. Again, in comparison with the *BMPR2* signaling pathway, *ALK-1* also signals through the Smad 1/5/8 pathway, which may explain the relationship between *ALK-1* mutations and the development of PAH [55,56]. Furthermore, like the *BMPR2* allele mutations, the overall effect of *ALK-1* mutations may depend on the presence of other modifier genes and the presence of exogenous stimuli [60,62].

Downstream Smad-dependent transcriptional controlled genes are involved in inhibition of cell proliferation and induction of apoptosis, and thus, BMPR2 signaling in

SMCS and ECs likely involves the inhibition of proliferation and induction of apoptosis, respectively. Although reduced BMPR2/Type 1 signaling in SMCs may result in uncontrolled proliferation, it is less clear how *BMPR2* and *ALK-1* mutations lead to increased proliferation of ECs, a pathological characteristic associated with the complex pulmonary lesions in PAH. Indeed, these loss-of-function mutations have been shown to increase the susceptibility of ECs to apoptosis [6].

1.5 Emerging Concepts and Novel Mechanisms in PAH

1.5.1 Inflammation and PAH

Inflammation is modulated by the presence and activation of inflammatory cells such as cytokines and growth factors. In particular, inflammation in PAH includes the interaction between activated inflammatory cells and non-inflammatory cells such as ECs and SMCs, as well as the development of inflammatory properties in ECs, SMCs, and fibroblasts [63]. PAH can often be acquired through complication of systemic inflammatory diseases such as Scleroderma. Scleroderma-triggered PAH is described by characteristic medial hypertrophy, intimal lesions, and plexiform-like lesions, where mononuclear inflammatory cells surround the vascular sites within the lesional growth but not within non-participating vascular lung structures [64]. Plexiform lesions surrounded by infiltrating inflammatory cells are seen in IPAH [65]. Importantly**,** evidence has shown that a large number of PAH patients who do not present with immunodeficiency or autoimmune disease have active lung inflammation [66]. Thus, various animal models have been used to establish the role of inflammatory mechanisms in PAH. These range from well-known models such as the toxic alkaloid monocrotaline (MCT)-induced PAH rat model to the chronic hypoxia-induced PAH rat model rats [67]. Additionally, perivascular inflammation of distal pulmonary vessels is

distinct in both heterozygous *BMPR2*-mutant mice and transgenic (Tg) mice over-expressing a deletional *BMPR2* mutant allele [68,69]. Various groups have described evidence demonstrating the presence of inflammatory cells, including macrophages and clustered T and B-lymphocytes, adjacent to remodeling vessels in PAH [64,65,70]. Inflammatory cytokines such as of interleukin-1ß (IL-1ß), IL-6, monocyte chemoattractant protein (MCP-1), and fractalkine, have been found to be upregulated in patients with IPAH or APAH [71-73]. Furthermore, ET-1, which is elevated in PAH patients, is known to stimulate neutrophils, activate mast cells, and stimulate the production of cytokines such as IL-1ß, IL-6, TNF-α, and TGF-ß [74]. Specifically, the MCT-treated rat model has been extensively used to understand the role of inflammation in PAH. Although this model does not display the characteristic plexiform lesions, it has raised an important question regarding the role of inflammatory cascades in vascular remodeling, including the initiation and development of plexiform lesions in human PAH [66].

1.5.2 Abnormal Vascular Cell Proliferation: The Cancer Paradigm of PAH

In many forms of human PAH, vaso-obliteration is present, in addition to pulmonary vascular muscularization. As mentioned previously, obliterating vascular lesions, including the characteristic plexiform lesions are found at regions distal of bifurcations in the pulmonary vascular tree of both IPAH and many other APAH patients. These lesions contain ECs, SMCs, and lymphocytes. It remains unclear as to whether or not one cell type initiates the formation of complex lesions; however, the pathological model of these "angioproliferative" lesions is based on the emergence of abnormally proliferative ECs, which are apoptosis-resistant [11,17]. Thus, the complex lesions present in PAH exhibit

some cancer-defining mechanisms such as angiogenesis and abnormal, uncontrolled cell growth [11,75]. Furthermore, evidence associates BMPs and their corresponding receptors with cell growth control, which may suggest *BMPR2* mutant alleles contribute to the cancer-like phenotype of PAH. Indeed, PAH patients exhibit altered growth of SMCs in response to BMPs [11,76]. Additionally, inhibition of the vascular endothelial growth receptor (VEGFR) under hypoxic conditions in rats potentiated the development of PAH along with vascular remodeling, including development of angioproliferative-like lesions in the lung. This effect was associated with marked increases in EC apoptosis and was inhibited by nonspecific caspase inhibitors suggesting that EC apoptosis induced by removal of VEGF survival signaling may be a trigger for the emergence of reactive hyper-proliferative cells [77]. Consistent with this concept is the observation mentioned above, that *BMPR2* signaling promotes EC survival and loss-of-function mutations would increase the susceptibility of EC to apoptosis. EC-SMC cross talk may also contribute to increased SMC proliferation in the context of inhibition of endothelial survival signaling. For example, VEGFR2 blockade *in vitro* induces the production of immune modulators such as TGF-$ß_1$ by ECs, which induces SMC proliferation [78]. As well, apoptotic endothelial nanovescicles have been shown to promote SMC hyperplasia, mediated by translationally controlled tumour protein (TCTP), which is a potent anti-apoptotic factor implicated in the malignant transformation of cancer cells [79]. In conclusion, within the complexity of PAH, it is likely that initial endothelial damage triggers multiple pathways leading to abundant endothelial cell proliferation, a mechanism involved in the formation of complex lesions characteristic of severe PAH.

1.5.3 Endothelial cell apoptosis and PAH: The Degenerative Hypothesis

As mentioned, pulmonary vascular remodeling includes both abnormal EC apoptosis and SMC proliferation, which may contribute to the development of the angioproliferative lesions. EC dysfunction, distal arteriole dropout, and conditions that favour hyper-proliferative ECs may ultimately lead to increased PVR [6]. Evidence from various PAH models has shown that endothelial cell apoptosis plays an important role in the development of this devastating disease.

1.5.3.1 Evidence from Sugen-chronic hypoxia and MCT-induced PAH rat models: VEGF signaling

The Sugen-chronic hypoxia rat model has highlighted the important role of endothelial apoptosis in the pathogenesis of PAH. In a study performed by Tarasaviciene-Stewart et al., rats treated with SU5416 (Sugen), a selective VEGF receptor inhibitor, under hypoxic conditions demonstrated worsening of PAH along with the development of vascular remodeling [77]. Specifically, increased levels of apoptotic endothelial cells localized to the internal elastic lamina of distal pulmonary arterioles and not at the site of luminal proliferation were found in Sugen-treated animals under both normoxic and hypoxic conditions. Additionally, treatment with a nonspecific caspase inhibitor abrogated the hemodynamic and marked vascular remodeling phenotype in the Sugen-chronic hypoxia model. This suggested that the increased levels of apoptosis due to inhibition of endothelial survival signaling triggered the development of hyper-proliferative ECs [77].

Furthermore, in a MCT-induced PAH model, apoptosis in endothelial cells, localized to small arterioles, was reduced following cell-based gene transfer of VEGF, suggesting that the improvement of vascular remodeling may involve the reduction of apoptosis induced by

VEGF [80]. Evidence from both the MCT and Sugen-chronic hypoxia animal models seems to show decreased levels of VEGF and support the role of endothelial cell apoptosis in PAH[6]. Nevertheless, the MCT model does not exhibit the intimal and obliterative lesions that are characteristic of human PAH, which are seen only in the Sugen model.

1.5.3.2 BMPR2 signaling in Cultured Endothelial Cells

As mentioned in section 1.4, the mechanistic link between the development of PAH and *BMPR2* signaling is unclear; however, evidence has demonstrated that *BMPR2* signaling triggers proliferation and apoptosis-resistance in SMCs. Our group was the first to demonstrate that *BMPR2* signaling promoted survival in cultured endothelial cells. Specifically, levels of apoptosis were significantly reduced in serum-deprived ECs treated with BMPs. Additionally, in both the presence and absence of serum, *BMPR2* gene silencing in ECs significantly increased levels of apoptosis [81]. A study by Southwood et al. has further demonstrated evidence supporting the role of the *BMPR2* pathway in vascular growth and survival in human fetal and embryonic lung tissue [82].

1.5.3.3 The Angiopoietin 1/Tie2 Endothelial Survival Pathway: Protective Role

Further evidence supporting the role of endothelial apoptosis in the pathogenesis of PAH stems from the Angiopoietin 1/Tie2 endothelial survival pathway. Angiopoietin 1 (*ANGPT1*) is a Tie2 agonist, which functions as an angiogenic and survival factor in endothelial cells and provides protection against inflammation and apoptosis, thereby acting as a vascular homeostatic factor. The role of *ANGPT1* has been controversial in the field of PAH. Although studies have demonstrated that over-expressing *ANGPT1* by adenoviral transfection potentiates PAH in rats, other studies have demonstrated that over-expressing *ANGPT1* by nonviral transfection reduces both right ventricular systolic pressure (RVSP)

and vascular remodeling in the chronic-hypoxia and MCT-induced PAH rat models [83-85]. These discrepancies are thought to be related to the use of viral vectors and their potential proinflammatory effects, as well as pulmonary vein clamping which was performed to aid with gene transfer [83]. Furthermore, studies demonstrated that *ANGPT1* expression and Tie2 activity are increased in the lung of PAH patients, whereas other groups have found that high basal expression levels of *ANGPT1* are present in the normal lung and remain unchanged in the lungs of PAH patients. Previous evidence has demonstrated high Ang1-Tie2 expression and activity in the lung compared to other organs [84,86-88]. Recently, a study using Tie2 heterozygous deficient mice demonstrated mild increases in RVSP at baseline and an exaggerated response following chronic-treatment with IL-6 or serotonin (5-HT). This response was associated with decreased *ANGPT1* levels and Tie2 activity, along with increased levels of peripheral lung apoptosis. Additionally, in Tie2 heterozygous deficient mice, inhibition of apoptosis using a pan-caspase inhibitor prevented the development of pulmonary hypertension in response to serotonin (5-HT). Since Tie2, an endothelial-selective receptor, is involved in maintaining vascular growth and remodeling, this evidence suggests that the *ANGPT1*-Tie2 pathway is important for promoting endothelial cell survival [89]. Collectively, this evidence strengthens the hypothesis that endothelial apoptosis as an important factor in the trigger and pathogenesis of PAH.

1.6 Transgenic PAH animal models: Understanding the Pathogenesis of PAH

A number of transgenic animal models have been developed to better understand the pathogenesis of PAH. The classic MCT rat model and chronic-hypoxia models, including those combined with Sugen-treatment, have their limitations. The chronic-hypoxia model has been used extensively but is not a true model of PAH (i.e. WHO group 1 PAH); rather it

is a model of WHO group 3 PAH. Moreover, many agents such as Fluoxetine and Rosuvastatin, that have reversed pathological changes in the MCT model, have not been proven to be effective in the human disease [90-92]. As mentioned earlier, the MCT-rat model exhibits pulmonary endothelial cell apoptosis, particularly localized to small pulmonary arterioles; however, it is associated with off-target toxicity to other organs including the liver and kidneys, which may contribute to high mortality in this model. Furthermore, these PAH models do not display the characteristic complex plexiform lesions typically presented in severe stages of the human disease. Thus, it is important to have a model that represents the remodeling process of PAH.

1.6.1 BMPR2 Transgenic Mice

Since the discovery of the heterozygous, loss-of-function *BMPR2* mutations in IPAH and FPAH patients, *BMPR2* Tg models in particular have been of interest for researchers in the field of PAH. Considering the important role of BMP/TGF signaling in development, *BMPR2* homozygous negative mice exhibit an embryonic lethal phenotype. In one study, *BMPR2* heterozygous mice exhibit modest increases in RVSP as well as modest pulmonary arteriole muscularization; however, in a second study this effect was not reported [93,94]. Additionally, in pursuit of a more robust PAH phenotype, mice expressing a SMC-selective dominant negative *BMPR2* allele were investigated [95]. These mice exhibit elevations in RVSP with some pulmonary arteriole muscularization; however, many features typical of the human disease are still absent. Furthermore, pulmonary EC-specific conditional *BMPR2* knockouts exhibit elevations in RVSP along with distal pulmonary arteriole muscularization and the presence of obliterate lesions [96]. More recently, a double Tg mouse model driving expression of a dominant negative *BMPR2* allele in a SMC-selective manner displayed

modest increases in RVSP, distal pulmonary arteriole muscularization, and more robust pulmonary vascular remodeling. Importantly, the dominant negative *BMPR2* Tg models do not represent the genetics of a patient with FPAH and therefore, downstream signaling pathways in this model may not correlate with the human disease [69]. As outlined, many pathways contribute to the pathogenesis of PAH and collectively this evidence suggests that *BMPR2* deficient models represent many characteristics of human PAH.

1.6.2 Limitations of Mouse Models: Resistance in Comparison to Rat Models

Over the years, mouse models have demonstrated higher resistance to the development of PAH in comparison to their respective rat models. For instance, lung vascular remodeling has been studied in both mice and rats following chronic exposure to hypoxia and under these conditions, mice display less pulmonary vascular remodeling and the extent of pulmonary vascular remodeling differs between mouse strains. A study performed by Hoshikawa et al. examined gene expression levels in Sprague-Dawley (SD) rats and C57BL/6 mice exposed to both acute and chronic hypoxic conditions. Both SD rats and C57BL/6 mice exhibit significant elevations in RVSP following three weeks of hypoxia whereas only SD rats exhibit a significant elevation in RVSP under acute hypoxic conditions. Most importantly, SD rats exposed to chronic hypoxia demonstrate changes in pulmonary arterial remodeling, whereas C57BL/6 mice show no pathological changes in the pulmonary vasculature. Furthermore, the same group demonstrated a distinct gene expression profile between the SD rats and C57BL/6 mice suggesting that rats may express higher levels of proteins involved in cell proliferation. In part, the differing gene expression profile between species may explain the differences in hypoxia-induced vascular remodeling between species [97].

In addition to the chronic hypoxia-induced PAH models, the Sugen/hypoxia model demonstrates differences in pulmonary vascular remodeling between the rat and mouse, particularly a less robust phenotype in the mouse. In a study conducted by Abe et al., SU5416-treated mice exposed to chronic hypoxia exhibited elevated RVSP, modest RVH, pulmonary vascular muscularization, and intimal lesions; however, the PAH-like phenotype was lost upon re-exposure to normoxic conditions [98]. In contrast, the rat Sugen/hypoxia model exhibits a more robust, irreversible PAH-like phenotype, reminiscent of the human disease [10,77]. In addition to the Sugen/hypoxia PAH models, Ye et al. investigated the distribution, metabolism, and clearance of Sugen between the two species, and demonstrated that systemic and renal clearance was much greater in the mouse [99]. Furthermore, RVSP hemodynamics correspond with RVH in rats, suggesting that RVH occurs in response to an increased afterload [100]. The weight ratio of the right ventricle to left ventricle plus septum wall (RV/LV+S) is used as an indicator of RVH. Both the MCT and Sugen/hypoxia PAH rat models exhibit severe RVH, an average RV/LS+S ratio of 0.67-0.76 [101]. Within mice models, only IL-6 over-expressing mice seem to exhibit comparable RVH measurements [101,102]. On another note, in comparison to the mouse, more blood vessel walls and a higher mean alveolar diameter are found in the rat lung, distinguishing mechanical properties between the two species [103]. Provided with this evidence, the many differences in anatomy, cellular composition, gene expression, and pharmacogenomics between mouse and rat may determine species-specific mechanisms leading to the development of PAH.

1.7. Unifying Hypothesis of the Central Role of Endothelial Cell Apoptosis in the Pathogenesis of PAH

As discussed, several lines of evidence suggest that endothelial damage, particularly endothelial apoptosis, is a central trigger in the development of PAH. Intra-acinar arterioles consist of a tiny endothelial layer with little or no support from smooth muscle cells and pericytes. Distal arterioles are located proximal to vascular capillary bed and control perfusion through the capillaries, ultimately determining the overall PVR. In line with the evidence presented above, the 'EC apoptosis in the pathogenesis of PAH' paradigm suggests that upon injury to the endothelium, EC apoptosis could lead directly to EC dysfunction, distal arteriole drop out and the subsequent loss of pulmonary microvasculature, as well as the emergence of hyper-proliferative ECs, SMCs, and fibroblasts, which could contribute to the proliferative or complex plexiform lesions found in many PAH patients. In the context of endothelial survival signaling, EC apoptosis could trigger the production of immune modulators such as TGF-$ß_1$, which induces SMC proliferation and could contribute to pulmonary arteriole muscularization as well as the formation of complex inflammatory lesions. These conditions could lead to reduced cross-sectional area of pulmonary arterioles, which could lead to loss of capillary bed perfusion, ultimately leading to increased PVR and the development of PAH (Figure 2). It is unclear as to whether or not one of these pathways predominates in the pathogenesis of PAH; however, the central role of EC apoptosis could provide new insight for prevention & detection strategies, as well as new PAH treatment strategies which could target and prevent EC loss and/or promote EC repair.

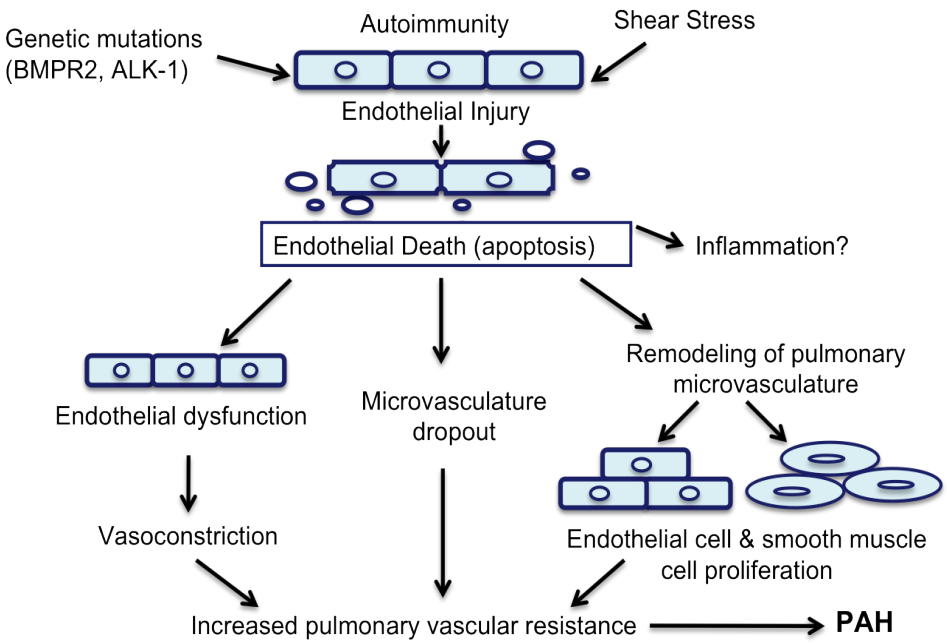

Figure 2. Hypothetical mechanism involving endothelial apoptosis in the pathogenesis of PAH. Factors such as BMPR2 and ALK-1 mutations associated with hereditary PAH, autoimmunity (APAH), and shear stress induce or predispose one to endothelial injury, which could trigger endothelial apoptosis and induce inflammation. Endothelial apoptosis could contribute to endothelial dysfunction, inducing vasoconstriction, as well as microvascular dropout and remodeling of the pulmonary microvasculature, including EC and SMC proliferation. All of these factors contribute to reduced cross-sectional area of the vasculature, which increases PVR and ultimately leads to increased PAP and PAH.

1.8 Hypothesis

Lung endothelial cell apoptosis will result in distal arteriolar degeneration, triggering pulmonary arteriole remodeling and the subsequent development of PAH.

1.9 Project Objective

Provided with the evidence that endothelial apoptosis plays an important role in the development of PAH, our lab has pursued the development of an endothelial-specific apoptosis-inducing PAH mouse model using a titratable molecular system that aims to produce a robust level of endothelial-specific apoptosis *in vivo*. Administration of a small dimerizing molecule, namely the AP20187 (AP) compound, should induce endothelial-specific apoptosis, providing us with an endothelial-targeted, Fas-induced apoptosis (EFIA) system. The overall goal of this project is to investigate and assess whether conditional and selective endothelial cell apoptosis will result in a PAH phenotype with characteristic pulmonary vascular structural and functional changes in EFIA Tg mice. In a preliminary study previously performed in the Stewart Lab, one of the founder EFIA Tg lines (E6711) exhibited pulmonary obliterative lesions; however, the phenotype was lost and shortly after, in absence of the AP compound, the emergence of a spontaneous structural phenotype in the 6780 EFIA (E6780) Tg line was observed. Lesions were observed in the peripheral lung in a subset of these mice. My objective was to reassess the 6711 and 6780 EFIA Tg lines at 12 weeks to determine if susceptibility is affected by age and if the phenotype was reproducible. *Chapter I* outlines these hemodynamic assessments and lung histopathology following treatment with 2 mg/kg of a dimerizing agent (AP20187) for 1 week.

Additionally, due to the loss and/or lack of phenotype in the described EFIA Tg mouse lines, an approach to potentially increase the expression of the EFIA transgene was

pursued. *Chapter II* outlines the strategy used to incorporate a stronger Tie2 promoter, namely the SuperTie2 (ST2) promoter, which was so graciously provided to us by Dr. Quertermous at Stanford. Furthermore, *Chapter II* outlines the initial *in vitro* transfection validation experiments performed to assess the functionality of the newly subcloned ST2 constructs.

Chapter I: Phenotyping 'First Generation' EFIA Transgenic Mice

Preface

A portion of the work presented in Chapter I has been conducted by other lab members. The generation of EFIA Tg mice was in collaboration with Dr. Turksen's group and a previous lab member, Jin-Yi Jiang, who also performed the initial experiments with the EFIA founder lines and performed the experiments presented in section 3.1 with the help of Yupu Deng. During my time on the project, our animal surgeon, Yupu Deng, graciously performed hemodynamic analyses and tissue collection. Our lab technician, Grace Li, maintained EFIA Tg mouse colonies, performed genotyping and assisted with end of studies. Grace Li and Mohamad Taha provided assistance with intraperitoneal AP injections. As primary on the project, I contributed to the study design, prepared for and assisted with end of studies, performed RVSP data analyses, processed all harvested tissue including fixation, paraffin embedding, sectioning, and histology, and performed all result analyses.

Chapter Objective

Provided with the evidence that endothelial apoptosis plays an important role in the development of PAH, our lab has pursued the development of EFIA Tg mice using a titratable molecular system that aims to produce a robust level of endothelial-specific apoptosis *in vivo*. Administration of a dimerizing compound, AP 20187, should induce endothelial-specific apoptosis. This chapter describes generation of the EFIA Tg mice, as well hemodynamic assessment and histological assessment of two EFIA Tg lines, namely the high-expressing (HE)-EFIA (E6780) and low-expressing (LE)-EFIA (E6711) lines following AP-transgene induction for 1 week. Initial assessments of lesion formation and relative apoptosis levels in lung tissue were performed and are described in this chapter.

2. Materials and Methods

2.1 Generation of EFIA Transgenic Mice

The Fas-Inducing Apoptosis (FIA) construct, developed by Ariad Pharmaceuticals, contains two FK-506 protein-binding domains and the cytoplasmic FAS death domain linked to the membrane-tethering region of the low affinity nerve growth factor receptor (ΔLNGFR) [104] (Figure 3). Previously, an endothelial fas-inducing apoptosis (EFIA) construct was created by incorporating a fragment of the 2.1 Kb endothelial-specific Tie-2 promoter to drive expression of FIA. EFIA mice were produced in collaboration with Dr. K. Turksen (Ottawa Hospital Research Institute, Ottawa, ON). The EFIA construct was microinjected into ova from super-ovulated CD1 mice to generate viable EFIA Tg mice. Seven Tg founder lines were generated and identified from genomic tail DNA by PCR analysis using FIA-specific primers (1446F 5'-ACA TGC CAC TCT CGT CTT-3'; 1696R 5'-TGG CTT CAT TGA CAC CAT-3'), spanning a sequence region encoding the second FK-BP and FADD. The founder lines were bred with CD1 mice. Except when noted, all data refers to animals from the current Tg lines, E6711, E6780. All experiments were approved by the University of Ottawa's Animal Care ethics committee and complied with the principles and guidelines of the Canadian Council on Animal Care.

2.2 Mouse Husbandry and Genotyping

For all experiments, the presence of the EFIA transgene was screened by PCR using genomic tail DNA and the original FIA-specific primers used to identify EFIA founder mice. EFIA mice were bred to CD1-wild-type (WT) mice and CD1 mice were used as controls in all *in vivo* experiments.

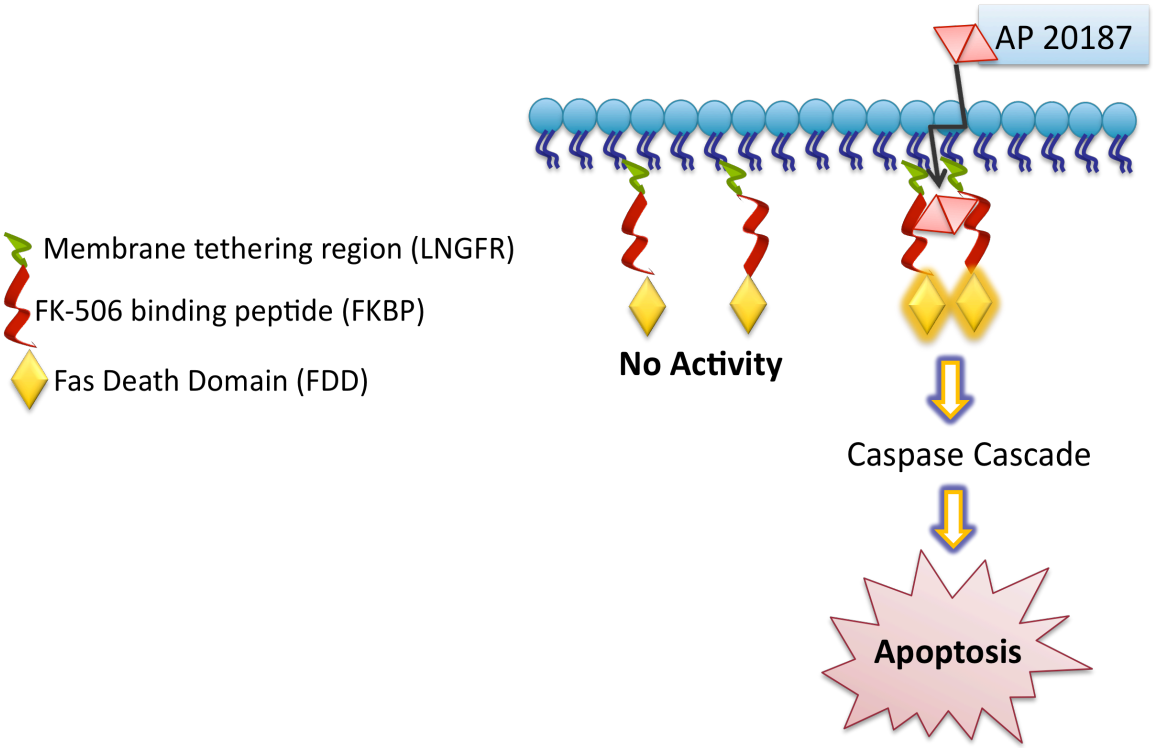

Figure 3. The FIA construct. The Fas-Induced Apoptosis (FIA) construct contains a membrane tethering region of the truncated low affinity nerve growth factor receptor (ΔLNGFR), two copies of the FK binding peptide (FKBP) dimerization domain, and a truncated cytoplasmic Fas domain. In the absence of the dimerizing agent it is inactive; however, administration of AP20187 (a FK506 analogue), dimerizes the FIA construct, leading to activation of apoptosis.

2.3 Dimerizer (AP) Treatment

AP20187 (AP) was originally a gift from Ariad Pharmaceuticals and later purchased through Clontech (B/B Homodimerizer, 635069). Lyophilized AP was dissolved in 100% ethanol at concentration of 12.5 mg/ml and stored at -20°C. For in vivo use, the 12.5 mg/ml stock was diluted to 0.40 mg/ml in an injection solution consisting of 4% ethanol, 10% polyethylene glycol-400 (PEG-400), and 2% Tween-20 in water. Each mouse was given daily interperitoneal injections for seven days with 2 mg AP/kg in a volume adjusted to individual body weight. Injection volumes ranged between 130 and 260 µl. Vehicle injections were performed in the same manner with 100% ethanol in place of dissolved AP. All intraperitoneal injections were administered within thirty minutes of injection solution preparation.

2.4 Hemodynamic Assessment

Direct right ventricular systolic pressure (RVSP) was measured following administration of an anesthetic mixture of ketamine (100 mg/kg, Ketalean, DIN 00612316) and xylazine (10 mg/kg, Rompun, DIN 02169592). After adequate sedation, an incision was made to expose the jugular vein. Subsequently, the jugular vein was tied off tightly at the cranial end, loosely tied at the caudal end, and a small, medial incision was made in the vein. Right ventricular pressure was measured using a 1.2 F pressure catheter transducer (Scisense, London, ON, FTS-1211B-0018) and proper readings were determined by observing sequential pressure loops recorded on LabScribe2 software (Scisense). The loose caudal tie was tightened for data collection. The average of three or four pressure loops was used to calculate RVSP. Following hemodynamic assessment, blood was collected from the inferior vena cava (IVC) and lung tissue was collected from every mouse. Right lung tissue

was divided into equal portions for protein or RNA extraction and placed into cryogenic vials (Corning, 430488). Lung samples for RNA extraction were immediately placed in RNAlater® stabilizing solution (Ambion AM7021), stored at 4°C overnight, and transferred to -80°C. Protein samples were flash frozen in liquid nitrogen and stored at -80ºC. The left lung was inflated with a 1:1 PBS:OCT solution by trachea infiltration. Half of the left lung was embedded in OCT medium (TissueTek 4583) for frozen sections and the remainder was fixed and processed for paraffin-embedded sections.

2.5 Tissue Processing: Paraffin-Embedding

Lung tissue harvested for histopathological assessments were placed in 4% paraformaldehyde (PFA; Appendix II) overnight. The next morning, tissue was transferred into Tru-Flow tissue cassettes (Fisher 15-200-403A), washed in phosphate buffered saline (PBS; Appendix II) for 6 hours at 4°C and subsequently transferred to 70% ethanol overnight. The Leica Asp 300S tissue processor was used following a programmed protocol: lung tissue was dehydrated in a series of graded ethanol washes 70% (3x), 80%, 95%, 100% (3x), immersed in 100% xylene (3x), and finally immersed in paraffin (62°C, 3x). Lung tissue was embedded into paraffin blocks and sliced into 5-µm sections using a Leica RM2255 microtome (Leica Microsystems, Wetzlar, Germany). Lung sections were placed in 70% ethanol, transferred to a 43°C water bath, gently mounted onto cover slides and dried in a 37°C incubator over night.

2.6 Histology

For all histological analyses, 5-µm paraffin-embedded tissue sections were deparaffinized in 100% Xylene, rehydrated in graded ethanol, and immersed in distilled water.

2.6.1 Hematoxylin and Eosin (H&E) Staining

Deparaffinized/rehydrated tissue sections were stained with concentrated hematoxylin (VectorLabs H-3404) for 10 minutes and subsequently rinsed under tap water for 5 minutes. Hematoxylin-stained tissue sections were placed in acid alcohol (Appendix II) for 5 minutes, rinsed under tap water for 5 minutes, soaked in Scott's solution (Appendix II) for 5 minutes, rinsed under tap water for 5 minutes, stained with Eosin (Fisher E-511, Appendix II) for 3 minutes, and finally rinsed under tap water for another 5 minutes. H&E stained lung sections were dehydrated by sequential dips in graded ethanol followed by immersion in 100% xylene (2 x 5 min). Tissue sections were sealed with Cytoseal XYL (Fisher 22050262), a xylene-based mounting medium and stored at room temperature (RT). Lungs sections from treated and non-treated WT mice and E6711 and E6780 Tg mice were stained with H & E and assessment was performed using ImageScope software. Lung sections were blinded and scanned for observable changes in gross morphology of pulmonary arterioles.

2.6.2 Terminal deoxynucleotidyl transferase-mediated dUTP Nick-End-Labeling (TUNEL) staining

Deparaffinized tissue sections were subjected to permeabilization with 20 µg/µl proteinase K (Promega TUNEL kit) for 10 minutes at RT. Following the manufacturers protocol, tissue sections were subjected to the Dead End™ Fluorometric TUNEL System

(Promega G3250) to identify fragmented DNA in cells undergoing apoptosis. Positive controls were treated with DNAseI (Ambion AM1906) and negative controls were treated with ddH_20 in place of rTdT. Processed tissue sections were counterstained with DAPI (Molecular Probes D21490, 1:4000) for 15 minutes. Slides were sealed with anti-fade mounting medium [1% N-propylgallate in glycerol and PBS (50:50)] and stored at 4°C.

2.6.3 Cleaved-Caspase 3 Immunohistochemistry (IHC)

Following deparaffinization, antigen retrieval was performed for 15 minutes in citrate buffer (Antigen unmasking solution, 1:100 dilution, VectorLabs H-3300) using a microwave. Slides were cooled to RT for 30 minutes, washed with PBS (2 x 5 min) and washed with ddH_2O for 5 minutes. Endogenous peroxidase activity was blocked by a 15-minute incubation with 3% hydrogen peroxide (Sigma 216763) and subsequently washed off with PBS (2 x 5 min). Slides were washed with PBS (2 x 5 min) and incubated with diluted goat serum [VECTASTAIN® Elite ABC kit (Rabbit IgG), VectorLabs PK-6101] for 30 minutes at RT. Following blocking, slides were incubated overnight at 4°C with monoclonal rabbit anti-cleaved caspase 3 antibody (1:600 dilution, Cell Signaling 9664S) that recognizes endogenous levels of the large fragment (17/19 kD) of activated caspase 3. Slides were washed with PBS (2 x 5 min) and incubated with diluted biotinylated secondary goat anti-rabbit antibody (VectorLabs PK-6101) 30 minutes at RT. Slides were washed with PBS (2 x 5 min) and incubated with VECTASTAIN® Elite ABC Reagent (VectorLabs PK-6101) for 30 minutes at RT, followed by washing with PBS (2 x 5 min). Slides were developed with Diaminiobenzidine (DAB) peroxidase substrate (ImmPACT™ DAB EqV, VectorLabs SK-4103) for 10 minutes at RT and immediately immersed in distilled water. Slides were counterstained with hematoxylin for 2 seconds and rinsed in running water for 2 minutes. To

"blue" hematoxylin staining, slides were dipped in 2% ammonium water and rinsed in ddH_2O for 5 minutes. Immunostained lung sections were dehydrated by sequential dips in graded ethanol followed by immersion in 100% xylene (2 x 5 min). Tissue sections were sealed with Cytoseal XYL stored at RT.

2.6.4 Microscopy

Whole tissue sections subjected to H&E staining and IHC were imaged using Aperio ScanScope CS. TUNEL stained sections were imaged using Confocal Fluoview FV1000 (Olympus, model BX61WI). All treatment groups were analyzed using the same brightness and intensity settings.

2.6.5 Quantification

Lung tissue sections stained for TUNEL and cleaved-caspase 3 were analyzed from five animals per group. Sections stained for TUNEL and cleaved-caspase 3 were analyzed using ImageJ (Java-based NIH Image 1.62) software. The appropriate threshold level was determined and used for all subsequent analyses.

Twelve fields per mouse were assessed for TUNEL positive cells. TUNEL images were captured at 20X magnification and only positive cells co-localized with DAPI were counted as positive. A TUNEL index was calculated as a percentage of apoptotic cells to total number of nucleated cells determined by DAPI staining. Quantification was performed in a blinded fashion. Cleaved-caspase 3 IHC lung sections were analyzed using ImageJ with a colour deconvolution plug-in. Six fields per animal were assessed for stained cells with activated-caspase 3. Images were captured at 40X magnification and positive cells found in both the cytoplasm and nucleus were counted as positive. An activated-caspase 3 index was

calculated as a percentage of apoptotic cells to total number of nucleated cells determined by hematoxylin staining.

2.7 Real-Time (RT)-qPCR

RT-qPCR EFIA primers were designed using Intregrated DNA Technology (IDT) software (EFIA#2 For 5'-CTG TGG TTG TGG GTC TTG TG -3'; EFIA#2 Rev 5'-CCT CCC ATC CCC TAA TGA CT -3'), spanning the region encoding LNGFR and first FK-BP. Lung tissue was disrupted and homogenized using TissueLyser II (Qiagen) and total RNA was extracted using an RNeasy Mini Kit (Qiagen 74106). RT reactions were performed with 1 µg total RNA using a QuantiTECT-RT kit (Qiagen 205313). PCR assays were conducted in low 96-well plates (Bio-Rad MLL-9601) using a CFX96 Real-Time System (Bio-Rad). Triplicates were used for each sample. The following 10 µl reaction mixture was used: 5 µl iTaq Universal SYBR Green SuperMix (Bio-Rad 1725121), 1 µl of primers at a final concentration of 5 µm, 1.5 µl RNase-free water, and 2.5 µl of cDNA (1:5 dilution). Primers were first optimized (Appendix) and the most optimal PCR cycling conditions were used for all experiments: denaturing at 95°C for 30s, 40 cycles at 95°C for 10s and 53.4°C for 30s, ending with a melt curve initiated at 55°C with 0.5°C increments/cycle up to 95°C. All EFIA samples were normalized using 18s as an internal control. Relative quantification was performed using the ΔΔCT method [105].

2.8 Statistics

All data are presented as mean ± standard error of the mean (SEM). Results were analyzed using a one-way analysis of variance (ANOVA) with a post hoc Bonferroni test on GraphPad Prism statistical software (San Diego, CA). A value of $p < 0.05$ was considered statistically significant.

3. Results

3.1 Preliminary characterization of LE-EFIA (E6711) at 8 weeks: LE-EFIA display a PAH phenotype following treatment with a dimerizing compound

To determine whether EFIA Tg mice develop a PAH-like phenotype in response to endothelial-specific apoptosis, 8-week old E6711 mice were treated with 2 mg/kg or 10 mg/kg AP20187 (AP) daily for 1 week and right ventricle systolic pressure (RVSP) by right ventricle catheterization was collected before sacrifice on day 8. RVSP values are presented in box plots (Figure 4A). Following EFIA transgene induction with 10 mg/kg AP, RVSP was significantly increased in E6711 mice compared to CD1-WT and E6711 controls at baseline (32 ± 1.3 mmHg, n=8; 23 mmHg ± 1.2, n=9; 24 ± 1.7 mmHg, n=6, respectively, $p \leq 0.001$), while 2 mg/kg treated E6711 mice displayed slightly lower RVSP although still significantly higher than WT control (28 ± 1.6 mmHg, n=8; 23 mmHg ± 1.2, n=9, respectively, $p \leq 0.01$) and E6711 vehicle-treated control (23.2 ± 0.9 mmHg, n=10, $p \leq 0.05$). RVSP in vehicle-treated WT mice were unaffected in comparison to that at baseline (23 ± 1.02 mmHg, n=5 vs. 23 mmHg ± 1.2, n=9).

The weight ratio of the right ventricle to left ventricle plus septum wall (RV/LV+S) is used as an indicator of RVH. RV/LV+S values following treatment with 2 mg/kg AP or 10 mg/kg daily for 1 week are presented in a box plot summarized in Figure 4B. Transgene induction with 2 mg/kg AP and 10 mg/kg AP resulted in significant elevations of RVSP in E6711 Tg mice compared to vehicle-treated WT mice (0.27 ± 0.01, n=8, $p \leq 0.05$, 0.28 ± 0.01, n=8, $p \leq 0.01$, 0.20 ± 0.02, n=5, respectively) An increasing trend was observed in E6711 Tg mice treated with 2 mg/kg and 10 mg/kg in comparison to E6711 and WT at baseline (0.26 ± 0.01, n=6; 0.23 ± 0.01, n=9, respectively). Peripheral lesions were found in a more several affected 6711-treated EFIA mouse (Figure 4C).

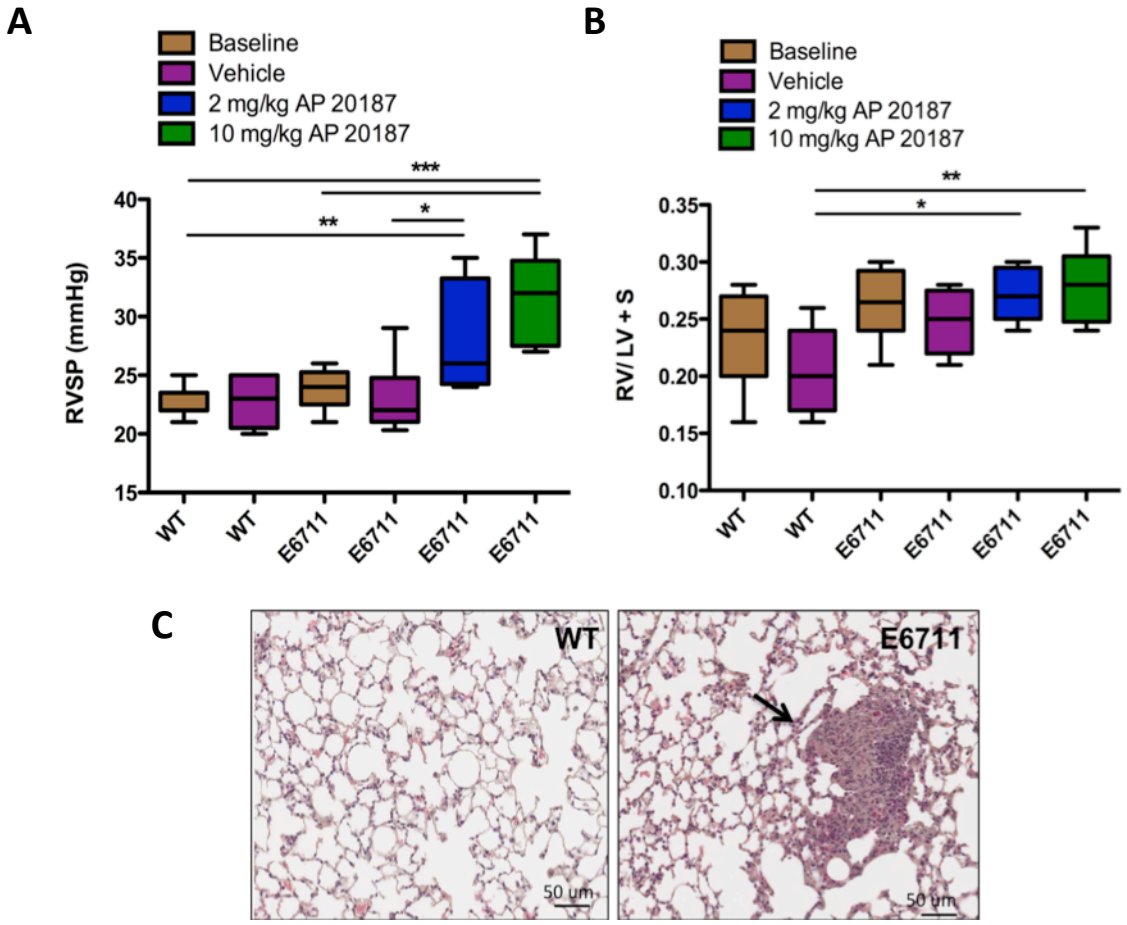

Figure 4. RVSP and RVH following EFIA transgene induction in E6711 mice. (A) Scatter plot representative of RVSP values in the E6711 founder line. (B) Box plot summarizing RVSP distribution in each experimental group and (C) induced arteriolar remodeling in the more severely affected EFIA mice (H&E staining). N=5-10/group. Whiskers in box plot represents maximum and minimum values with median line. Scale bar represents 10 µm. * = p≤0.05; ** = p≤0.01, *** = p≤0.001 by ANOVA with Bonferroni post-hoc test.

3.2 Reassessment of EFIA mRNA abundance in EFIA Tg Mice: E6780 exhibits elevated EFIA mRNA expression in comparison to E6711 and E6712 Tg lines

To determine and compare relative EFIA mRNA expression levels between three EFIA Tg lines, RT-qPCR was performed using primers targeting the mutated FKBP portion of the EFIA transgene. The highest EFIA mRNA levels were detected in E6780 (high expressing (HE)-EFIA) and the lowest detected in E6712 (Table 1, Figure 5). For experimental purposes, the E6711 Tg line is termed low expressing (LE)-EFIA. All EFIA mRNA levels were normalized to ribosomal 18s.

3.3 Preliminary characterization of HE- and LE-EFIA at 12 weeks

3.3.1 HE- & LE-EFIA exhibit modest hemodynamic changes following treatment with a dimerizing compound at 12 weeks

To determine whether mice over-expressing the fas-inducing apoptosis construct develop a PAH-like phenotype in response to endothelial-specific apoptosis, 12-week old EFIA mice were treated with 2 mg/kg AP20187 (AP) daily for 1 week and sacrificed on day 8. Right ventricle systolic pressure (RVSP) data by right ventricle catheterization was collected before sacrifice. RVSP values indicative of pulmonary pressure are summarized in Figure 6 and are presented in both scatter and box plots. No significant increases in RVSP were observed E6780, E6711, and E6712 compared to CD1-WT controls. An increasing trend in RVSP was observed in treated E6711 compared to CD1-WT controls. Mean RVSP values are summarized in Table 2.

RV/LV+S values following treatment with 2 mg/kg AP daily for 1 week are presented in both scatter and box plots and are summarized in Figure 6. No significant increases in RVH were detected in E6780, E6711, or E6712 mice compared to CD1-WT

controls. Again, an increasing trend in RVSP was observed in treated E6711 compared to baseline and CD1-WT controls. Mean RV/LV+S values are summarized in Table 2.

3.3.2 Pathological assessment of gross lung morphology reveals no observable pulmonary lesions

Previous results from Tg founder lines E6711 and E6780 revealed pulmonary remodeling with presence of pulmonary obliterate lesions. Thus, lung sections from E6711, E6780, and WT mice, following treatment with 2 mg/kg AP for 1 week, were stained with H&E and gross morphology was analyzed by observation. All sections were blinded before analysis. In comparison to baseline and WT controls, treated EFIA lung tissue lacked any significant signs of arteriolar remodeling or a proliferative cell phenotype. Representative H&E histology is presented in Figure 7.

Table 1. EFIA mRNA abundance in EFIA Tg mice by RT-qPCR

Tg Line or WT	Number of Mice	Mean Relative EFIA mRNA level ($x10^{-6}$)	Ct Value
E6711	5	55.82	26-34
E6712	5	0.4760	33-34
E6780	5	203.90	24-25
CD1	5	0.2681	33-39

Mean Relative EFIA mRNA Data is represented by the ΔΔCT method.

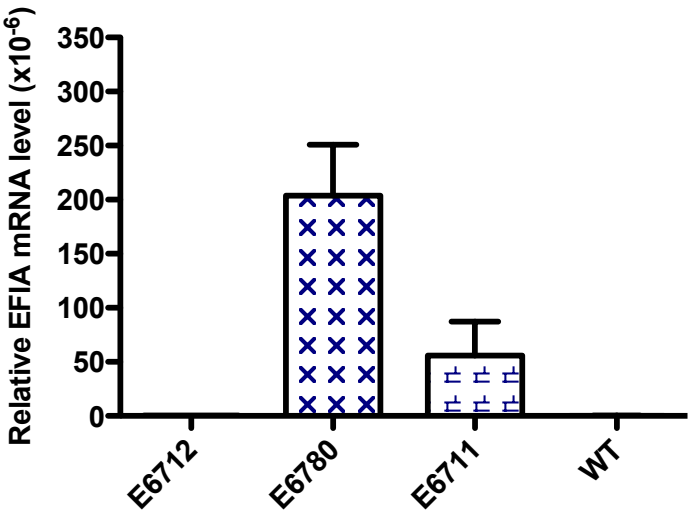

Figure 5. Relative EFIA mRNA expression levels in the lung of three EFIA Tg lines. Bar graph representing EFIA mRNA levels in the lung of 3 Tg lines following EFIA transgene induction for 1 week. EFIA mRNA levels are normalized to 18s. Bar represents mean + SEM.

Table 2. RVSP and RV/LV+S in Three Tg EFIA lines following AP treatment

	WT		**E6712**	**E6711**		**E6780**	
	Baseline (n=23)	*AP (n=12)*	*Baseline (n=5)*	*Baseline (n=8)*	*AP (n=9)*	*Baseline (n=11)*	*AP (n=11)*
RVSP	21± 0.48	21 ± 0.52	21 ± 1.07	23 ± 0.81	24 ± 0.97	22 ± 0.97	22 ± 0.77
RV/LV +S	0.27 ± 0.0048	0.28 ± 0.0089	0.31 ± 0.012	0.28 ± 0.0075	0.31 ± 0.011	0.28 ± 0.0068	0.29 ± 0.0072

Data are represented as mean ± standard error of the mean.

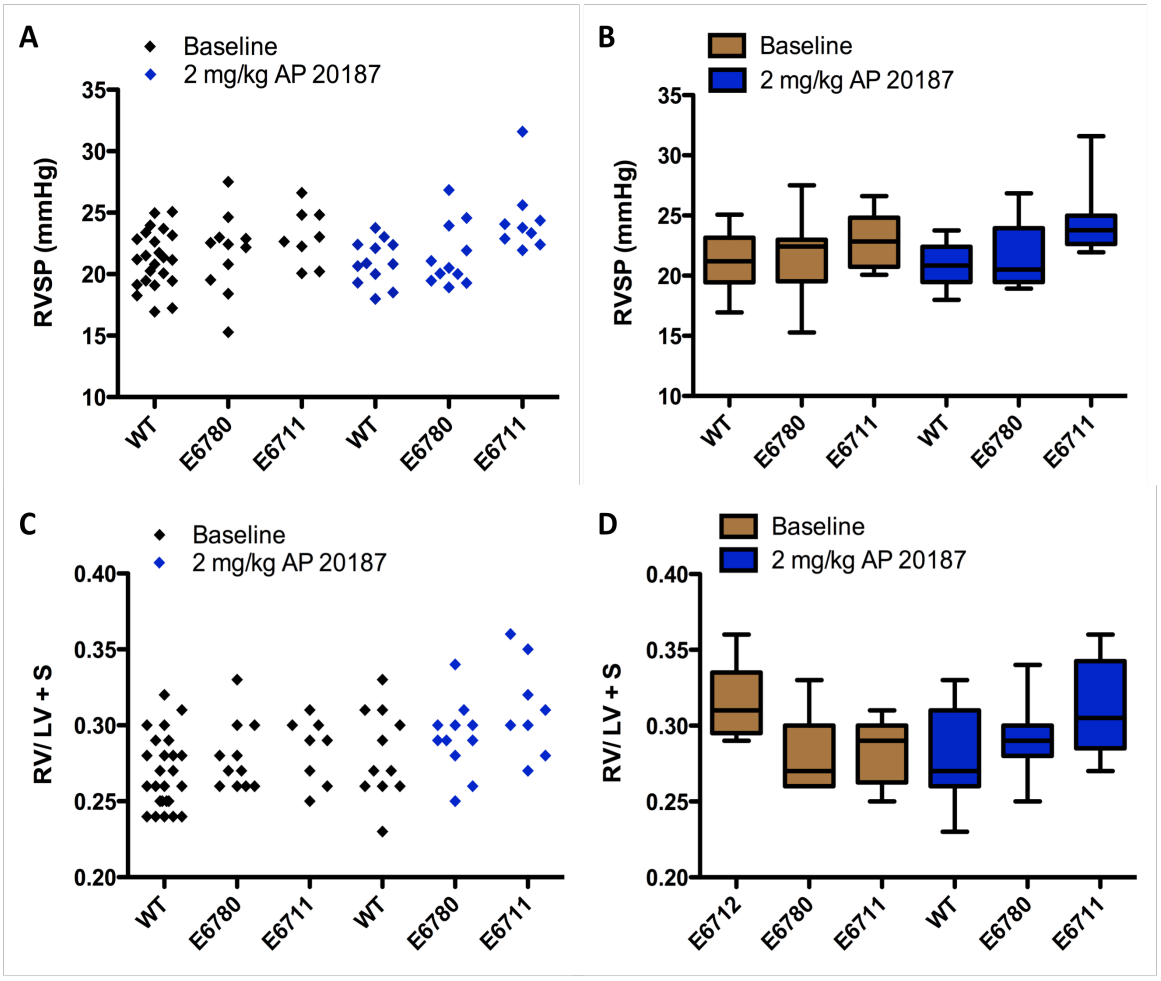

Figure 6. RVSP and RVH following EFIA transgene induction in E6780 mice. (A) Scatter plot representative of RVSP values in 3 Tg EFIA lines. **(B)** Box plot summarizing RVSP distribution in each experimental group. RVH measurements in three EFIA Tg lines. No significant changes in RVSP or RVH were seen in AP-treated mice compared to baseline or WT controls (n=8-23/group). **(C)** Scatter plot representative of RV/LV+S values in 3 Tg lines. **(D)** Box plot summarizing RV/LV+S values of each experimental group. Whiskers in box plot represents maximum and minimum values with median line.

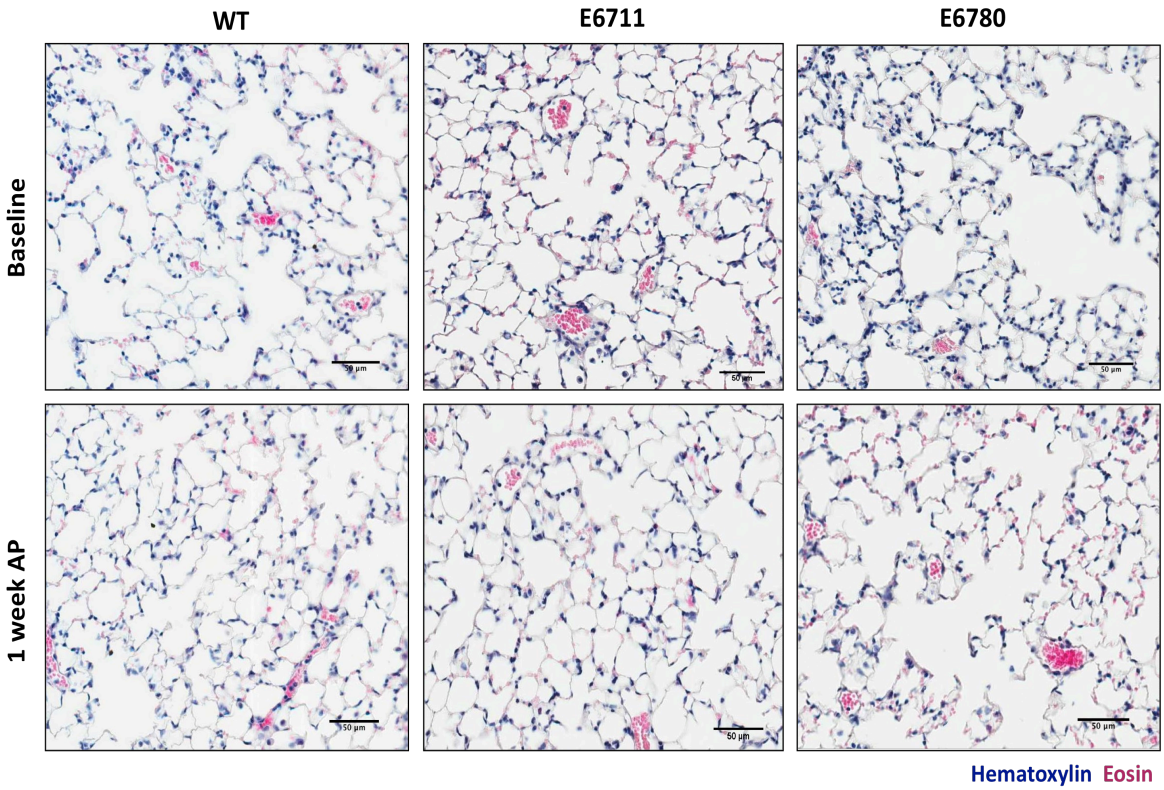

Figure 7. Representative hematoxylin and eosin staining in EFIA Tg mice following treatment with dimerizing compound (AP) for one week. Lung sections were stained with hematoxylin and eosin. Representative lung histology in E6711, E6780, and WT mice, both treated and non-treated (n=8-23/group). Scale bar represents 50 µm.

3.4 Patterns of apoptosis in the lung of HE-EFIA (E6780) following AP treatment

3.4.1 TUNEL staining and activated caspase-3 detection reveal increasing levels of apoptosis in HE-EFIA (E6780) Tg mice and activated caspase-3 detection deems more sensitive to apoptosis

Provided evidence to suggest that apoptosis plays a major role in the pathogenesis of PAH and the notion that E6780 mice exhibit higher EFIA mRNA levels, pulmonary apoptosis levels in peripheral lung tissue were assessed. HE-EFIA and WT mice were treated with 2 mg/kg AP daily for 7 days and sacrificed on day 8. TUNEL staining was performed on lung sections at baseline and following transgene induction. Representative TUNEL staining and quantification is presented in (Figure 8). No significant changes were found in treated E6780 compared to baseline and CD1 controls, although a trend towards increased levels of apoptosis were observed in E6780 at baseline.

To further explore patterns of apoptosis, identical lung sections were assessed for activated caspase-3 immunoreactivity. Cleaved-caspase 3 (CC3) is the main effector caspase in the apoptotic pathway and has been shown to be more sensitive than the popular TUNEL assay [106]. Representative CC3 IHC staining and quantification is presented in (Figure 9). Again, no significant changes were found in treated E6780 compared to baseline and CD1 controls, although a trend towards increased levels of apoptosis were observed in E6780 at baseline.

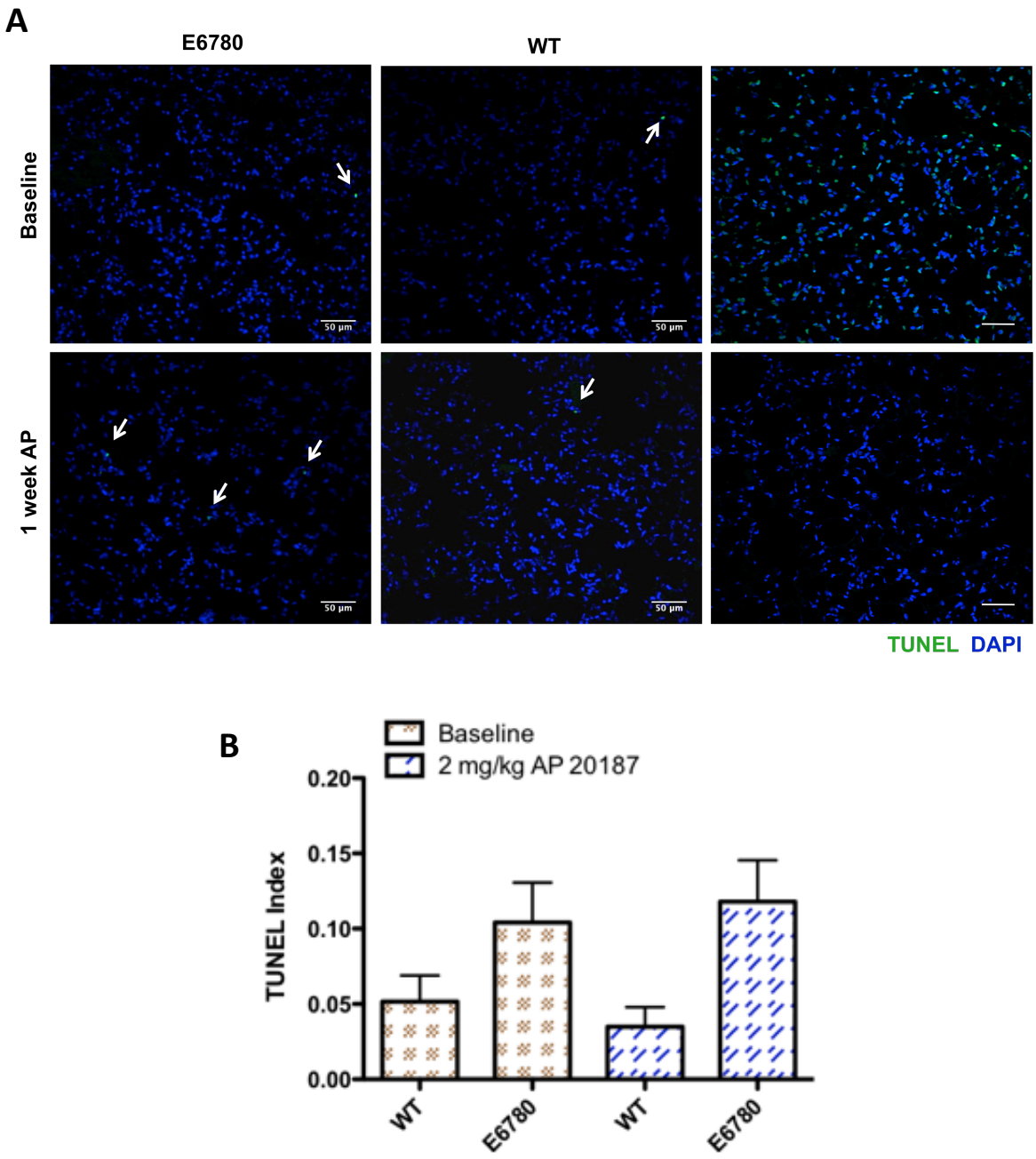

Figure 8. Peripheral lung apoptosis patterns assessed by TUNEL following EFIA Tg induction in E6780 mice. (A) Paraffin lung sections of E6780 and WT mice stained with TUNEL (green) and DAPI nuclear counterstain (blue) after 1 week of AP transgene induction (top left and centre, bottom left and centre; n=5/group). Positive (top right) and negative (bottom right) controls are shown. Arrows indicate positive cells. Scale bar represents 50 µm. **(B)** Quantification of TUNEL-positive cells. Bar represents mean + SEM.

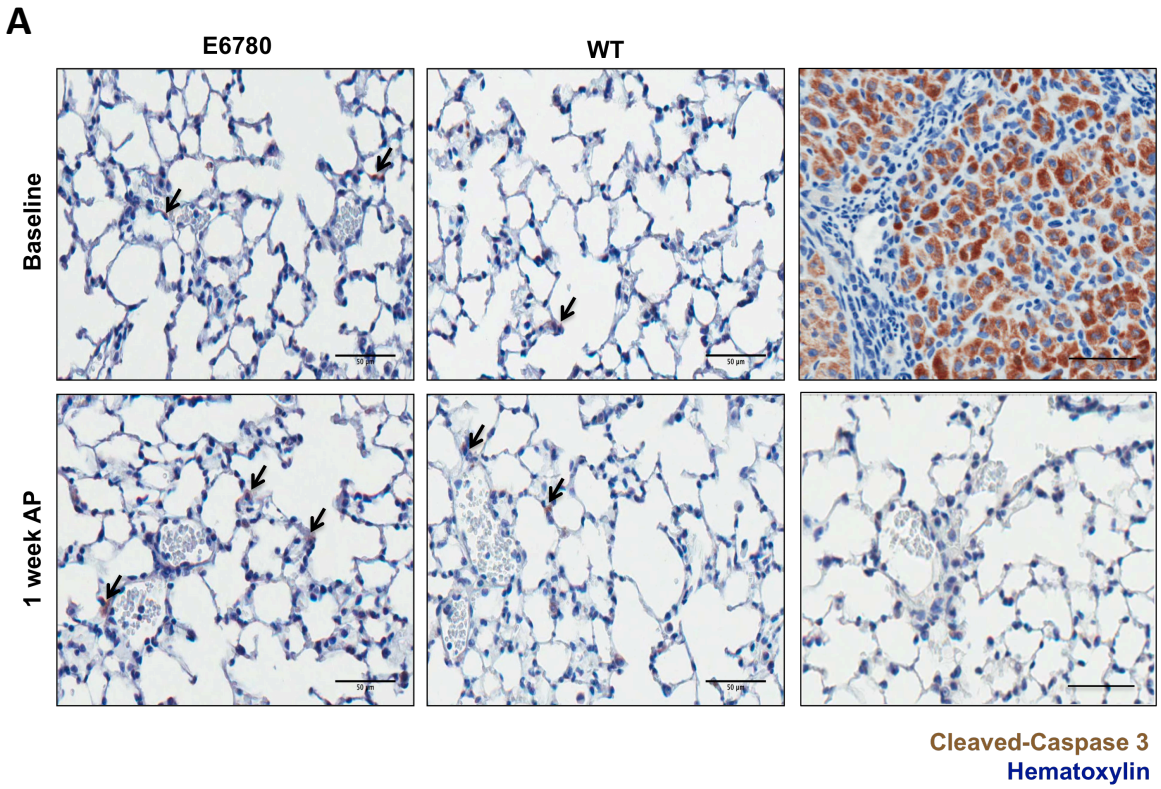

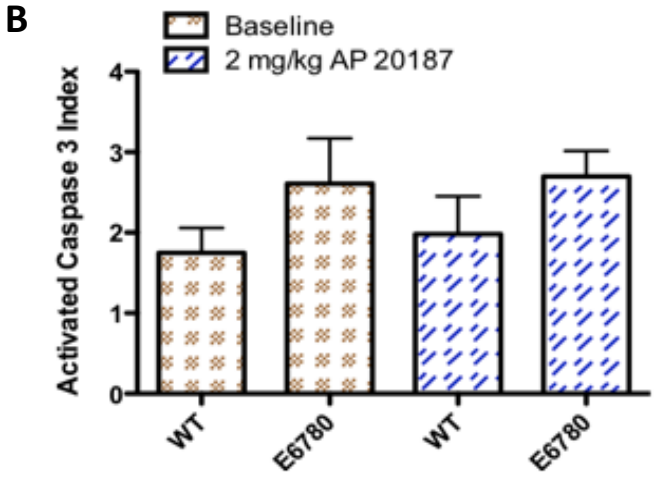

Figure 9. Peripheral lung apoptosis patterns assessed by activated caspase 3 following EFIA Tg induction in E6780 mice. (A) DAB staining (brown) representative of activated caspase 3 with DAPI nuclear counterstaining (blue) on paraffin lung sections of E6780 and WT mice after 1 week of AP transgene induction (top left and centre, bottom left and centre; n=5/group). Positive control in spleen tissue (top right) and isotype control in lung tissue (bottom right) are shown. Arrows indicate positive cells. Scale bar represents 50 µm. **(B)** Quantification of activated caspase 3 cells. Bar represents mean + SEM.

Chapter II: Generating a More Robust EFIA System for 'Second Generation' EFIA Transgenic Mice

Chapter Objective

Due to the loss and/or lack of phenotype in the described EFIA Tg mouse lines, this chapter outlines the strategy used to incorporate a stronger Tie2 promoter, namely the 'SuperTie2' promoter, to enhance the expression of FIA within endothelial cells containing the EFIA transgene. ST2 has been designed using a fragment of the 2.1 kb Tie-2 promoter with 1.7 kb of an enhancer element from the first intron, that which is required for robust expression in adult mice [107]. Interestingly, a consensus octamer element within a 223 base pair (bp) enhancer region is required for endothelial cell-specific activity *in vivo* [108].

In addition to the endothelial-specific promoter, since the FIA transgene contains regions similar to endogenous proteins, the reporter gene, DsRed-Express 2 (DSRE2), was chosen to incorporate into the EFIA construct to provide more robust detection. DSRE2 has low cytotoxicity and phototoxicity due to its reduced aggregation tendency compared to wild-type DsRed. Additionally, we can induce bicistronic expression of FIA and DSRE2 by incorporating the encephalomyocarditis virus (EMCV) internal ribosome entry site 2 (IRES2) along with DSRE2 [109]. Furthermore, this chapter outlines the initial *in vitro* transfection validation experiments performed in three different endothelial cells (HUVEC, BAEC and EOMA) to assess the functionality of the newly sub-cloned ST2 constructs.

4. Materials and Methods

4.1 Construction of SuperTie2 Constructs

4.1.1 SuperTie2 (ST2)-FIA-DsRedExpress2 Construction

FIA was excised from pVAX1-FIA with BamH1 [(New England Biolabs (NEB)], purified using QIAQuick gel extraction kit (Qiagen 28704), and sub-cloned into a BamHI restriction site located in the multiple cloning site (MCS) of pIRES2-DsRedExpress2 (DSRE2; Clontech 632540) backbone using T4 DNA ligase (NEB M0202). Ligated DSRE2-FIA was transformed into Top 10 chemically competent cells (Invitrogen C404006), purified using QIAprep spin miniprep kit (Qiagen 27104), and successful ligation was determined by linearizing with EcoRI (NEB) followed by sequencing with a CMV forward primer (StemCore, Ottawa, ON).

DSRE2-FIA was excised from DSRE2 plasmid with PCR primers designed to incorporate ClaI and SalI restriction sites at the 5' and 3' ends, respectively. ClaI-DSRE2-FIA-SalI PCR product was purified using the QIAQuick gel extraction kit, digested with ClaI (NEB) and SalI-HF (NEB), and sub-cloned into the MCS of SuperTie2 (ST2) plasmid using T4 DNA ligase. Ligated ST2-DSRE2-FIA was transformed into Top 10 chemically competent cells, purified using QIAprep spin miniprep kit, and successful ligation was determined by digestion with HindIII-HF (NEB) followed by sequencing with a bGH polyA reverse primer (StemCore, Ottawa, ON).

4.1.2 SuperTie2-FIA Construction

FIA was excised from pVAX1-FIA using PCR with forward and reverse primers designed to incorporate a ClaI restriction site. ClaI-FIA-ClaI PCR product was purified using the QIAQuick gel extraction kit, digested with ClaI, and sub-cloned into the MCS of

ST2 plasmid using T4 DNA ligase. Ligated ST2-FIA was transformed into XL10-Gold ultracompetent cells (Stratagene 200314), purified using QIAprep spin miniprep kit, and successful ligation was determined by digestion with BamHI-HF (NEB) followed by sequencing with a bGH polyA reverse primer (StemCore, Ottawa, ON).

4.1.3 SuperTie2-pIRES2-DSRE2 Construction

DSRE2 was excised from DSRE2 plasmid using PCR with forward and reverse primers designed to incorporate a ClaI restriction site. ClaI-DSRE2-ClaI PCR product was purified using the QIAQuick gel extraction kit, digested with ClaI, and sub-cloned into the MCS of ST2 plasmid using T4 DNA ligase. Ligated ST2-DSRE2 was transformed into Top 10 chemically competent cells, purified using QIAprep spin miniprep kit, and successful ligation was determined by digestion with BamHI-HF (NEB) followed by sequencing with a bGH polyA reverse primer (StemCore, Ottawa, ON).

4.1.4 SuperTie2-EGFP Construction

EGFP was excised from pIRES-EGFP plasmid (Clontech 60641) using PCR with forward and reverse primers designed to incorporate a ClaI restriction site. ClaI-EGFP-ClaI PCR product was purified using the QIAQuick gel extraction kit, digested with ClaI, and sub-cloned into the MCS of ST2 plasmid using T4 DNA ligase. Ligated ST2-EGFP was transformed into Top 10 chemically competent cells, purified using QIAprep spin miniprep kit, and successful ligation was determined by digestion with SalI-HF and ClaI followed by sequencing with a bGH reverse primer (StemCore, Ottawa, ON).

4.2 Cell Culturing

Human umbilical vein endothelial cells (HUVEC) were purchased from Lonza (CC-2519) and were cultured in endothelial growth medium-2 (EGM-2) medium containing 2% fetal bovine serum (FBS) and growth factors (Lonza CC-3156) at 37°C in an atmosphere of 5% CO_2. HUVEC were grown to 80-90% confluence before subculturing and 90-95% confluence for protein lysis or electroporation. HUVEC were frozen down in Synth-a-Freeze cryopreservation medium containing 10% dimethylsulfoxide (DMSO) (Gibco A12542-01) at a concentration of 5 x 10^6 cells//ml, cooled to 4°C, placed in Nalgene Cryo 1°C freezing container (Thermo Scientific 5100-0001) and cooled to -80°C overnight and transferred to liquid nitrogen for long term storage.

Bovine aortic endothelial cells (BAEC) were purchased from Lonza (BW-6002) and were cultured in EGM-MV medium containing 2% FBS and growth factors (Lonza CC-3125), following the same protocol as HUVEC. BAEC were frozen down following the same protocol as HUVEC.

Mouse endothelioma (EOMA) cells were purchased from ATCC (CRL-2586) and were cultured in DMEM (Gibco 1995-065) medium supplemented with 10% FBS (Lonza CC4102B) at 37°C in an atmosphere of 5% CO_2. EOMA cells were grown to 80-90% confluence and split in a 1:3-1:5 ratio for subculturing purposes. EOMA cells were frozen down in DMEM supplemented with 10%FBS and 5% DMSO (Sigma D2438).

Chinese hamster ovary (CHO)-K1 cells were purchased from ATCC (CCL-61) and were cultured in F-12 Ham's medium (Gibco 1176-054) supplemented with 10% FBS (Lonza CC4102B), 2 mM L-glutamine (Gibco 25030) and 1% penicillin/streptomycin (Gibco 15140) at 37°C in an atmosphere of 5% CO_2. CHO-K1 cells were grown to 80-90%

confluence and split in a 1:4-1:12 ratio for subculturing purposes. CHO-K1 cells were frozen down frozen down following the same protocol as HUVEC.

4.3 Tie2 Immunoblotting

4.3.1 Protein Extraction and Quantification

Proteins were extracted from HUVEC, BAEC, and EOMA cells after homogenization in approximately 150 µl of ice-cold RIPA lysis buffer (Appendix II). Homogenized cells were incubated at 4°C while shaking for 10 minutes. Cell lysate was centrifuged (14000 xg) for 15 minutes at 4°C. Extracted protein was quantified with the DC protein assay kit II (Bio-Rad 5000111), following manufacturer's protocol. Duplicates of each sample along with bovine serum albumin (BSA) standards were loaded into a 96-well plate (Corning 3596) and incubated for 15 minutes at RT. Absorbance was read at 750 nm using the POLARstar Omega microplate reader (BMG Labtech).

4.3.2 Gel Electrophoresis and Transfer

Protein samples were denatured in Laemmli buffer (Appendix II) for 5 minutes at 95°C, cooled for 5 minutes on ice, and loaded into a NuPAGE® Bis-Tris 4-12% gel (Invitrogen NP0321PK2). 20-30 µg of protein was loaded into each well and gels were run at 180 V in NuPAGE® MOPS SDS running buffer (Invitrogen NP0001) until the protein ladder reached the bottom of the gel. Protein samples were transferred from NuPAGE Bis-Tris gel to a nitrocellulose membrane using the iBLOT system (Invitrogen). Following transfer, membranes were stained with Ponceau-S red (Sigma P7170) stain to visualize protein transfer.

4.3.3 Immunoblotting

Membranes were blocked with 5% nonfat dry milk in 0.1% TBS-T (Appendix) for 1 hour at RT and incubated with rabbit anti-Tie-2 primary antibody (1:000 dilution, C-20, Santa Cruz sc-324) or monoclonal mouse anti-β-actin (1:5000 dilution, Sigma A5441) in blocking buffer overnight at 4ºC. Membranes were washed in 0.1% TBS-T (3 x 5 min) followed by incubation with a goat anti-rabbit horseradish peroxidase (HRP)-conjugated secondary antibody (1:2500 dilution, Bio-Rad 170-6515) or goat anti-mouse HRP (1:2500, Bio-Rad 170-6516) in blocking buffer for 1 hour at RT. If using Bio-Rad's Precision Plus Protein WesternC (161-0363) ladder, 0.5 µl of streptavidin-HRP (Bio-Rad 161-0381) was added to the secondary antibody incubation. An enhanced chemiluminescence detection system, ECL Plus (GE Healthcare RPN2132) was used to detect immunoblotting. Bands were visualized with Versadoc imaging system (Bio-Rad). Protein loading and signal intensity was normalized to β-actin.

4.4 Transient Transfections

Unless indicated otherwise, 2500-5000 cells/cm^2 were seeded into T-75 flasks (Corning 430641) and grown to 90% confluence before transfection. Cells were stained with trypan blue and counted using a hemocytometer to determine cell viability and concentration. Cells were transfected by nuclear-targeting electroporation using the Amaxa™ Nucleofector™ 4D system (Lonza).

4.4.1 HUVEC

For each transfection, 0.5 million (M) cells/sample were resuspended in 100 µl of P5 primary cell 4D-Nucleofector™ solution (Lonza V4XP-5024). Each sample mastermix

consisted of 100 µl of cell suspension and 1-6 µg of plasmid DNA. Electroporation was performed using the manufacturer's optimized pulse program for HUVEC (CA-167). Following transfection, cells were resuspended in 500 µl of EGM-2 media and seeded into culture system of choice. Analysis was performed at 24, 48, or 72 hours.

4.4.2 CHO-K1 Cells

Transfection was performed using a similar protocol to that of HUVEC, with a few exceptions: 1) Cells were grown in F-12 Ham's medium; 2) Transfection was performed using the DT-133 pulse program on the 4D-Nucleofector™ using the SF cell line 4D-Nucleofector™ Kit. Analysis was performed at 24 or 48 hours.

4.4.3 BAEC

Transfections were performed using the same protocol as HUVEC with EGM-MV medium. Initial transfection optimization was performed using the primary cell optimization 4D-Nucleofector™ kit (Lonza V4XP-9096) with maxGFP™. The CA-167 pulse was used for all subsequent BAEC transfections. Analysis was performed at 24 or 48 hours.

4.4.4 EOMA Cells

Transfections were performed using the same protocol as HUVEC with a few exceptions: 1) cells were grown to 75-80% confluence; 2) cells were grown in DMEM medium and; 3) cells were incubated at 37°C for 5 minutes following resuspension in 500 µl of media. Initial transfection optimization performed using the cell line optimization 4D-Nucleofector™ kit (Lonza V4XC-9064) with maxGFP™. Optimization was performed using 15 pulses with three Nucleofector™ solutions (SG, SF, and SE) in a nucleocuvette strip. Subsequent transfections were performed using the SG cell line 4D-Nucleofector™ kit

(Lonza V4XC-3012) was used for Fluorescent analysis was performed at 48 hours with Nikon Eclipse TE2000-E inverted fluorescent microscope.

4.5 DsRed Immunofluorescence

Immunofluorescence (IF) was performed on transfected cells grown on an 8- or 4-well chamber slide. Cells were washed 3x with Dulbecco's PBS (DPBS; Gibco 17-512F), fixed at RT for 20 minutes with 4% PFA (Appendix II), washed again 3x with DPBS, and permeabilized for 5 minutes with 0.2% Triton X-100 (Appendix II). Fixed and permeabilized cells were washed 3 x with DPBS, blocked in 1% BSA in PBS, washed 3x with DPBS, and incubated for 1 hour at RT with polyclonal rabbit anti-DsRed antibody (1:150 dilution, Clontech 632496). Following incubation with primary antibody, cells were washed 5x with DPBS and incubated for 1 hour at RT with goat anti-rabbit AlexFluor 488 (1:200 dilution, Invitrogen A-11008) and subsequently washed 5x with DPBS. Cells were counterstained with DAPI (1:4000, Molecular Probes D21490) washed 5x with DPBS. Counterstained cells were subsequently mounted with Mowiol mounting medium (Appendix II) and sealed with glass cover slips (VWR 48393-059)

4.6 Microscopy

Images of DSRE2 IF staining and EGFP expression in 4- or 8-well chambers slides were acquired using the Zeiss Axio Imager M2 fluorescent microscope. Images of DSRE2 and EGFP expression in 6- and 12-well dishes were acquired using the Nikon Eclipse TE2000-E fluorescent microscope. All images of cells during normal culturing practices were acquired using the Nikon Eclipse T5100 microscope.

5. Results

5.1 Generation of new Tie2 constructs: Incorporation of the "stronger" SuperTie2 promoter and DsRedExpress2

The ST2 construct, spanning from the T7 region to the T3 region, was sequenced before initiating subcloning experiments. Four ST2 plasmids were constructed, namely: 1) SuperTie2-FIA-DsRedExpress2 (ST2-FIA-DSRE2); 2) SuperTie2-FIA (ST2-FIA); 3) SuperTie2-IRES2-DsRedExpress2 (ST2-DSRE2) and; 4) SuperTie2-EGFP (ST2-EGFP). See Table 3 for list of plasmids. All plasmids were confirmed by both restriction enzyme digestion and sequencing.

5.2 Sub-cloning Fas-Induced Apoptosis construct and DsRed-Express2 into SuperTie2 plasmid

5.2.1 The FIA construct and DSRE2 were sub-cloned into SuperTie2

Digestion with EcoRI confirmed a correct linearized DNA fragment of approximately 7.2 Kb, which was subsequently sequenced to confirm insertion of the FIA construct into DSRE2 (Figure 10). Due to few restriction sites available in the MCS of the ST2 construct, SalI and ClaI sites were chosen for ligation of DSRE2-FIA into ST2. Correct ligation was confirmed through digestion of plasmid DNA samples with HindIII (Figure 10). Furthermore, sequencing confirmed correct ligation in the ST2-FIA-DSRE2 construct. Refer to section 4.1.1 for details.

5.2.2 FIA alone was sub-cloned into SuperTie2

The ST2-FIA-DSRE2 plasmid is approximately 10.5 Kb and thus FIA was also sub-cloned into ST2 in absence of DSRE2. Purified DNA was digested with BamHI to confirm

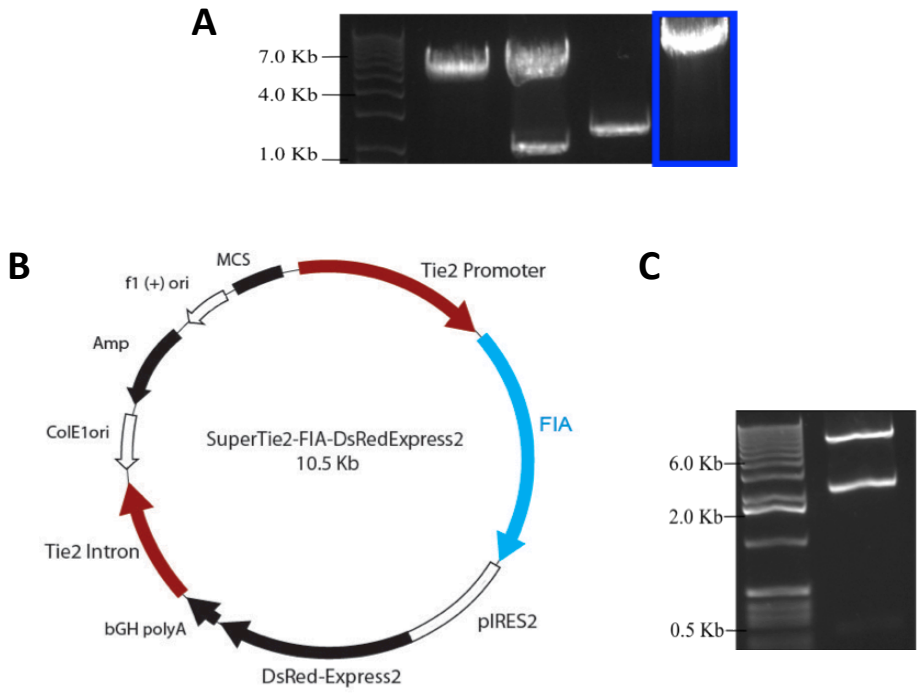

Figure 10. The ST2-FIA-DSRE2 construct. FIA was inserted into the DSRE2 plasmid and **(A)** represents FIA-DSRE2 fragment digested with EcoRI. Correct ligation yields a 7.4 Kb linearized plasmid (blue box). FIA and DSRE2 were sub-cloned into the MCS of ST2 at SalI and ClaI restriction sites and the ST2-FIA-DSRE2 construct was purified with an endofree maxiprep. **(B)** ST2-FIA-DSRE2 plasmid map and the (**C**) ST2 + FIA-DSRE2 ligated colony digested with HindIII. Correct ligation yields a 235 bp fragment.

correct ligation (Figure 11). Sequencing confirmed insertion of FIA into the MCS of ST2 expression vector. See section 4.1.2 for details.

5.2.3 DSRE2 was sub-cloned into SuperTie2

The construction of ST2-DSRE2 was pursued for use as a control during *in vitro* validation transfection experiments with ST2 constructs. Purified DNA was digested with BamHI to confirm correct ligation (Figure 12). Sequencing confirmed insertion of FIA into the MCS of ST2 expression vector. Refer to section 4.1.3 for details.

5.2.4 EGFP was sub-cloned into SuperTie2

The construction of ST2-EGFP was pursued after confirming lack of DSRE2 expression following transfection with ST2 constructs. Purified DNA was digested with SalI and ClaI to confirm correct ligation (Figure 13). Sequencing confirmed insertion of EGFP into the MCS of ST2 expression vector. Refer to section 4.1.4 for details.

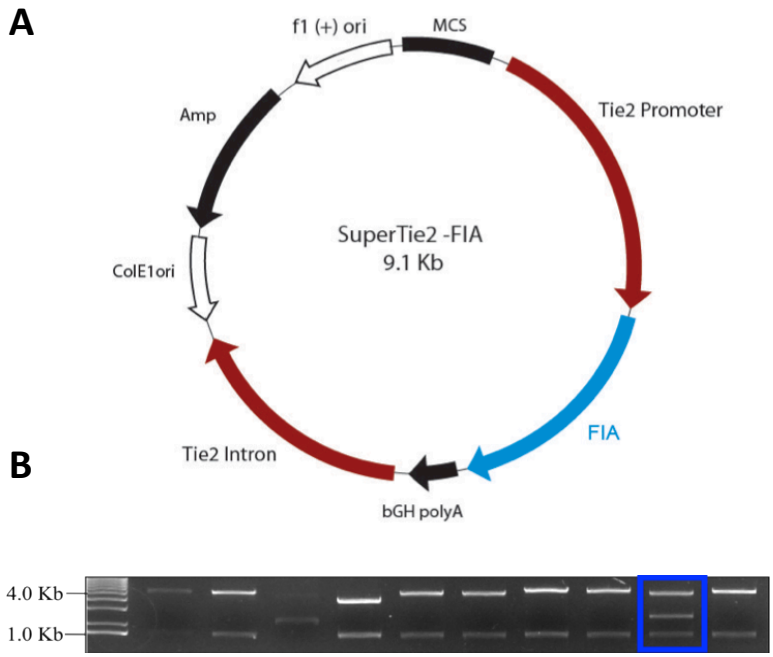

Figure 11. The ST2-FIA construct. FIA was inserted into the MCS of ST2 at ClaI restriction sites and ST2-FIA was purified in endotoxin free conditions. **(A)** ST2-FIA plasmid map and **(B)** ligated colonies digested with BamHI. Correct ligation yields three fragments: 1668 bp, 2420 bp, and 4959 bp (blue box).

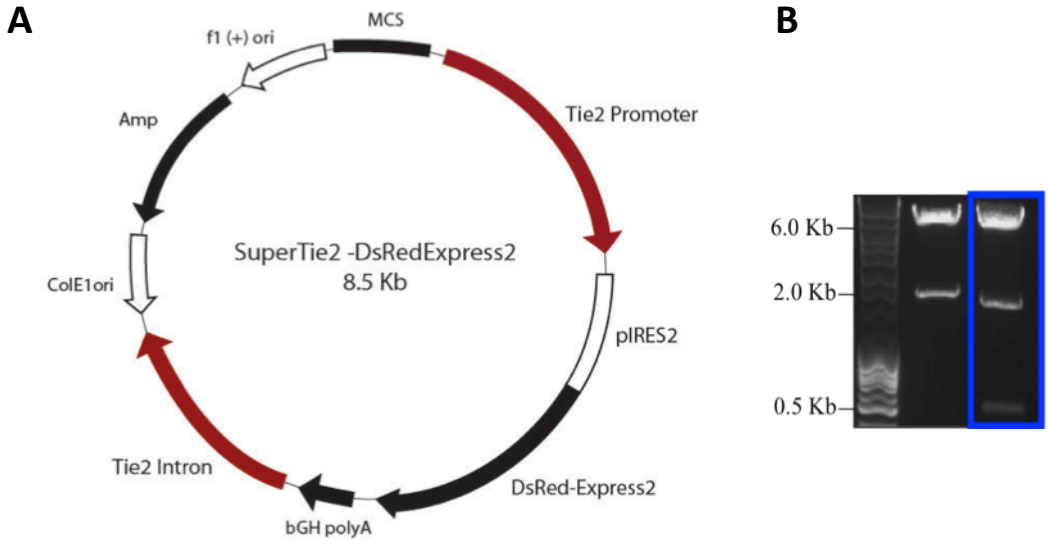

Figure 12. The ST2-DSRE2 construct. DSRE2 was inserted in the MCS of ST2 at ClaI restriction sites and ST2-DSRE2 was purified in endotoxin free conditions. **(A)** ST2-DSRE2 plasmid map and **(B)** ligated colonies digested with BamHI. Correct ligation yields three fragments: 517 bp, 1668 bp, and 6283 bp (blue box).

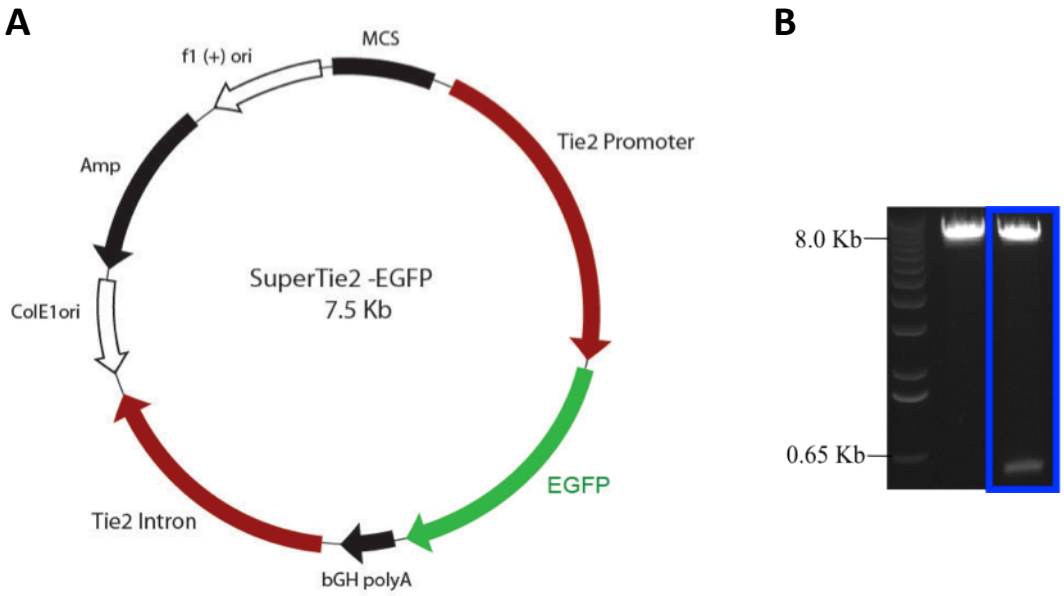

Figure 13. The ST2-EGFP construct. FIA was inserted into the MCS of ST2 at ClaI restriction sites and ST2-EGFP was purified in endotoxin free conditions. **(A)** ST2-EGFP plasmid map and **(B)** ligated colonies digested with SalI and ClaI. Correct ligation yields two fragments: 7.1 Kb and 750 bp (blue box).

Table 3. List of plasmids

Plasmid	Size (kb)	Purification Method	Concentration (μg/μL)[2]	A260/A280[3]	A260/A230[4]
maxGFP™	3.4	Lonza	1.0	-	-
pIRES-EGFP	5.3	Midiprep	1.0	-	-
pIRES-DSRE2	5.3	Maxiprep[1]	0.31	1.87	2.27
ST2-EGFP	7.5	Midiprep	3.22	1.87	2.27
ST2-DSRE2	8.5	Midiprep	0.23	1.86	2.28
ST2-FIA	9.1	Maxiprep[1]	1.166	1.89	2.32
ST2-FIA-DSRE2	10.5	Maxiprep[1]	1.298	1.88	2.31

[1] Qiagen Endofree purification kit
[2] Concentration as determined by Nanodrop (Thermo Scientific).
[3] Ratio represents DNA purity as determined by Nanodrop. A ratio of 1.80 is considered pure DNA.
[4] Ratio represents another level of DNA purity. A ratio > 2.0 represents pure DNA without organic contamination

5.3 *In vitro* validation of ST2 constructs

5.3.1 Confirmation of Tie2 Expression in HUVEC, BAEC, and EOMA cells

HUVEC and BAEC were initially chosen to perform *in vitro* validation of the new ST2 constructs. Mouse EOMA cells were pursued later in transfection studies with the idea that they would be easier to transfect than primary endothelial cells. Immunoblots targeting Tie2 protein were performed on whole cell extracts. Tie2 protein expression and thus, an endothelial-phenotype were confirmed in HUVEC, BAEC, and EOMA cells (Figure 14). β-actin was used as a loading control.

5.3.2 Endothelial Cell Transfections

Endothelial cells are notoriously difficult to transfect, with high cells toxicity and low transfection efficiency after transfection [110]. Nucleofection has been recently identified as a promising transfection method for HUVECs and other hard-to-transfect cells [110,111]. A brief electric field is applied to the cells causing the formation of pores in the cell membrane due to ionic forces. DNA can pass through these pores and thereby transfect the cells. The cells are suspended in a specific solution, that which stabilizes the cells in the electric field.

5.3.3 HUVEC: DSRE2 expression is not observed without DsRed-IF

HUVEC were transfected with maxGFP™ (2 μg) and DSRE2 (1-3 μg) by nucleofection following manufacturer's protocol and analyzed at 24 and 48 hours under a fluorescent microscope (Trial H1, Table 4). GFP expression was observed; however no evidence of DSRE2 expression was observed. A second transfection with DSRE2 (2 μg) and

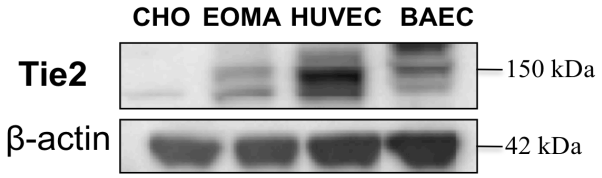

Figure 14. Tie2 Immunoblots (**A)** confirming positive Tie2-expression in HUVEC and BAEC whole cell lysate. (**B)** Immunoblot comparing relative Tie2 protein expression between EOMA cells, HUVEC, and BAEC. CHO-K1 cells represent negative control. β-actin represents protein-loading control.

Table 4. Summary of HUVEC Nucleofection Trials

Trial[1]	Analysis (hours)	DsRed IF[2]	Fluorescence or transfection efficiency (μg)						
			Max GFP™	pIRES-EGFP	ST2-EGFP	pIRES-DSRE2	ST2-DSRE2	ST2-FIA-DSRE2	ST2-FIA
H1	24, 48	N[3]	Y (2)	-	-	N (1, 2, 3)	-	-	-
H2	24, 48	N	Y (2)	-	-	N (2)	-	N (2, 3, 4)	-
H3	48	Y	Y (2)	-	-	7% (2)	-	N (2,3)	-
H4	24, 72	Y	Y (2)	-	-	Y (2)	N (2)	N (3)	(3.4)[4]
H5	24	Y	-	-	-	Y (2)	N (2)[4]	N (6)[4]	(3.5)[4]
H6	24, 48	N	-	-	-	11.7% (4)[5]	N (2)[5]	N (4)[5]	-
H7	48	-	-	Y (2)	Y (2,4)	(2, 4)[4]	-	(2, 4)[4]	-
H8	48	N	-	-	Y (2)	N (2)	-	(2)[4]	(2)[4]

[1] H = HUVEC
[2] Indicates whether or not DsRed-IF was performed; [3] Y (Yes) or N (N0)
[4] Cells were lysed for RNA extraction
[5] Cells were lysed for protein extraction

ST2-FIA-DSRE2 (2-4 μg) was performed and analyzed at 24 and 48 hours (Trial H2, Table 4). Again, DSRE2 (2-4 μg) was performed and analyzed at 24 and 48 hours (Trial H2, Table 4). Again, GFP expression was observed; however there was no evidence of DSRE2 expression in any conditions. Despite analysis at two time points and different concentrations of DNA, positive DSRE2 cells were not observed. IF targeting DsRed was performed in all subsequent trials.

5.3.4 HUVEC: Positive DSRE2 expression following DsRed-IF but not under ST2 promoter conditions

DsRed-IF was performed to enhance any DSRE2 signal present in transfected cells. CHO-K1 cells were included in one trial to compare relative expression of GFP and DSRE2 expression to that in HUVEC. In trial H3 (Table 4), HUVEC and CHO-K1 cells were transfected with maxGFP™ (2 μg), DSRE2 (2 μg), and ST2-FIA-DSRE2 (2 & 3 μg) and DsRed-IF was performed at 48 hours. Positive GFP expression (~40.7%) was observed in both HUVEC and CHO cells. DSRE2 expression (~6.8%) were observed in HUVEC pIRES-DSRE2-transfection condition HUVEC, with less efficiency in CHO-K1 cells (~4.1%); however, DSRE2-positive cells were not observed following HUVEC transfection with ST2-FIA-DSRE2 (Figure 15). Trial H4 (Table 4) addressed a potential shortcoming from the previous trial; the possibility of cellular toxicity induced by the FIA construct. The ST2-DSRE2 construct was sub-cloned and included in Trial H4 along with the ST2-FIA construct (2 μg and 3 μg, respectively) and transfected cells were analyzed at 24 and 72 hours. Again, positive DSRE2 expression was not seen under control of the ST2, in absence of the FIA construct. Despite further trials (H5-H7, Table 4), with varying amounts of DNA

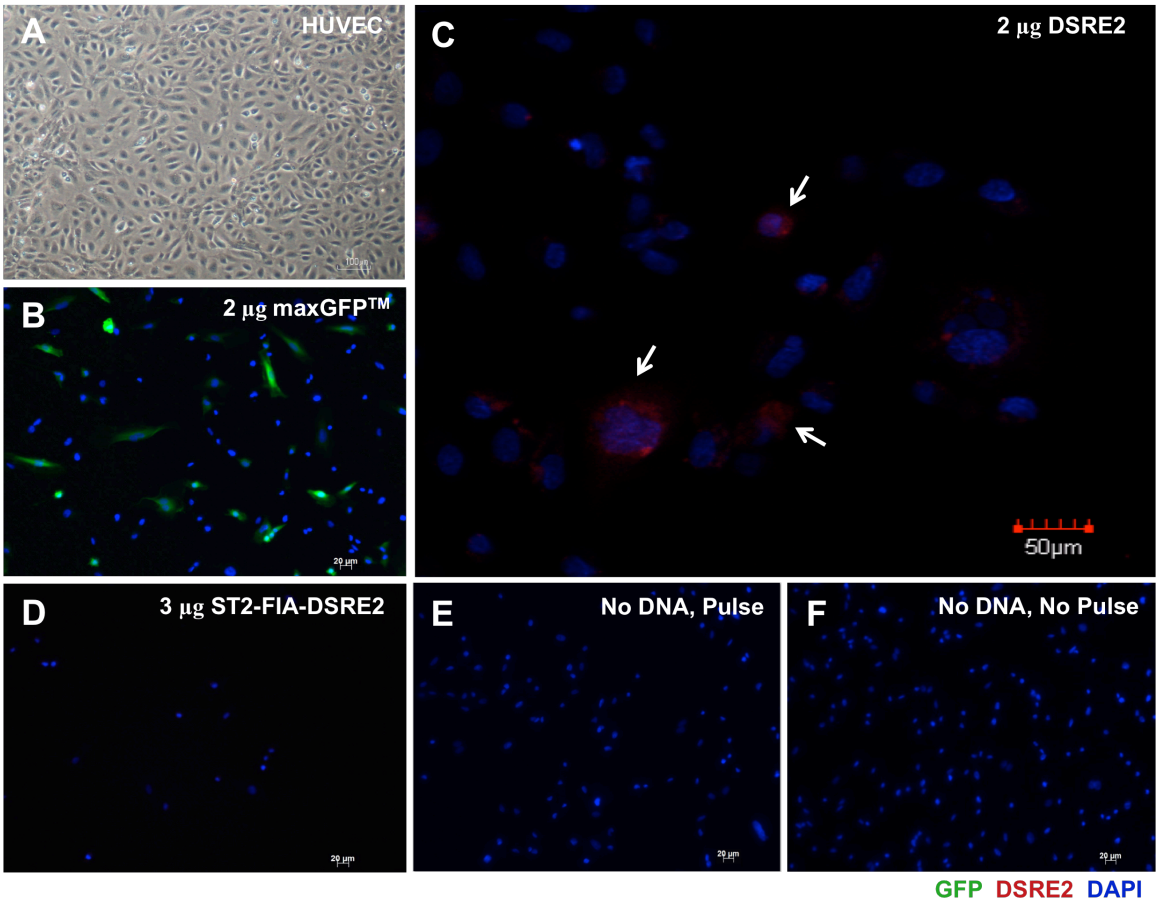

Figure 15. Electroporated HUVEC are positive for DSRE2 but not under control of the ST2 promoter. HUVEC were transfected followed by DsRed-IF (red) with DAPI nuclear counterstain (blue) at 48 hours. No IF was performed on positive transfection control **(B)** maxGFP™. **(C)** HUVEC were DSRE2-positive under control of the CMV promoter but not for **(D)** 3 µg ST2-FIA-DSRE2 or 2 & 4 µg (no shown). **(A)** Representative HUVEC before nucleofection. **(E)** No DNA + pulse and **(F)** no DNA, no pulse controls are shown. DNA mass/0.5M cells indicated in top right corner. Scale bar represents 20 µm, except for **(C)** 50 µm.

and DsRed-IF, DSRE2-positive cells were never observed following transfection with ST2 constructs and DSRE2 expression was consistently minimal (Figure 15).

5.3.5 HUVEC: Positive EGFP expression driven by ST2 promoter

ST2-EGFP was constructed to address promoter functionality and was tested in later transfection trials (H7, H8, Table 4). ST2-EGFP (2, 4 μg) expression was compared to that of pIRES-EGFP (2, 4 μg) and non-transfected cells at 48 hours. Transfected HUVEC were fixed and stained with DAPI nuclear stain. Positive EGFP expression was observed in ST2-EGFP conditions. These results confirm positive ST2 promoter function in HUVEC. ST2-EGFP transfected cells revealed stronger EGFP expression than pIRES-EGFP transfected HUVEC; however, efficiency remained low (Figure 16).

5.3.6 BAEC: DsRed-IF reveals DSRE2 expression, but not under control of ST2 promoter

The Quertermous group at Stanford originally used BAEC in the initial *in vitro* ST2 promoter study [112]. Given the low transfection efficiency of DSRE2 compared to GFP in HUVEC, transfection using BAEC was pursued. GFP expression was analyzed after 24 hours. Initially, a trial with pulse EH-100 (Trial B1, Table 5), that which was optimized for human aortic endothelial cells, was tested; however, little cells survived following transfection. Thus, nucleofection optimization with maxGFP™ (2 μg) was performed to find an optimal electroporation pulse. The number of GFP-positive cells/field was examined and pulse EH-100 resulted in the second highest BAEC transfection efficiency (~18.8%), but was observed to result in less cell death compared to pulse DY-138, that which had the highest observed transfection efficiency (~22%). Representative images of BAEC pulsed by

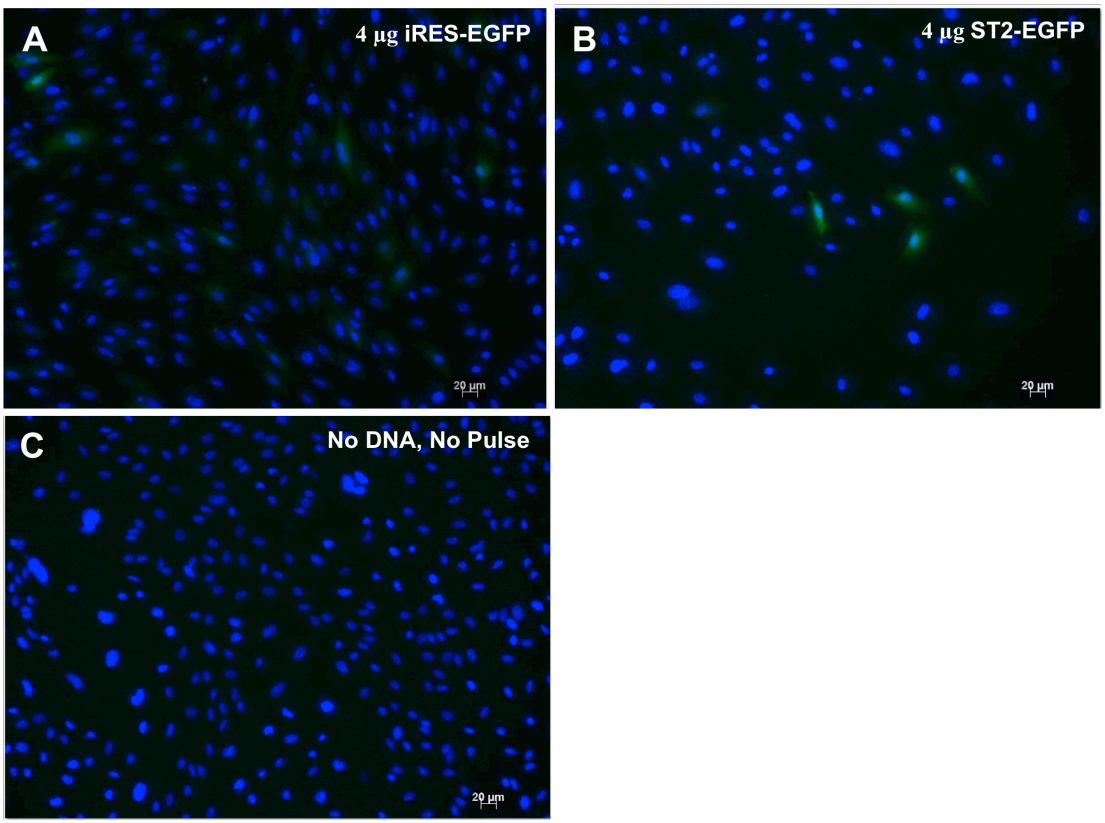

Figure 16. Electroporated HUVEC are positive for EGFP under control of ST2 promoter. HUVEC were transfected (Trial H7) and counterstained with DAPI (blue) at 48 hours. HUVEC were positive for **(A)** pIRES-EGFP and **(B)** ST2-EGFP. **(C)** No DNA, no pulse control is shown. DNA mass/0.5M cells indicated in top right corner. Scale bar represents 20 µm.

Table 5. Summary of BAEC and EOMA transfection trials and analyses

Trial[1]	Pulse	Analysis (hours)	Fluorescence or transfection efficiency (µg)							
			DsRed IF[2]	Max GFP™	pIRES-EGFP	ST2-EGFP	pIRES-DSRE2	ST2-DSRE2	ST2-FIA-DSRE2	ST2-FIA
B1	EH-100	24, 48	N	#	-	-	#	#	#	#
B2	EP-114	24, 48	Y	Y (2)	-	-	N (2)	N (2)	N (4)	-(3.5)
B3	CA-167	48	Y	Y (2)	-	-	3% (4)	-	N (4)	-
B4	CA-167	24, 48	Y	-	-	N (2)	N (2)	N (2)	N (2)	-
B5	CA-167	48	N	Y (2)	-	Y (2)	-	-	-(2)[4]	-(2)[4]
B6	CA-167	24, 48	N	-	N (2)	Y (2)	-	-	-(2)[5]	-(2)[5]
E1	EH-100	24, 48	Y	Y (2)	-	-	Y (1)	N (1)	N (1)	-

[1] B = BAEC; E = EOMA
[2] Indicates whether or not DsRed-IF was performed; [3] Y (Yes) or N (N0)
[4] Cells lysed for RNA extraction
[5] Viability too low for RNA extraction

EP-114, DY-138, CA-167, as well as FF-138, a condition with extremely poor cell viability, are shown in Figure 17. Pulse EP-114 was used in a subsequent BAEC nucleofection (Trial B2, Table 5). Nucleofection using pulse EP-114 was performed with maxGFP™ (2 μg), DSRE2 (2 μg), ST2-DSRE2 (2 μg), and ST2-FIA-DSRE2 (4 μg); however, cell viability following transfection was extremely low (Figure 18). In addition to low cell viability, BAECs displayed large variability within culture conditions recommended by the manufacturer. The no DNA, no pulse control transfection conditions displayed poor cell viability compared to that of HUVEC, following the same protocol. BAEC growth only reached 10-20% confluence at six days when seeded at maximum seeding density, 5000 cells/cm^2.

All subsequent BAEC transfections were conducted with pulse CA-167, which showed slightly lower transfection efficiency (13.0%), but better cell viability compared to pulse EP-114 as observed. BAEC were transfected with DSRE2 (2 μg) and ST2-FIA-DSRE2 (4 μg) and analyzed with DsRed-IF at 48 hours. Cell viability was improved in comparison to trial B2 and DSRE2 expression (3%) was observed (Trial B3, Table 5); however, again DSRE2 expression was not observed following transfection with ST2-FIA-DSRE2 (Figure 18). Trial B4 (Table 5) was carried out to investigate immunoblotting with anti-DsRed antibody; however, DSRE2-positive cells were not observed following DsRed-IF and thus, protein lysates were discarded. Trial B5 and B6 (Table 5) were performed for RT-qPCR assays with FIA-specific primers (not shown) with the addition of ST2-EGFP. Although low efficiency, EGFP-positive cells were observed in both trials (B5 & B6) at 48 hours (Figure 19). Transfected-BAEC in trial B6 had poor viability at 48 hours and thus, RNA extraction was not performed. Despite transfection optimization, DSRE2 transfection

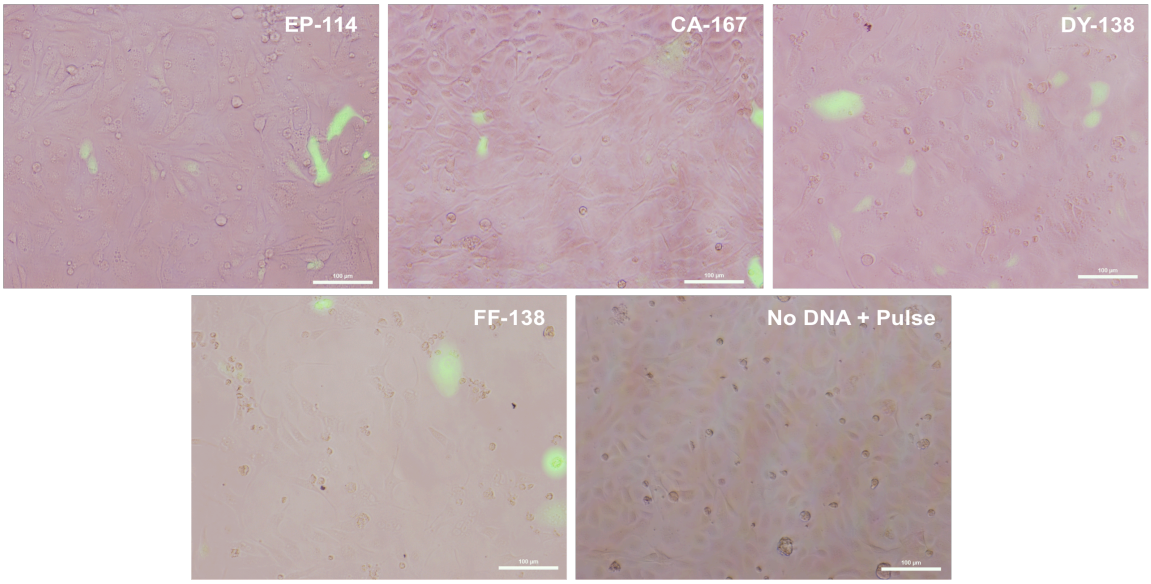

Figure 17. Representative Images of BAEC Nucleofection Optimization. BAEC were transfected with GFP (green) and imaged in media at 48 hours using fluorescent microscopy. Four of seven pulse conditions are shown; pulse name indicated in top right corner (n=1). Scale bar represents 100 um.

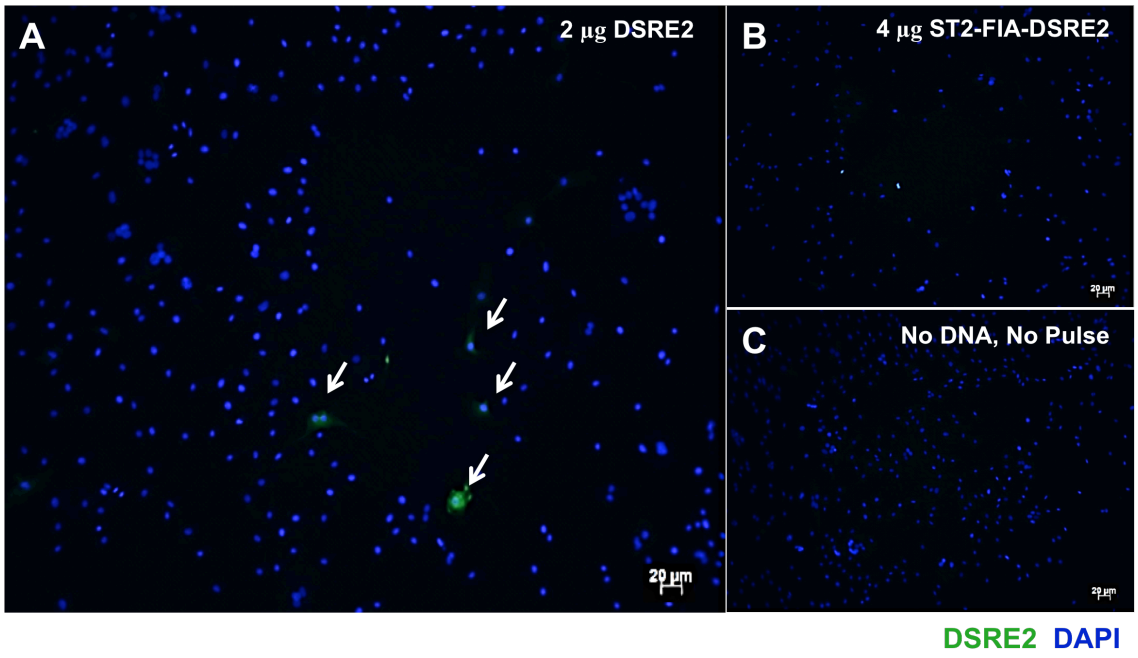

Figure 18. BAEC are positive for DSRE2. Anti-DsRed IF (green) on transfected BAEC with pulse CA-167 (Trial B6) was performed at 48 hours and counterstained with DAPI nuclear stain (blue). **(A)** Positive DSRE2 expression (arrows) in control plasmid condition but not in **(B)** SuperTie2-FIA-DsRedExpress2 condition. **(C)** No DNA, no pulse control is shown. DNA mass/0.5M cells indicated in top right corner. Scale bar represents 20 µm.

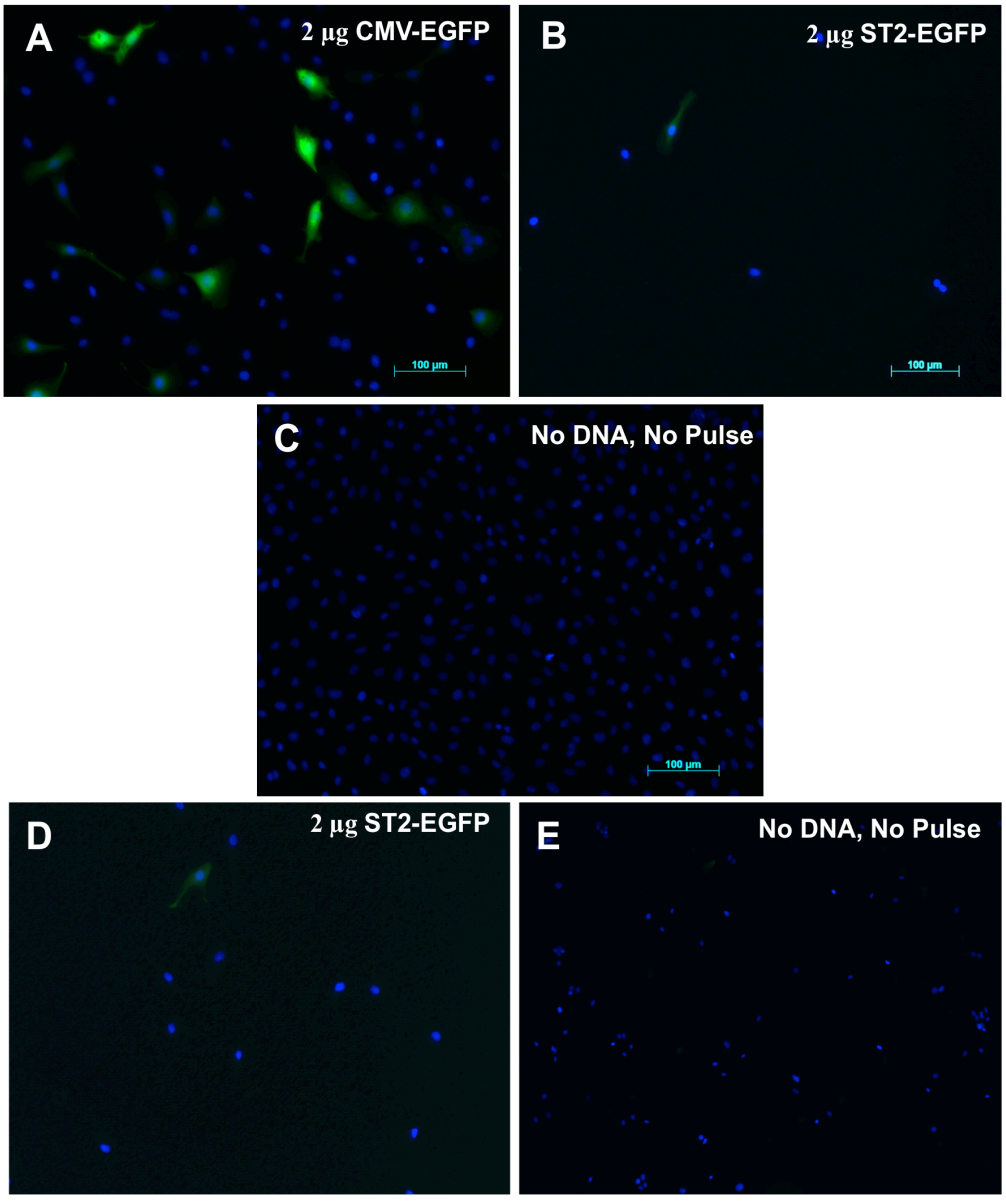

Figure 19. BAEC are positive for ST2-EGFP. BAEC were transfected (Trial B5, B6) with pulse CA-167 and counterstained with DAPI (blue) at 48 hours. In trial B5, BAEC were positive for **(A)** GFP in control condition and **(B)** EGFP in ST2-EGFP condition. **(C)** No DNA, no pulse control is shown. In trial B6, BAEC were positive for EGFP in **(D)** ST2-EGFP condition. **(E)** No DNA, no pulse control is shown. DNA mass/0.5M cells indicated in top right corner. Scale bar represents 100 µm.

efficiency was lower than that in HUVEC and BAEC viability deemed more sensitive to culturing conditions.

5.3.7 EOMA: DsRed-IF reveals DSRE2 expression, but not under control of ST2 promoter

Mouse EOMA cells, an endothelial cell line, were third in line for ST2-construct transfections. EOMA cells were pursued as an 'easier-to-transfect' cell line in comparison to the primary endothelial cells (HUVEC and BAEC). EOMA Nucleofection optimization was performed using maxGFP™ (2 μg) with three nucleofection solutions (SE, SF, & SG) and 11 different pulse programs. EOMA cells were analyzed at 24 and 48 hours. Very poor viability was observed in all pulse conditions with SE nucleofection solution. Interestingly, GFP transfection efficiency was much lower than any previous nucleofections with HUVEC, which reached up to 40%. Only pulse EH-100 in SG nucleofection solution, had fairly good transfection efficiency with good cell viability. Pulse EH-100 and SG nucleofection solution was used for one subsequent transfection experiment (Trial E1, Table 5). DSRE2-positive cells were not observed at 24 hours and low expression was seen with DsRed-IF at 48 hours. In coordinance with HUVEC and BAEC transfection, DSRE2 expression was not observed in any ST2-construct conditions, even when DsRed-IF was performed. Furthermore, GFP transfection efficiency was surprisingly low, with only two positive cells in a chosen field of view (Figure 20). Considering poor EOMA cell viability, low transfection efficiency with maxGFP™, and evidence that lab purified ST2 constructs affect cell viability even more so than GFP, further transfection experiments with EOMA cells were not performed.

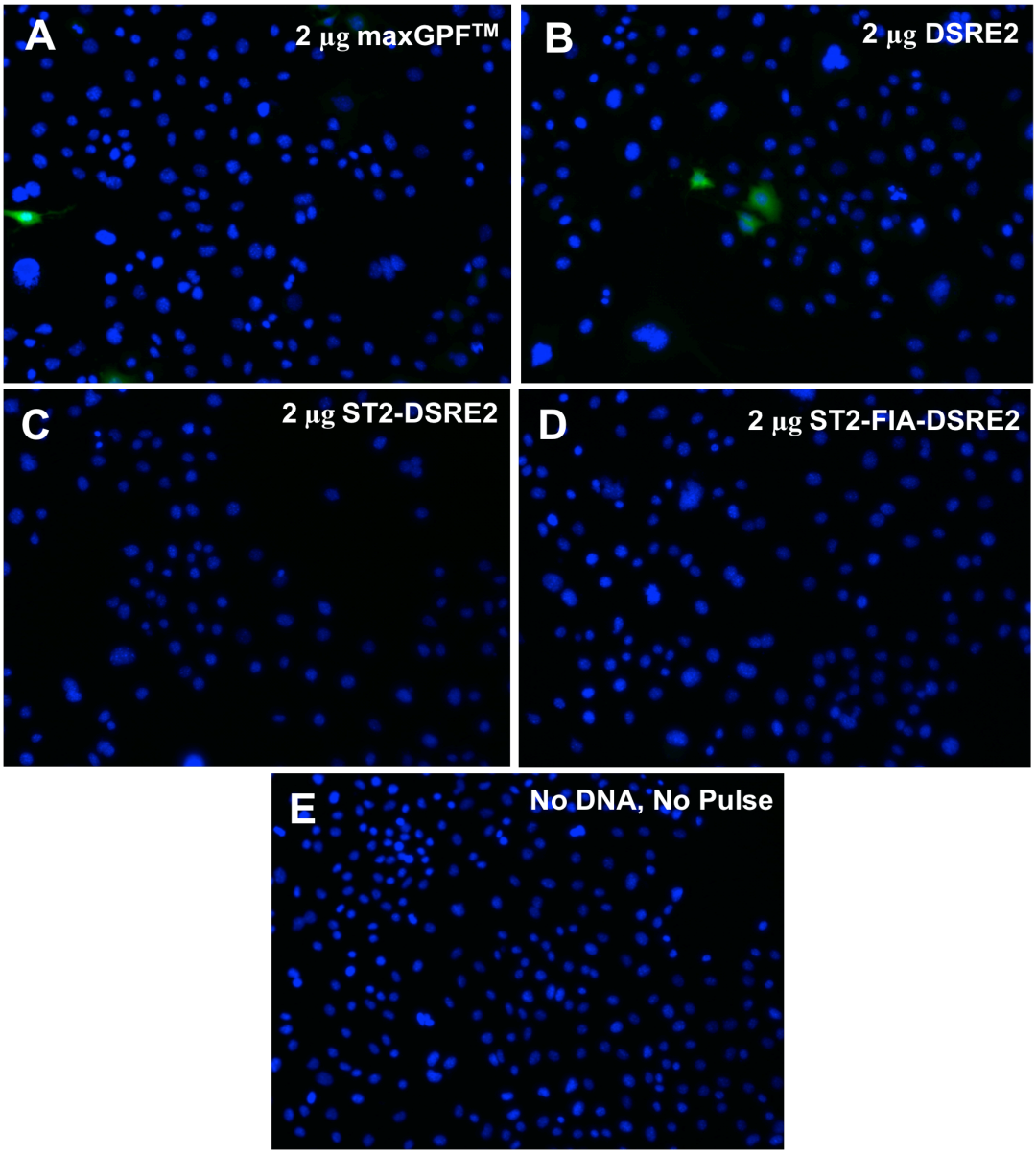

Figure 20. EOMA cells transfected with pulse EH-100. DsRed-IF (green) performed at 48 hours and counterstained with DAPI nuclear stain (blue). **(A)** GFP only stained with DAPI **(B)** EOMA cells had positive DSRE2 expression but no expression was seen in either **(C)** ST2-DSRE2 or **(D)** ST2-FIA-DSRE2 conditions **(E)** No DNA, no pulse control is shown. DNA mass/0.5M cells indicated in top right corner. Scale bar not shown.

6. General Discussion

Pulmonary arterial hypertension is a complex, lethal disease of multifactorial origin, characterized by vascular remodeling, particularly at the level of distal pulmonary arterioles. Although the pathogenesis of this lethal disease remains unclear, evidence, as outlined in section 1.2, has suggested that factors inducing vascular remodeling, such as the imbalance of vasoconstrictor/growth factor production, play an important role in the pathobiology underlying the development of PAH [6]. Despite modern day therapies targeting the imbalance between vasoconstrictors and vasodilators within the pulmonary vascular system, the mean life expectancy upon diagnosis remains at 3-5 years, and post-operative status remains poor following lung transplantation [47].

In consideration of the multifactorial origin of PAH, there are a number of areas of interest that could lead to a better understanding of the pathogenesis of PAH. The first is perivascular inflammation, which may provide insight into the role of inflammatory cascades in vascular remodeling including the initiation and development of the characteristic complex lesions [66]. The second area of interest includes downstream Smad-dependent and Smad-independent mechanistic pathways of BMPR2 mutations, which could provide insight into the mechanistic link between BMPR2 mutations and the pathophysiology of PAH [57]. The third area of interest and the focus of this thesis is the role of EC apoptosis in the structural changes associated with the development of PAH. The EC apoptosis hypothesis posits that initial damage to the endothelium results in programmed-cell death, which triggers reactive changes in vascular cell growth and survival that in turn produce the characteristic functional and pathological abnormalities of PAH. These include degeneration and “dropout” of the distal pulmonary arteriole as well as the

emergence of abnormal hyperproliferative and apoptotic-resistant vascular cells that are associated with complex intimal and plexiform lesions, ultimately leading to elevated PVR, increased PAP, and RHF (Figure 1).

6.1 Development of the endothelial fas-induced apoptosis (EFIA) transgenic model

As outlined in sections 1.3 and 1.5, many pathways including inflammation surrounding distal pulmonary vessels, BMPR2 signaling, and most importantly, EC apoptosis, contribute to the pathogenesis of PAH. Historically, EC dysfunction has served as the basis for the development of therapies used to treat PAH. Although EC dysfunction is apparent in PAH patients, EC apoptosis at the level of the distal pulmonary arteries could trigger and/or potentiate this process [6,15]. Our main aim is to target an apoptosis-inducing transgene to ECs to elucidate the central role of endothelial apoptosis in the development of PAH. Ideally, sustained expression of an endothelial-specific transgene can be accomplished using an endothelial-specific promoter.

Over-expressing a fas-induced apoptosis (FIA) construct was originally used to trigger death in T lymphocytes and macrophages *in vitro* and *in vivo*, respectively [104,113]. The FIA construct contains a membrane tethering region of the truncated low affinity nerve growth factor receptor, two mutant copies of the FK binding peptide (FKBP) dimerization domain, and a truncated cytoplasmic fas domain. Fas is a member of the tumor necrosis factor (TNF) receptor superfamily and dimerization of fas leads to the recruitment of a fas activating death domain (FADD), activating a caspase cascade that induces apoptosis [113]. The fas-induced apoptosis system was designed to respond to a synthetic dimerizing agent, AP 20187, with specificity for the engineered or mutated FKBP instead of the endogenous form. In the first studies using the fas-based suicide system, introduction of the FIA

construct with the use of a retroviral vector into T lymphocytes resulted in a dose-dependent depletion of T lymphocytes [113]. *In vivo* studies performed by Burnet *et al* demonstrated up to 94% macrophage depletion in macrophage-specific fas-inducing apoptosis mice following administration of 10 mg/kg AP20187 for five consecutive days [104]. Under the hypothesis that endothelial-specific apoptosis is a significant contributor in the pathogenic process of PAH, our lab incorporated this FIA construct into a plasmid vector containing an endothelial-specific Tie-2 promoter and developed endothelial-specific apoptosis-inducing (EFIA) Tg mice.

6.2 Lessons from preliminary data

The results presented in Chapter I represent preliminary data on the development of an endothelial-specific apoptosis-inducing (EFIA) Tg mouse model. Preliminary characterization of E6711 Tg mice at 8 weeks of age demonstrated a dose response to AP; however, despite significant (albeit modest) changes in RVSP and RVH, the phenotype of this transgenic line was eventually lost. The original EFIA mice were outbred with CD1 wild-type mice, which may have introduced genetic drift over generations of outbreeding. Interestingly, preliminary data demonstrated proliferative lesions in a subset of these mice (Section 3, Figure 4). Although levels of EC apoptosis were not assessed in the preliminary E6711 experiments, the lesions presented are inflammatory in nature and could demonstrate a response to apoptosis at the level of the distal arterioles. This could be supported by the pathological model of "angioproliferative' lesions as described in section 1.5.2 whereby endothelial apoptosis may lead to the selection of apoptosis-resistant ECs. However, only a small subset of EFIA Tg mice exhibited proliferative lesions in the peripheral lung. Since the

PAH phenotype was lost after several breeding generations, the quantity of endothelial apoptosis may not be sufficient to induce vascular remodeling.

The three established EFIA transgenic lines, E6780, E6711, and E6712 consistently demonstrated lung EFIA expression at the mRNA level, with E6712 having the lowest relative EFIA mRNA levels (Figure 5). We re-assessed the E6711 and E6780 Tg mice at 12 weeks following transgene inductions for 1 week with 2 mg/kg of AP. This protocol had previously demonstrated a hemodynamic response in 8 week old E6711 Tg mice, as well as a slight elevation in RV/LV + S ratio. With reference to the results from the preliminary study in 8-week-old E6711 Tg mice (Figure 4), the 2 mg/kg dose was chosen over the 10 mg/kg dose based on the hypothesis that the lower dose may exacerbate the hemodynamic response in the aged Tg mice. Upon reassessment of E6711 and E6780, RVSP and RVH remained relatively normal in comparison to WT controls (Figure 4 & 6). E6780 (HE-EFIA) Tg mice exhibited higher levels of EFIA mRNA in comparison to E6711 (LE-EFIA) and E6712 Tg mice (Figure 5). However, even with lower levels of EFIA mRNA, E6711 Tg mice demonstrated a greater hemodynamic response, leading towards the development of PAH. The same observation was found in the analyses of RV/LV +S data, indicative of RVH (Figure 6).

Considering the elevated EFIA mRNA expression in HE-EFIA, relative apoptosis levels were examined in paraffin-embedded lung tissue. Quantification of stained cells was performed and apoptotic indices were calculated for TUNEL-positive cells and activated-caspase 3 cells. The sensitivity of the cleaved-caspase 3 assay exceeded that of the TUNEL assay, which has been previously reported [106]. Both assays demonstrated a trend towards increased levels in apoptosis in HE-EFIA compared to WT, although HE-EFIA treated with the dimerizing compound did not display increased levels of apoptosis compared to baseline.

At baseline, a modest increase in apoptosis levels in EFIA lung tissue compared to WT could be attributed to self-dimerization of the FIA construct within the EFIA transgene. It has been reported that fas can induce apoptosis in absence of the dimerizing agent or transgene inducer [113]. This self-dimerization could be attributed to self-association of the death domain. Based on the levels of apoptosis in the peripheral lung of HE-EFIA mice, higher levels of apoptosis are necessary to induce changes in pulmonary hemodynamics.

6.3 Insight into the variable phenotype presented in the EFIA Model

6.3.1 Transgene expression

There are several promoters that have been used to drive EC-specific expression in transgenic mice: the human von Willebrand factor (vWF) promoter, the murine endothelin-1 promoter, and the murine tyrosine kinase promoters, Tie1 and Tie2/Tek. Despite expression in ECs, the murine endothelin-1 promoter is also expressed in epithelial cells, and thus is an undesirable candidate for targeted endothelial apoptosis. The vWF promoter targets ECs in embryological development as well as in the adult brain [112]. Additionally, vWF displays heterogeneous expression between different pulmonary blood vessels, with less expression in the distal arterioles and capillaries; however, in PAH, this vessel-type specific expression is not observed [114].

Ultimately, the Tie1 and Tie2/Tek promoters are the best candidates for endothelial-specific expression for the purpose of our study, as expression is seen in a large portion of the endothelium throughout all stages of development. The Fadel group demonstrated that Tie2 promoter constructs transfected *in vitro* revealed EC-specific expression. An upstream fragment of 2.3 Kb in the Tie2 gene was shown to be EC–specific *in vitro* and also exhibited

endothelial-specific gene expression in transgenic mice. [112] Specifically, the upstream enhancer region was required for endothelial-specific expression of the LacZ gene in transgenic mice [115]. Other groups have demonstrated that the Tie2 promoter contains the appropriate transcriptional regulatory elements to drive endothelial-specific expression [108,116]. The endothelial-specific Tie2 promoter is one of the most important factors regulating transgene expression in this study and the Tie2 promoter deemed sufficient during preliminary experiments using the Tie2-FIA construct.

As presented above, EFIA mRNA levels in the E6780 line were relatively high in comparison to the E6711 and E6712 Tg lines; however, in my study, we did not see a significant RVSP response in any of these mice. The Tie2 promoter has proven to be functional in other studies, and thus, the variable phenotype observed between the EFIA lines is not clear. Transgenes are randomly inserted into the murine genome and transgene expression will depend on site-specific location, which includes other sequences surrounding the insertion site. The transgene must first be successfully transcribed into its corresponding mRNA and subsequently translated into functional protein. The same transgene inserted into two different sites could exhibit two different levels of functionality. Additionally, the expression level of a transgene is often a factor of its copy number and increased gene dosage leads to higher levels of gene product [117]. This factor could explain why the E6780 line exhibits a higher EFIA mRNA expression level than the E6711 or E6712 lines. E6780 mice may have a higher EFIA transcript level; however, the number of copies integrated in to the genome may be less than that of the E6711 mice, which are more sensitive to the AP compound.

Furthermore, ECs may develop mechanisms to avoid apoptosis, which is also a mechanism hypothesized to be involved in the development of plexiform or complex lesions

associated with IPAH [118]. This could have been a factor in the E6780 line, which demonstrated less sensitivity to the AP compound. Other genetic traits that could be involved include the outbred CD1 wild-type mice leading to increased heterogeneity within the EFIA transgenic lines.

6.3.2 The Multiple-Hit Hypothesis and PAH

Although PAH can be a monogenetic disease in the case of mutations in the *Bmpr2* gene, even then it exhibits variable penetrance and only ~20% of mutation carriers will develop clinical disease [53]. This suggests that the Bmpr2 mutation alone is insufficient to cause disease and other genetic or environmental influences are needed. Loss-of-function genetic mutations in *BMPR2* (and possibly *ALK-1,* a type 1 BMP receptor) can predispose to EC apoptosis [6,81]. EC apoptosis could lead directly to degeneration of the fragile precapillary arterioles that consist of endothelial tubes supported by thin matrix and basement membrane. Thus, loss of the endothelium at this level could result in drop out of distal lung arterioles compromising the normal low-pressure pulmonary circulation. As well, it has been reported that EC apoptosis is a trigger for subsequent reactive changes in the lung vasculature, such as the emergence of hyperproliferative ECs leading to vascular remodeling and the formation of obliterate lesions as described earlier in section 1.5.2 [77].

Additional endogenous and/or environmental triggers may be necessary to potentiate vascular changes in PAH. More specifically, inflammation is a widely recognized factor involved in the pathogenesis of both IPAH and APAH. PAH patients exhibit perivascular inflammation by which inflammatory cells surround the pulmonary vasculature. IPAH and APAH patients also demonstrate elevated circulating levels and pulmonary expression of IL-6 along with other pro-inflammatory cytokines and chemokines [119]. Furthermore,

evidence from Tg mice overexpressing IL-6 demonstrated spontaneous vascular remodeling and a PAH-phenotype (up to 60 mmHg RVSP) [102]. Ultimately, within the complexity of PAH, multiple triggers at both the genetic and environmental levels likely produce additive effects on the vascular changes involved in the full pathogenic process of PAH.

6.3.3 Possible phenotype modifying influences in the EFIA model

There are a number of factors that could influence the PAH phenotype in the EFIA model. In the previous sections, I discussed the potential role of varying levels of gene expression between transgenic lines, and even within a given line, since the transgene promoter activity can be gradually silenced over progressive generation [120]. Moreover, this transgenic model was established in the CD1 background, which is outbred and thus there may be slight differences in genetic modifiers between individual mice that could have a profound influence on the phenotype. Genetic modifiers could influence phenotype at a number of levels, including the susceptibility to EC apoptosis as well as the response of the neighboring vascular cells and the innate immune system to this EC injury and loss. As discussed previously, reactive vascular proliferation and inflammation are thought to be critical mechanisms in the pathogenesis of this disease.

Additionally, environmental factors could be playing an important role. Small changes that introduce an additional stress may have a large effect. For example, even minute contamination or undetected infection could prime the immune system and alter the response of subtle stimulus such as low grade EC apoptosis. Indeed, my study may shed light on a fundamental unanswered question in the PAH field; namely, why a mutation in the BMPR2 gene, which is ubiquitously expressed in all cells and tissues of the body, results in such a specific abnormality that is largely limited to small arteries only in the lung. The

answer may lie in unique characteristics of the lung, which like the skin and the gut, is exposed directly to the outside environment through the airways and is thus a first line of defense upon exposure to the environment. Additionally, the fragile distal pulmonary arteriolar bed lacks smooth muscle cells characteristic of similar sized systemic arterioles. The lack of supporting cells may not only make the pulmonary arteriolar endothelial lining more susceptible to injury, but may also make it more likely that EC apoptosis at this level could lead to structural and functional microvascular abnormalities.

Furthermore, by its exposure to the external environment, the lung contains a highly developed innate immune system, which may contribute to the destruction of microvasculature in PAH and exacerbate EC apoptosis. Again, considering the need for "multiple-hits" as outlined in the previous section, the innate immune system likely needs triggering for the full pathogenic process of PAH to occur. Endothelial apoptosis could activate the innate immune system, exacerbating vascular remodeling and distal arteriole dropout, leading to more robust hemodynamic changes. As mentioned in section 1.5.1, upregulation of inflammatory cytokines such as IL-6 and MCP-1 is common in patients with IPAH as well as perivascular inflammation, which has also been observed in animal models such as Tg mice over-expressing a deletional *BMPR2* mutant allele [69].

6.4 Additional strategies to induce endothelial-specific apoptosis

In light of the issues presented above, a number of areas need to be addressed. One of the most promising strategies to overcome the limitations described in the previous sections is to produce a more robust phenotype in the EFIA Tg mouse model. This involves incorporating a 'stronger' endothelial-specific promoter into the construct to enhance the expression of FIA within ECs containing the EFIA transgene. The first generation of EFIA

mice were generated using a Tie2 promoter system that did not contain the Tie2 intron, or enhancer region, as described in section 6.3.1. Schlaeger *et al* has demonstrated that a 1.7 kb internal fragment of the Tie2 intron contains cis-acting sequences that are essential for *in vivo* expression. The same group demonstrated that 1.7 kb fragment was necessary and sufficient to enhance Tie2 expression in BAECS. Further findings by the same group demonstrated that the 1.7 Kb fragment enhanced EC-specific transcription independently of its position and orientation [116]. The following section introduces a new strategy using the Tie-2 promoter with the enhancer region, namely the SuperTie2 (ST2) promoter.

To address the outbred CD1 limitation, it might be necessary to backcross an EFIA transgenic line into an inbred strain, such as C57blJ. This may introduce a larger level of homogeneity between EFIA mice in regards to genetic modifiers, which could generate a more robust phenotype. Furthermore, the issue with innate immunity in the lung could be addressed through co-administration with IL-6, which may potentiate endothelial-apoptosis and the subsequent vascular changes obstructing the pulmonary circulation. As mentioned earlier, patients with IPAH have consistently higher serum and lung levels of IL-6 and evidence from IL-6 over-expressing Tg mice has also shown that IL-6-induced inflammation is associated with vascular remodeling [102,119]. Thus, co-administration of IL-6 and the AP compound could potentiate vascular remodeling in EFIA Tg mice and exacerbate the development of PAH

6.5 Incorporating a stronger Tie2 promoter

As mentioned above, the initial strategy pursued to generate a more robust EFIA phenotype was based on an optimized, ST2 promoter, designed by the Quetermous group at Stanford. The “ST2” promoter consists of a fragment of the 2.1 kb Tie-2 promoter along

with a 1.7 kb portion of an enhancer element from the first intron of the Tie2 gene. The Quetermous group identified that the enhancer element was an absolute requirement for robust expression in the endothelium of adult mice [107].

6.5.1 Optimizing SuperTie2 Transfection

The function of the ST2 promoter must be validated *in vitro* via EC transfection with optimal post-transfection cell viability and efficiency. Optimal transfection efficiency is determined by many factors including cell type, cell confluence, cell passage, vector size and purity, promoters, and the transfection protocol. In addition to these factors ECs in particular are known for their hard-to-transfect nature and poor transfection efficiency.

The ability to transfect ECs with high efficiency is essential for the ability to test the functionality of the newly constructed EFIA vector *in vitro*. A number of strategies have been pursued to achieve high transfection efficiencies in primary ECs. Standard nonviral techniques using cationic phosphate, cationic liposome or DEAE-dextran do not produce transfection efficiencies higher than 30% in ECs. Primary ECs are susceptible to toxic effects of transfection reagents and thus, the best transfection strategy encompasses high efficiency and low cytotoxicity to maintain sufficient cell viability for subsequent *in vitro* assays. Lipofectamine LTX, a chemical transfection reagant, has been shown produce transfection efficiencies up to 30% in HUVEC at shorter periods of time (24 hours versus 48 hours) [121]. HUVEC, like most primary ECs have a slow proliferation rate and a short lifespan, usually no more than 10-12 passages *in vitro*. As such, HUVEC behave more like *in vivo* cells than immortalized cells and can serve as an *in vitro* surrogate for studying ECs that line vasculature. In view of the issues presented above, nucleofection, a new electroporation technology, is promising as it can result in transfection efficiencies up to

50% in primary cells including primary ECs [110]. Using an optimized electroporation condition and a proprietary buffer, the nucleofection technology reduces the amount of time cells spent in transfection reagent. Cells are stabilized in a buffer, allowing an electrotransfer of vector or plasmid into nuclei.

In my study, HUVEC, BAEC, and EOMA cells were used for transfection via electroporation with Amaxa's 4D-Nucleofector™. BAEC were selected based on their use in initial studies with the ST2 promoter and the EOMA cell line was selected for their better resistance to cell death compared to primary ECs (HUVEC and BAEC); however, following transfection in both EOMA cells and BAEC, both viability and transfection efficiency were worse in comparison to HUVEC. HUVEC usually had better cell viability before transfection, which likely contributed and thus, HUVEC were chosen for subsequent transfections to validate the new ST2 constructs. Despite following the manufacturer protocols, BAECs and EOMA cells both displayed poor cell viability and growth during culturing conditions. These limitations likely contributed to the deleterious effect of transfection on survival in these cell lines, considering that electroporation can induce greater than 50% cell death even under optimal conditions [110]. We expected that both BAEC and HUVEC would reach 90% confluence around 3 days when seeded at 5000 cells/cm^2; however in our reported culture conditions, BAEC exhibited growth arrest after 2-3 days, at no more than 50% confluence.

Throughout EC transfections, both DNA quality and quantity was considered to ensure the best transfection conditions. Plasmids were purified using an endotoxin-free procedure. Reduced cell viability in EOMA cells and BAEC appeared to be a result of DNA toxicity and not a result of the electroporation (Figure 15). Transfections were performed

using either 2 ug or 4 ug of plasmid DNA based on the Amaxa™ primary cell optimization protocol.

Overall, despite the previous use of BAEC in initial ST2 studies and the use of an EC line that is purportedly "easy" to culture, cell viability and observed transfection efficiency remained higher in HUVEC compared to BAEC and EOMA cells. Ideally, transfection efficiency would have been at least 30% to perform subsequent functional assays. Low cell viability preceding transfection and DNA toxicity contributed to low transfection efficiencies and low cell viability following transfection.

6.5.2 DSRE2 reporter gene and sub-optimal protein expression

DSRE2 was chosen as a convenient fluorescent marker of transgene expression since, in addition to providing the potential of detection based on its emission spectrum, there is a DsRed-specific antibody that can be used in the case that detection of the fluorescent signal is too low. DSRE2 also has low cytotoxic properties [109]. Selecting an antibody for detection of the FIA gene becomes difficult considering portions of the FIA gene are similar to the endogenous FADD protein and FK binding peptide. The manufacturers of DSRE2 state that DSRE2 should facilitate both strong and stable fluorescence when used in the production of Tg animals [109]. Additionally, DSRE2 protein can take up to 48 hours to be expressed and thus, transfection analyses were performed at 24 and 48 hours, with one trial analyzed at 72 hours (Trial H4, Table 4) [109]. Initial ST2-validation nucleofections revealed that DSRE2 under control of the CMV promoter could not be detected without the use of a DsRed antibody. Despite using a CMV plasmid, DSRE2 expression was never visualized by its direct emissions in transfected cells when immunofluorescence was not performed. The DSRE2 plasmid contains an IRES2 site, which

can affect the magnitude of translation. [122] As described in section 5.2.1, the IRES2-DSRE2 fragment was inserted into the ST2 construct following the Tie2 promoter and FIA gene. Thus, the IRES2 initiates translation of the second gene, DSRE2. IRES sites normally translate proteins at a lesser efficiency, which could explain low DSRE2 expression observed following electroporation. However, when transfecting HUVEC with pIRES-EGFP driven by the CMV promoter, GFP was indeed visualized (Figure 16) and thus, the IRES site is likely not the only factor contributing to the expression of DSRE2. ST2-transfection studies presented in chapter II were not consistent with reports on minimal DSRE2 cytotoxicity in mammalian cells and increased brightness in comparison to other red fluorescent proteins [123]. Transfections with CMV-DSRE2 induced some cellular toxicity but to a lesser extent than that of ST2-DSRE2 and ST2-FIA-DSRE2, which are larger constructs at 8.5 Kb and 10.5 Kb, respectively. Plasmid size can also have a large impact on expression of transfected genes and thus, it is likely that these relatively large plasmids may have also limited the expression of both DSRE2 and FIA proteins.

Strack *et al* reports the relative brightness of DSRE2, calculated as the product of the quantum yield and extinction coefficient, to be 14,952 [109]. Although the properties of the tetrameric DSRE2 fluorescent protein include reduced cytotoxicity in comparison to wild-type DsRed, the brightness of DsRed is significantly higher at 36,565 and DSRE2 appears to function poorly compared to EGFP[109]. The limitation of low DSRE2 brightness was eliminated with the use of IF.

As mentioned above, a significant factor involved in the expression of DSRE2 is the pIRES2 site preceding the DSRE2 encoding region. IRES2 from the encephalomyocarditic virus (EMVC) allows for cap-independent translation of DSRE2 using an internal start site, resulting in bicistronic expression of our gene of interest and DSRE2. Protein expression

from IRES sites cannot be predicted and the cellular environment and nature of IRES are believed to play a role in the strength of internal translational initiation [122]. Based on evidence from the work present in chapter II, we can conclude that indeed, the IRES had a significant effect on the translation and/or expression of DSRE2 following transfection with CMV-DSRE2, ST2-DSRE2, and ST2-FIA-DSRE2. Firstly, the CMV promoter drives both maxGFP™ and DSRE2; however, DSRE2 contains an IRES. Thus, maxGFP™ expression is much brighter and transfection efficiency is higher in HUVEC (Figure 15). Although both maxGFP™ and IRES-EGFP are driven by the CMV promoter, IRES-EGFP expression is less bright in HUVEC (Figure 15 & 16). Additionally, transfection with a plasmid expressing EGFP under the direct control of the ST2 promoter resulted in a much brighter fluorescence than when HUVECs were transfected with the IRES-EGFP construct, despite the use of the ST2 promoter in both (Figure 16). Indeed, DSRE2 expression with IRES under control of the ST2 promoter could not be visualized without the use of a DsRed-specific antibody whereas ST2-EGFP was clearly visualized under fluorescent light. Thus, IRES is likely an important factor responsible for the lack of robust DSRE2 expression under control of the ST2 promoter. An additional factor contributing low expression of DSRE2 following transfection with the ST2-FIA-DSRE2 construct could be spontaneous cell death via self-dimerization of the FIA construct or self-association of the death domain; however transfection with ST2-DSRE2 resulted in similar cell viability as visualized [113].

Relatively good viability and high transfection efficiency are required in order to perform subsequent RT-qPCR, western, or flow cytometry analyses. Based on the results presented here, cell viability was consistently low in HUVEC, BAEC, and EOMA cells following nucleofection and thus, not optimal to perform functional analyses following transfection.

6.5.3 Transfecting primary endothelial cells: difficulties and shortcomings

As previously stated, primary cells are more susceptible to toxic agents than immortalized cell lines, which makes transfection difficult. Specifically, ECs are in direct contact with blood and thus, act as a barrier, but also control the passage of cells and other materials between blood and surrounding tissues or blood from air as in the lungs [124]. Essentially, this function of controlled trafficking in and out of the bloodstream could explain why primary ECs and EC lines such as endothelioma cells are hard to transfect [125]. Generally, endothelial trafficking is maintained by membrane-bound receptors specific for numerous macromolecules including proteins, hormones, metabolites, and lipid-transporting molecules. Thus, the endothelial membrane has restricted passageways making transfection of ECs difficult.

Again, on the level of plasmid transfection, nucleofection has proven to be a promising method for transfection of primary ECs [110,111]. Nucleofection was pursued in light of the concerns mentioned above and in section 6.5.1. Although good cell viability with positive GFP expression was consistently observed after transfection with Lonza's maxGFP™ plasmid, cell viability remained low when electroporation was performed with the larger plasmids such as ST2-FIA (9.1 Kb), ST2-DSRE2 (8.5 Kb), and ST2-FIA-DSRE2 (10.5 Kb).

Cell viability and transfection efficiency are the most important for post-transfection analyses and thus, in light of the results presented here, alternative transfection strategies are required. As previously mentioned, plasmid based transfection system do offer certain advantages, but the magnitude of expression is generally lower with plasmids than that with viral vectors. Adenoviral vectors are commonly used for transient transfections and result in

less cytotoxicity compared to plasmid DNA. Thus, successful EC transfection may ultimately require the use of viral vectors. Furthermore, viral vectors can also be used as a means to introduce endothelial-specific transgenes *in vivo* [125] and could serve as a basis to generate EFIA mice.

6.5.4 Summary: *In vitro* ST2 validation

The establishment of an endothelial-specific model for induction of apoptosis remains an important goal to investigate the role of apoptosis in the pathogenesis of PAH. Overall, DSRE2 deemed to be a poor reporter gene in that positive DSRE2 expression was never observed under fluorescent microscopy in both BAEC and HUVEC transfected with ST2-FIA-DSRE2 and ST2-DSRE2. Considering all necessary conditions for optimal transfection in primary cells, transfection of ECs, especially with an endothelial-specific promoter should not be performed in the presence of IRES. Relatively good viability and high transfection efficiency are required to perform subsequent functional assays. Furthermore, an alternative method, such as the use of an adenoviral vector, could enhance transfection efficiency in ECs for the purpose of validating a vector or plasmid that will be used for in vivo gene transfer or microinjection to produce a transgenic model.

6.6 Conclusion

Over-expression of the FIA construct targeted to ECs resulted in several intriguing observations relating to EC apoptosis in the development of a PAH phenotype. These include modest increases in RVSP and RVH in the original founder lines as well as the development of striking lung lesions localized to the distal arterioles (section 3.1). In many instances there was evidence that these lesions were obliterate, resulting occlusion of the vascular lumen. Unfortunately, this PAH phenotype was inconsistent in the E6711 & E6780

Tg mice, and despite our best attempts to characterize the independent transgenic lines and control for the possible factors, which could account for the loss of this phenotype over time, we have not been successful. For this reason, my thesis was largely focused on developing a more robust transgenic model with better induction of the EFIA transgene and in vivo expression and activity.

Much of the work described in this thesis relates to my attempts to design a new EFIA construct that could be used to establish 'second generation' EFIA mice. This work will build on our preliminary data from the 'first generation' EFIA transgenic model to establish the central role of lung EC apoptosis in initiating the structural and hemodynamic abnormalities of PAH. Ultimately, a strategy to induce robust endothelial apoptosis or endothelial specific cell death *in vivo,* will not only provide a unique animal model to better understand the pathogenesis of this devastating disease, but may also lead to novel treatment strategies designed to reduce EC loss or promote vascular repair.

6.7 Future Directions

Establishing an endothelial-specific apoptosis inducing system *in vivo* may require a more detailed approach to investigate the role of EC apoptosis in the development of PAH. Animal models have revealed that a single factor such as a genetic mutation may not be sufficient to reproduce the complete pathogenic process of PAH. Multiple-hits as outlined in section 6.3.2 are likely required. This could involve backcrossing to a susceptible background, co-administration of IL-6 or the incorporation of a stronger promoter to drive expression of the FIA protein.

Considering both the *in vivo* and *in vitro* EFIA results presented in this thesis, the endothelial-specific Tie2 promoter may ultimately be too weak to over-express FIA in ECs

at a level high enough to induce pathological changes in the pulmonary vasculature of Tg mice. A couple major modifications concerning promoter strength and transgenic mice could address the issues presented in the approach to induce increased levels of apoptosis in the lung. Mouse models display a relative resistance to the development of PAH in comparison to rat models (section 1.6.2). Thus, targeting rats rather than mice could be beneficial when developing a rodent model of PAH; however, the development of transgenic rats is expensive and cumbersome so alternative strategies could be considered.

Recently, studies have demonstrated successful, lung endothelia-targeted gene transfer *in vivo* using the JetPEI reagent, a cationic polymer manufactured by Polyplus, which localizes almost exclusively to lung tissue. In comparison to other tissues, Gao et al demonstrated up to a 10-fold increase in lung-localization of transfected siRNA using *in vivo* JetPEI [126]. The same group reported that retroviral infection results in limited autotoxicity in both cell lines and T lymphocytes and suggested that extreme levels of autotoxicity can occur in the case of transient transfections in which FAS expression levels are extremely high. The EFIA construct presented in chapter I could be subcloned for *in vivo* gene transfer with the use of *in vivo* JetPEI and the FIA construct under control of a strong ubiquitous promoter, such as CMV, since the transfection strategy may provide selective endothelial targeting.

Ultimately, a successful rodent model of PAH will provide valuable insight into the many pathways involved in the pathogenesis of PAH. The use of a novel animal model will help us investigate interactions between triggers, define new hypotheses, and allow us to develop new strategies to inhibit the development of PAH and/or reverse established PAH.

References

1. Rich, S., Dantzker, D.R., Ayres, S.M., Bergofsky, E.H., Brundage, B.H., Detre, K.M., Fishman, A.P., Goldring, R.M., Groves, B.M., Koerner, S.K., and et al. (1987). Primary pulmonary hypertension. A national prospective study. Ann Intern Med *107*, 216-223.
2. Lane, K.B., Machado, R.D., Pauciulo, M.W., Thomson, J.R., Phillips, J.A., 3rd, Loyd, J.E., Nichols, W.C., and Trembath, R.C. (2000). Heterozygous germline mutations in BMPR2, encoding a TGF-beta receptor, cause familial primary pulmonary hypertension. Nat Genet *26*, 81-84.
3. Cogan, J.D., Pauciulo, M.W., Batchman, A.P., Prince, M.A., Robbins, I.M., Hedges, L.K., Stanton, K.C., Wheeler, L.A., Phillips, J.A., 3rd, Loyd, J.E., and Nichols, W.C. (2006). High frequency of BMPR2 exonic deletions/duplications in familial pulmonary arterial hypertension. Am J Respir Crit Care Med *174*, 590-598.
4. Simonneau, G., Robbins, I.M., Beghetti, M., Channick, R.N., Delcroix, M., Denton, C.P., Elliott, C.G., Gaine, S.P., Gladwin, M.T., Jing, Z.C., Krowka, M.J., Langleben, D., Nakanishi, N., and Souza, R. (2009). Updated clinical classification of pulmonary hypertension. J Am Coll Cardiol *54*, S43-54.
5. Thomson, J.R., Machado, R.D., Pauciulo, M.W., Morgan, N.V., Humbert, M., Elliott, G.C., Ward, K., Yacoub, M., Mikhail, G., Rogers, P., Newman, J., Wheeler, L., Higenbottam, T., Gibbs, J.S., Egan, J., Crozier, A., Peacock, A., Allcock, R., Corris, P., Loyd, J.E., Trembath, R.C., and Nichols, W.C. (2000). Sporadic primary pulmonary hypertension is associated with germline mutations of the gene encoding BMPR-II, a receptor member of the TGF-beta family. J Med Genet *37*, 741-745.
6. Jurasz, P., Courtman, D., Babaie, S., and Stewart, D.J. (2010). Role of apoptosis in pulmonary hypertension: from experimental models to clinical trials. Pharmacol Ther *126*, 1-8.
7. Stewart, S., and Rassl, D. (2009). Advances in the understanding and classification of pulmonary hypertension. Histopathology *54*, 104-116.
8. Heath, D., and Edwards, J.E. (1958). The pathology of hypertensive pulmonary vascular disease; a description of six grades of structural changes in the pulmonary arteries with special reference to congenital cardiac septal defects. Circulation *18*, 533-547.
9. Sakao, S., and Tatsumi, K. (2011). Vascular remodeling in pulmonary arterial hypertension: multiple cancer-like pathways and possible treatment modalities. Int J Cardiol *147*, 4-12.
10. Abe, K., Toba, M., Alzoubi, A., Ito, M., Fagan, K.A., Cool, C.D., Voelkel, N.F., McMurtry, I.F., and Oka, M. (2010). Formation of Plexiform Lesions in Experimental Severe Pulmonary Arterial Hypertension. Circulation *121*, 2747-2754.
11. Rai, P.R., Cool, C.D., King, J.A., Stevens, T., Burns, N., Winn, R.A., Kasper, M., and Voelkel, N.F. (2008). The cancer paradigm of severe pulmonary arterial hypertension. Am J Respir Crit Care Med *178*, 558-564.
12. Aird, W.C. (2003). Endothelial cell heterogeneity. Crit Care Med *31*, S221-230.
13. Chen, Y.F., and Oparil, S. (2000). Endothelial dysfunction in the pulmonary vascular bed. Am J Med Sci *320*, 223-232.
14. Nicod, L.P. (2007). The endothelium and genetics in pulmonary arterial hypertension. Swiss Med Wkly *137*, 437-442.

15. Budhiraja, R., Tuder, R.M., and Hassoun, P.M. (2004). Endothelial dysfunction in pulmonary hypertension. Circulation *109*, 159-165.
16. Christman, B.W., McPherson, C.D., Newman, J.H., King, G.A., Bernard, G.R., Groves, B.M., and Loyd, J.E. (1992). An imbalance between the excretion of thromboxane and prostacyclin metabolites in pulmonary hypertension. N Engl J Med *327*, 70-75.
17. Cool, C.D., Stewart, J.S., Werahera, P., Miller, G.J., Williams, R.L., Voelkel, N.F., and Tuder, R.M. (1999). Three-dimensional reconstruction of pulmonary arteries in plexiform pulmonary hypertension using cell-specific markers. Evidence for a dynamic and heterogeneous process of pulmonary endothelial cell growth. Am J Pathol *155*, 411-419.
18. Gurbanov, E., and Shiliang, X. (2006). The key role of apoptosis in the pathogenesis and treatment of pulmonary hypertension. Eur J Cardiothorac Surg *30*, 499-507.
19. Steudel, W., Ichinose, F., Huang, P.L., Hurford, W.E., Jones, R.C., Bevan, J.A., Fishman, M.C., and Zapol, W.M. (1997). Pulmonary vasoconstriction and hypertension in mice with targeted disruption of the endothelial nitric oxide synthase (NOS 3) gene. Circ Res *81*, 34-41.
20. Ignarro, L.J. (1989). Biological actions and properties of endothelium-derived nitric oxide formed and released from artery and vein. Circ Res *65*, 1-21.
21. Moncada, S., Palmer, R.M., and Higgs, E.A. (1991). Nitric oxide: physiology, pathophysiology, and pharmacology. Pharmacol Rev *43*, 109-142.
22. Ozaki, M., Kawashima, S., Yamashita, T., Ohashi, Y., Rikitake, Y., Inoue, N., Hirata, K.I., Hayashi, Y., Itoh, H., and Yokoyama, M. (2001). Reduced hypoxic pulmonary vascular remodeling by nitric oxide from the endothelium. Hypertension *37*, 322-327.
23. Fagan, K.A., Fouty, B.W., Tyler, R.C., Morris, K.G., Jr., Hepler, L.K., Sato, K., LeCras, T.D., Abman, S.H., Weinberger, H.D., Huang, P.L., McMurtry, I.F., and Rodman, D.M. (1999). The pulmonary circulation of homozygous or heterozygous eNOS-null mice is hyperresponsive to mild hypoxia. J Clin Invest *103*, 291-299.
24. Mason, N.A., Springall, D.R., Burke, M., Pollock, J., Mikhail, G., Yacoub, M.H., and Polak, J.M. (1998). High expression of endothelial nitric oxide synthase in plexiform lesions of pulmonary hypertension. J Pathol *185*, 313-318.
25. Giaid, A., and Saleh, D. (1995). Reduced expression of endothelial nitric oxide synthase in the lungs of patients with pulmonary hypertension. N Engl J Med *333*, 214-221.
26. Perrella, M.A., Edell, E.S., Krowka, M.J., Cortese, D.A., and Burnett, J.C., Jr. (1992). Endothelium-derived relaxing factor in pulmonary and renal circulations during hypoxia. Am J Physiol *263*, R45-50.
27. Kelly, L.K., Wedgwood, S., Steinhorn, R.H., and Black, S.M. (2004). Nitric oxide decreases endothelin-1 secretion through the activation of soluble guanylate cyclase. Am J Physiol Lung Cell Mol Physiol *286*, L984-991.
28. Le Cras, T.D., Tyler, R.C., Horan, M.P., Morris, K.G., Tuder, R.M., McMurtry, I.F., Johns, R.A., and Abman, S.H. (1998). Effects of chronic hypoxia and altered hemodynamics on endothelial nitric oxide synthase expression in the adult rat lung. J Clin Invest *101*, 795-801.

29. Xue, C., and Johns, R.A. (1996). Upregulation of nitric oxide synthase correlates temporally with onset of pulmonary vascular remodeling in the hypoxic rat. Hypertension *28*, 743-753.
30. Fike, C.D., Kaplowitz, M.R., Thomas, C.J., and Nelin, L.D. (1998). Chronic hypoxia decreases nitric oxide production and endothelial nitric oxide synthase in newborn pig lungs. Am J Physiol *274*, L517-526.
31. Vane, J.R., Anggard, E.E., and Botting, R.M. (1990). Regulatory functions of the vascular endothelium. N Engl J Med *323*, 27-36.
32. Geraci, M.W., Gao, B., Shepherd, D.C., Moore, M.D., Westcott, J.Y., Fagan, K.A., Alger, L.A., Tuder, R.M., and Voelkel, N.F. (1999). Pulmonary prostacyclin synthase overexpression in transgenic mice protects against development of hypoxic pulmonary hypertension. J Clin Invest *103*, 1509-1515.
33. Hoshikawa, Y., Voelkel, N.F., Gesell, T.L., Moore, M.D., Morris, K.G., Alger, L.A., Narumiya, S., and Geraci, M.W. (2001). Prostacyclin receptor-dependent modulation of pulmonary vascular remodeling. Am J Respir Crit Care Med *164*, 314-318.
34. Tuder, R.M., Cool, C.D., Geraci, M.W., Wang, J., Abman, S.H., Wright, L., Badesch, D., and Voelkel, N.F. (1999). Prostacyclin synthase expression is decreased in lungs from patients with severe pulmonary hypertension. Am J Respir Crit Care Med *159*, 1925-1932.
35. Haynes, W.G., and Webb, D.J. (1998). Endothelin as a regulator of cardiovascular function in health and disease. J Hypertens *16*, 1081-1098.
36. Rosendorff, C. (1997). Endothelin, vascular hypertrophy, and hypertension. Cardiovasc Drugs Ther *10*, 795-802.
37. Sakurai, T., Yanagisawa, M., Takuwa, Y., Miyazaki, H., Kimura, S., Goto, K., and Masaki, T. (1990). Cloning of a cDNA encoding a non-isopeptide-selective subtype of the endothelin receptor. Nature *348*, 732-735.
38. Shetty, S.S., Okada, T., Webb, R.L., DelGrande, D., and Lappe, R.W. (1993). Functionally distinct endothelin B receptors in vascular endothelium and smooth muscle. Biochem Biophys Res Commun *191*, 459-464.
39. McEwan, P.E., Valdenaire, O., Sutherland, L., Webb, D.J., and Gray, G.A. (1998). A nonradioactive method for localization of endothelin receptor mRNA in situ. J Cardiovasc Pharmacol *31 Suppl 1*, S443-446.
40. Wong, J., Vanderford, P.A., Winters, J., Soifer, S.J., and Fineman, J.R. (1995). Endothelinb receptor agonists produce pulmonary vasodilation in intact newborn lambs with pulmonary hypertension. J Cardiovasc Pharmacol *25*, 207-215.
41. Kirchengast, M., and Munter, K. (1999). Endothelin-1 and endothelin receptor antagonists in cardiovascular remodeling. Proc Soc Exp Biol Med *221*, 312-325.
42. Stewart, D.J., Levy, R.D., Cernacek, P., and Langleben, D. (1991). Increased plasma endothelin-1 in pulmonary hypertension: marker or mediator of disease? Ann Intern Med *114*, 464-469.
43. Giaid, A., Yanagisawa, M., Langleben, D., Michel, R.P., Levy, R., Shennib, H., Kimura, S., Masaki, T., Duguid, W.P., and Stewart, D.J. (1993). Expression of endothelin-1 in the lungs of patients with pulmonary hypertension. N Engl J Med *328*, 1732-1739.
44. Li, H., Chen, S.J., Chen, Y.F., Meng, Q.C., Durand, J., Oparil, S., and Elton, T.S. (1994). Enhanced endothelin-1 and endothelin receptor gene expression in chronic hypoxia. J Appl Physiol *77*, 1451-1459.

45. Frasch, H.F., Marshall, C., and Marshall, B.E. (1999). Endothelin-1 is elevated in monocrotaline pulmonary hypertension. Am J Physiol *276*, L304-310.
46. Langleben, D., Christman, B.W., Barst, R.J., Dias, V.C., Galie, N., Higenbottam, T.W., Kneussl, M., Korducki, L., Naeije, R., Riedel, A., Simonneau, G., Hirsch, A.M., Rich, S., Robbins, I.M., Oudiz, R., McGoon, M.D., Badesch, D.B., Levy, R.D., Mehta, S., Seeger, W., and Soler, M. (2002). Effects of the thromboxane synthetase inhibitor and receptor antagonist terbogrel in patients with primary pulmonary hypertension. Am Heart J *143*, E4.
47. Stringham, R., and Shah, N.R. (2010). Pulmonary arterial hypertension: an update on diagnosis and treatment. Am Fam Physician *82*, 370-377.
48. Badesch, D.B., Abman, S.H., Simonneau, G., Rubin, L.J., and McLaughlin, V.V. (2007). Medical therapy for pulmonary arterial hypertension: updated ACCP evidence-based clinical practice guidelines. Chest *131*, 1917-1928.
49. Rubin, L.J., Badesch, D.B., Barst, R.J., Galie, N., Black, C.M., Keogh, A., Pulido, T., Frost, A., Roux, S., Leconte, I., Landzberg, M., and Simonneau, G. (2002). Bosentan therapy for pulmonary arterial hypertension. N Engl J Med *346*, 896-903.
50. Janssens, S., Flaherty, D., Nong, Z., Varenne, O., van Pelt, N., Haustermans, C., Zoldhelyi, P., Gerard, R., and Collen, D. (1998). Human endothelial nitric oxide synthase gene transfer inhibits vascular smooth muscle cell proliferation and neointima formation after balloon injury in rats. Circulation *97*, 1274-1281.
51. McLaughlin, V.V., Genthner, D.E., Panella, M.M., and Rich, S. (1998). Reduction in pulmonary vascular resistance with long-term epoprostenol (prostacyclin) therapy in primary pulmonary hypertension. N Engl J Med *338*, 273-277.
52. Newman, J.H., Wheeler, L., Lane, K.B., Loyd, E., Gaddipati, R., Phillips, J.A., 3rd, and Loyd, J.E. (2001). Mutation in the gene for bone morphogenetic protein receptor II as a cause of primary pulmonary hypertension in a large kindred. N Engl J Med *345*, 319-324.
53. Yuan, J.X., and Rubin, L.J. (2005). Pathogenesis of pulmonary arterial hypertension: the need for multiple hits. Circulation *111*, 534-538.
54. Stewart, D.J. (2005). Bone Morphogenetic Protein Receptor-2 and Pulmonary Arterial Hypertension: Unraveling a Riddle Inside an Enigma? Circulation Research *96*, 1033-1035.
55. Ramos, M.F., Lame, M.W., Segall, H.J., and Wilson, D.W. (2008). Smad signaling in the rat model of monocrotaline pulmonary hypertension. Toxicol Pathol *36*, 311-320.
56. Schmierer, B., and Hill, C.S. (2007). TGFbeta-SMAD signal transduction: molecular specificity and functional flexibility. Nat Rev Mol Cell Biol *8*, 970-982.
57. Rudarakanchana, N., Flanagan, J.A., Chen, H., Upton, P.D., Machado, R., Patel, D., Trembath, R.C., and Morrell, N.W. (2002). Functional analysis of bone morphogenetic protein type II receptor mutations underlying primary pulmonary hypertension. Hum Mol Genet *11*, 1517-1525.
58. Nohe, A., Hassel, S., Ehrlich, M., Neubauer, F., Sebald, W., Henis, Y.I., and Knaus, P. (2002). The mode of bone morphogenetic protein (BMP) receptor oligomerization determines different BMP-2 signaling pathways. J Biol Chem *277*, 5330-5338.
59. Atkinson, C., Stewart, S., Upton, P.D., Machado, R., Thomson, J.R., Trembath, R.C., and Morrell, N.W. (2002). Primary pulmonary hypertension is associated with

reduced pulmonary vascular expression of type II bone morphogenetic protein receptor. Circulation *105*, 1672-1678.

60. Trembath, R.C., Thomson, J.R., Machado, R.D., Morgan, N.V., Atkinson, C., Winship, I., Simonneau, G., Galie, N., Loyd, J.E., Humbert, M., Nichols, W.C., Morrell, N.W., Berg, J., Manes, A., McGaughran, J., Pauciulo, M., and Wheeler, L. (2001). Clinical and molecular genetic features of pulmonary hypertension in patients with hereditary hemorrhagic telangiectasia. N Engl J Med *345*, 325-334.
61. Harrison, R.E., Flanagan, J.A., Sankelo, M., Abdalla, S.A., Rowell, J., Machado, R.D., Elliott, C.G., Robbins, I.M., Olschewski, H., McLaughlin, V., Gruenig, E., Kermeen, F., Halme, M., Raisanen-Sokolowski, A., Laitinen, T., Morrell, N.W., and Trembath, R.C. (2003). Molecular and functional analysis identifies ALK-1 as the predominant cause of pulmonary hypertension related to hereditary haemorrhagic telangiectasia. J Med Genet *40*, 865-871.
62. Smoot, L.B., Obler, D., McElhinney, D.B., Boardman, K., Wu, B.L., Lip, V., and Mullen, M.P. (2009). Clinical features of pulmonary arterial hypertension in young people with an ALK1 mutation and hereditary haemorrhagic telangiectasia. Arch Dis Child *94*, 506-511.
63. Tuder, R.M., and Voelkel, N.F. (1998). Pulmonary hypertension and inflammation. J Lab Clin Med *132*, 16-24.
64. Cool, C.D., Kennedy, D., Voelkel, N.F., and Tuder, R.M. (1997). Pathogenesis and evolution of plexiform lesions in pulmonary hypertension associated with scleroderma and human immunodeficiency virus infection. Hum Pathol *28*, 434-442.
65. Tuder, R.M., Groves, B., Badesch, D.B., and Voelkel, N.F. (1994). Exuberant endothelial cell growth and elements of inflammation are present in plexiform lesions of pulmonary hypertension. Am J Pathol *144*, 275-285.
66. Dorfmuller, P., Perros, F., Balabanian, K., and Humbert, M. (2003). Inflammation in pulmonary arterial hypertension. Eur Respir J *22*, 358-363.
67. Stenmark, K.R., Meyrick, B., Galie, N., Mooi, W.J., and McMurtry, I.F. (2009). Animal models of pulmonary arterial hypertension: the hope for etiological discovery and pharmacological cure. Am J Physiol Lung Cell Mol Physiol *297*, L1013-1032.
68. Song, Y., Coleman, L., Shi, J., Beppu, H., Sato, K., Walsh, K., Loscalzo, J., and Zhang, Y.Y. (2008). Inflammation, endothelial injury, and persistent pulmonary hypertension in heterozygous BMPR2-mutant mice. Am J Physiol Heart Circ Physiol *295*, H677-690.
69. West, J., Harral, J., Lane, K., Deng, Y., Ickes, B., Crona, D., Albu, S., Stewart, D., and Fagan, K. (2008). Mice expressing BMPR2R899X transgene in smooth muscle develop pulmonary vascular lesions. Am J Physiol Lung Cell Mol Physiol *295*, L744-755.
70. Caslin, A.W., Heath, D., Madden, B., Yacoub, M., Gosney, J.R., and Smith, P. (1990). The histopathology of 36 cases of plexogenic pulmonary arteriopathy. Histopathology *16*, 9-19.
71. Humbert, M., Monti, G., Brenot, F., Sitbon, O., Portier, A., Grangeot-Keros, L., Duroux, P., Galanaud, P., Simonneau, G., and Emilie, D. (1995). Increased interleukin-1 and interleukin-6 serum concentrations in severe primary pulmonary hypertension. Am J Respir Crit Care Med *151*, 1628-1631.
72. Balabanian, K., Foussat, A., Dorfmuller, P., Durand-Gasselin, I., Capel, F., Bouchet-Delbos, L., Portier, A., Marfaing-Koka, A., Krzysiek, R., Rimaniol, A.C.,

Simonneau, G., Emilie, D., and Humbert, M. (2002). CX(3)C chemokine fractalkine in pulmonary arterial hypertension. Am J Respir Crit Care Med *165*, 1419-1425.
73. Itoh, T., Nagaya, N., Ishibashi-Ueda, H., Kyotani, S., Oya, H., Sakamaki, F., Kimura, H., and Nakanishi, N. (2006). Increased plasma monocyte chemoattractant protein-1 level in idiopathic pulmonary arterial hypertension. Respirology *11*, 158-163.
74. Teder, P., and Noble, P.W. (2000). A cytokine reborn? Endothelin-1 in pulmonary inflammation and fibrosis. Am J Respir Cell Mol Biol *23*, 7-10.
75. Tuder, R.M., Cool, C.D., Yeager, M., Taraseviciene-Stewart, L., Bull, T.M., and Voelkel, N.F. (2001). The pathobiology of pulmonary hypertension. Endothelium. Clin Chest Med *22*, 405-418.
76. Morrell, N.W., Yang, X., Upton, P.D., Jourdan, K.B., Morgan, N., Sheares, K.K., and Trembath, R.C. (2001). Altered growth responses of pulmonary artery smooth muscle cells from patients with primary pulmonary hypertension to transforming growth factor-beta(1) and bone morphogenetic proteins. Circulation *104*, 790-795.
77. Taraseviciene-Stewart, L., Kasahara, Y., Alger, L., Hirth, P., Mc Mahon, G., Waltenberger, J., Voelkel, N.F., and Tuder, R.M. (2001). Inhibition of the VEGF receptor 2 combined with chronic hypoxia causes cell death-dependent pulmonary endothelial cell proliferation and severe pulmonary hypertension. FASEB J *15*, 427-438.
78. Sakao, S., Taraseviciene-Stewart, L., Wood, K., Cool, C.D., and Voelkel, N.F. (2006). Apoptosis of pulmonary microvascular endothelial cells stimulates vascular smooth muscle cell growth. Am J Physiol Lung Cell Mol Physiol *291*, L362-368.
79. Sirois, I., Raymond, M.A., Brassard, N., Cailhier, J.F., Fedjaev, M., Hamelin, K., Londono, I., Bendayan, M., Pshezhetsky, A.V., and Hebert, M.J. (2011). Caspase-3-dependent export of TCTP: a novel pathway for antiapoptotic intercellular communication. Cell Death Differ *18*, 549-562.
80. Campbell, A.I., Zhao, Y., Sandhu, R., and Stewart, D.J. (2001). Cell-based gene transfer of vascular endothelial growth factor attenuates monocrotaline-induced pulmonary hypertension. Circulation *104*, 2242-2248.
81. Teichert-Kuliszewska, K. (2006). Bone Morphogenetic Protein Receptor-2 Signaling Promotes Pulmonary Arterial Endothelial Cell Survival: Implications for Loss-of-Function Mutations in the Pathogenesis of Pulmonary Hypertension. Circulation Research *98*, 209-217.
82. Southwood, M., Jeffery, T.K., Yang, X., Upton, P.D., Hall, S.M., Atkinson, C., Haworth, S.G., Stewart, S., Reynolds, P.N., Long, L., Trembath, R.C., and Morrell, N.W. (2008). Regulation of bone morphogenetic protein signalling in human pulmonary vascular development. J Pathol *214*, 85-95.
83. Sullivan, C.C., Du, L., Chu, D., Cho, A.J., Kido, M., Wolf, P.L., Jamieson, S.W., and Thistlethwaite, P.A. (2003). Induction of pulmonary hypertension by an angiopoietin 1/TIE2/serotonin pathway. Proc Natl Acad Sci U S A *100*, 12331-12336.
84. Kugathasan, L. (2005). Role of Angiopoietin-1 in Experimental and Human Pulmonary Arterial Hypertension. Chest *128*, 633S-642S.
85. Zhao, Y.D., Campbell, A.I., Robb, M., Ng, D., and Stewart, D.J. (2003). Protective role of angiopoietin-1 in experimental pulmonary hypertension. Circ Res *92*, 984-991.
86. Thistlethwaite, P.A., Lee, S.H., Du, L.L., Wolf, P.L., Sullivan, C., Pradhan, S., Deutsch, R., and Jamieson, S.W. (2001). Human angiopoietin gene expression is a

marker for severity of pulmonary hypertension in patients undergoing pulmonary thromboendarterectomy. J Thorac Cardiovasc Surg *122*, 65-73.

87. Eddahibi, S., Guignabert, C., Barlier-Mur, A.M., Dewachter, L., Fadel, E., Dartevelle, P., Humbert, M., Simonneau, G., Hanoun, N., Saurini, F., Hamon, M., and Adnot, S. (2006). Cross talk between endothelial and smooth muscle cells in pulmonary hypertension: critical role for serotonin-induced smooth muscle hyperplasia. Circulation *113*, 1857-1864.
88. Wong, A.L., Haroon, Z.A., Werner, S., Dewhirst, M.W., Greenberg, C.S., and Peters, K.G. (1997). Tie2 expression and phosphorylation in angiogenic and quiescent adult tissues. Circ Res *81*, 567-574.
89. Kugathasan, L., Ray, J.B., Deng, Y., Rezaei, E., Dumont, D.J., and Stewart, D.J. (2009). The angiopietin-1-Tie2 pathway prevents rather than promotes pulmonary arterial hypertension in transgenic mice. J Exp Med *206*, 2221-2234.
90. Li, X.L., Guan, R.J., and Li, J.J. (2012). Attenuation of monocrotaline-induced pulmonary arterial hypertension in rats by rosuvastatin. J Cardiovasc Pharmacol *60*, 219-226.
91. Kawut, S.M., Bagiella, E., Lederer, D.J., Shimbo, D., Horn, E.M., Roberts, K.E., Hill, N.S., Barr, R.G., Rosenzweig, E.B., Post, W., Tracy, R.P., Palevsky, H.I., Hassoun, P.M., and Girgis, R.E. (2011). Randomized clinical trial of aspirin and simvastatin for pulmonary arterial hypertension: ASA-STAT. Circulation *123*, 2985-2993.
92. Han, D.D., Wang, Y., Zhang, X.H., Liu, J.R., and Wang, H.L. (2012). Fluoxetine protects against monocrotaline-induced pulmonary arterial remodeling by inhibition of hypoxia-inducible factor-1alpha and vascular endothelial growth factor. Can J Physiol Pharmacol *90*, 445-454.
93. Beppu, H., Ichinose, F., Kawai, N., Jones, R.C., Yu, P.B., Zapol, W.M., Miyazono, K., Li, E., and Bloch, K.D. (2004). BMPR-II heterozygous mice have mild pulmonary hypertension and an impaired pulmonary vascular remodeling response to prolonged hypoxia. Am J Physiol Lung Cell Mol Physiol *287*, L1241-1247.
94. Long, L., MacLean, M.R., Jeffery, T.K., Morecroft, I., Yang, X., Rudarakanchana, N., Southwood, M., James, V., Trembath, R.C., and Morrell, N.W. (2006). Serotonin increases susceptibility to pulmonary hypertension in BMPR2-deficient mice. Circ Res *98*, 818-827.
95. West, J., Fagan, K., Steudel, W., Fouty, B., Lane, K., Harral, J., Hoedt-Miller, M., Tada, Y., Ozimek, J., Tuder, R., and Rodman, D.M. (2004). Pulmonary hypertension in transgenic mice expressing a dominant-negative BMPRII gene in smooth muscle. Circ Res *94*, 1109-1114.
96. Hong, K.H., Lee, Y.J., Lee, E., Park, S.O., Han, C., Beppu, H., Li, E., Raizada, M.K., Bloch, K.D., and Oh, S.P. (2008). Genetic ablation of the BMPR2 gene in pulmonary endothelium is sufficient to predispose to pulmonary arterial hypertension. Circulation *118*, 722-730.
97. Hoshikawa, Y., Nana-Sinkam, P., Moore, M.D., Sotto-Santiago, S., Phang, T., Keith, R.L., Morris, K.G., Kondo, T., Tuder, R.M., Voelkel, N.F., and Geraci, M.W. (2003). Hypoxia induces different genes in the lungs of rats compared with mice. Physiol Genomics *12*, 209-219.
98. Ciuclan, L., Bonneau, O., Hussey, M., Duggan, N., Holmes, A.M., Good, R., Stringer, R., Jones, P., Morrell, N.W., Jarai, G., Walker, C., Westwick, J., and

Thomas, M. (2011). A novel murine model of severe pulmonary arterial hypertension. Am J Respir Crit Care Med *184*, 1171-1182.

99. Ye, C., Sweeny, D., Sukbuntherng, J., Zhang, Q., Tan, W., Wong, S., Madan, A., Ogilvie, B., Parkinson, A., and Antonian, L. (2006). Distribution, metabolism, and excretion of the anti-angiogenic compound SU5416. Toxicol In Vitro *20*, 154-162.
100. Oka, M., Homma, N., Taraseviciene-Stewart, L., Morris, K.G., Kraskauskas, D., Burns, N., Voelkel, N.F., and McMurtry, I.F. (2007). Rho kinase-mediated vasoconstriction is important in severe occlusive pulmonary arterial hypertension in rats. Circ Res *100*, 923-929.
101. Gomez-Arroyo, J., Saleem, S.J., Mizuno, S., Syed, A.A., Bogaard, H.J., Abbate, A., Taraseviciene-Stewart, L., Sung, Y., Kraskauskas, D., Farkas, D., Conrad, D.H., Nicolls, M.R., and Voelkel, N.F. (2012). A brief overview of mouse models of pulmonary arterial hypertension: problems and prospects. Am J Physiol Lung Cell Mol Physiol *302*, L977-991.
102. Steiner, M.K., Syrkina, O.L., Kolliputi, N., Mark, E.J., Hales, C.A., and Waxman, A.B. (2009). Interleukin-6 overexpression induces pulmonary hypertension. Circ Res *104*, 236-244, 228p following 244.
103. Faffe, D.S., Rocco, P.R., Negri, E.M., and Zin, W.A. (2002). Comparison of rat and mouse pulmonary tissue mechanical properties and histology. J Appl Physiol *92*, 230-234.
104. Burnett, S.H., Kershen, E.J., Zhang, J., Zeng, L., Straley, S.C., Kaplan, A.M., and Cohen, D.A. (2004). Conditional macrophage ablation in transgenic mice expressing a Fas-based suicide gene. J Leukoc Biol *75*, 612-623.
105. Livak, K.J., and Schmittgen, T.D. (2001). Analysis of relative gene expression data using real-time quantitative PCR and the 2(-Delta Delta C(T)) Method. Methods *25*, 402-408.
106. Duan, W.R., Garner, D.S., Williams, S.D., Funckes-Shippy, C.L., Spath, I.S., and Blomme, E.A. (2003). Comparison of immunohistochemistry for activated caspase-3 and cleaved cytokeratin 18 with the TUNEL method for quantification of apoptosis in histological sections of PC-3 subcutaneous xenografts. J Pathol *199*, 221-228.
107. Teng, P.I., Dichiara, M.R., Komuves, L.G., Abe, K., Quertermous, T., and Topper, J.N. (2002). Inducible and selective transgene expression in murine vascular endothelium. Physiol Genomics *11*, 99-107.
108. Fadel, B.M., Boutet, S.C., and Quertermous, T. (1999). Octamer-dependent in vivo expression of the endothelial cell-specific TIE2 gene. J Biol Chem *274*, 20376-20383.
109. Strack, R.L., Strongin, D.E., Bhattacharyya, D., Tao, W., Berman, A., Broxmeyer, H.E., Keenan, R.J., and Glick, B.S. (2008). A noncytotoxic DsRed variant for whole-cell labeling. Nat Methods *5*, 955-957.
110. Kang, J., Ramu, S., Lee, S., Aguilar, B., Ganesan, S.K., Yoo, J., Kalra, V.K., Koh, C.J., and Hong, Y.K. (2009). Phosphate-buffered saline-based nucleofection of primary endothelial cells. Anal Biochem *386*, 251-255.
111. Thiel, C., and Nix, M. (2006). Efficient transfection of primary cells relevant for cardiovascular research by nucleofection. Methods Mol Med *129*, 255-266.
112. Fadel, B.M., Boutet, S.C., and Quertermous, T. (1998). Functional analysis of the endothelial cell-specific Tie2/Tek promoter identifies unique protein-binding elements. Biochem J *330 (Pt 1)*, 335-343.

113. Thomis, D.C., Marktel, S., Bonini, C., Traversari, C., Gilman, M., Bordignon, C., and Clackson, T. (2001). A Fas-based suicide switch in human T cells for the treatment of graft-versus-host disease. Blood *97*, 1249-1257.
114. Muller, A.M., Skrzynski, C., Skipka, G., and Muller, K.M. (2002). Expression of von Willebrand factor by human pulmonary endothelial cells in vivo. Respiration *69*, 526-533.
115. Schlaeger, T.M., Qin, Y., Fujiwara, Y., Magram, J., and Sato, T.N. (1995). Vascular endothelial cell lineage-specific promoter in transgenic mice. Development *121*, 1089-1098.
116. Schlaeger, T.M., Bartunkova, S., Lawitts, J.A., Teichmann, G., Risau, W., Deutsch, U., and Sato, T.N. (1997). Uniform vascular-endothelial-cell-specific gene expression in both embryonic and adult transgenic mice. Proc Natl Acad Sci U S A *94*, 3058-3063.
117. Picciotto, M.R., and Wickman, K. (1998). Using knockout and transgenic mice to study neurophysiology and behavior. Physiol Rev *78*, 1131-1163.
118. Masri, F.A., Xu, W., Comhair, S.A., Asosingh, K., Koo, M., Vasanji, A., Drazba, J., Anand-Apte, B., and Erzurum, S.C. (2007). Hyperproliferative apoptosis-resistant endothelial cells in idiopathic pulmonary arterial hypertension. Am J Physiol Lung Cell Mol Physiol *293*, L548-554.
119. Savale, L., Tu, L., Rideau, D., Izziki, M., Maitre, B., Adnot, S., and Eddahibi, S. (2009). Impact of interleukin-6 on hypoxia-induced pulmonary hypertension and lung inflammation in mice. Respir Res *10*, 6.
120. Calero-Nieto, F.J., Bert, A.G., and Cockerill, P.N. (2010). Transcription-dependent silencing of inducible convergent transgenes in transgenic mice. Epigenetics Chromatin *3*, 3.
121. Hunt, M.A., Currie, M.J., Robinson, B.A., and Dachs, G.U. (2010). Optimizing transfection of primary human umbilical vein endothelial cells using commercially available chemical transfection reagents. J Biomol Tech *21*, 66-72.
122. Hennecke, M., Kwissa, M., Metzger, K., Oumard, A., Kroger, A., Schirmbeck, R., Reimann, J., and Hauser, H. (2001). Composition and arrangement of genes define the strength of IRES-driven translation in bicistronic mRNAs. Nucleic Acids Res *29*, 3327-3334.
123. Strack, R.L., Hein, B., Bhattacharyya, D., Hell, S.W., Keenan, R.J., and Glick, B.S. (2009). A rapidly maturing far-red derivative of DsRed-Express2 for whole-cell labeling. Biochemistry *48*, 8279-8281.
124. Alberts, B., Johnson, A., and Lewis, J. (2002). Blood Vessels and Endothelial Cells (New York, Garland Science).
125. Lindemann, D., and Schnittler, H. (2009). Genetic manipulation of endothelial cells by viral vectors. Thromb Haemost *102*, 1135-1143.
126. Gao, S., Dagnaes-Hansen, F., Nielsen, E.J., Wengel, J., Besenbacher, F., Howard, K.A., and Kjems, J. (2009). The effect of chemical modification and nanoparticle formulation on stability and biodistribution of siRNA in mice. Mol Ther *17*, 1225-1233.
127. McLaughlin, V.V., and McGoon, M.D. (2006). Pulmonary arterial hypertension. Circulation *114*, 1417-1431.

Appendix I - Table S1: World Health Organization Classification of Functional Status for PAH [127].

Class I	•No limitations during normal or physical activity
Class II	•Slight limtations during physical activity; no symptoms at rest
Class III	•Marked limitation during physical activity; symptoms during normal activity; no symptoms at rest
Class IV	•Unable to perform any physical activity without symptoms; symptoms present at rest; discomfort during any activity

Appendix II –Solutions

Histology

Scott's solution	**Eosin solution**	**Acid Alcohol**	**4% PFA**
6 g $MgSO_4 \cdot 7H_2O$ 1.05 g $NaHCO_3$ 300 mL ddH_2O	3 g Eosin/300 mL ddH_2O 100 µl glacial acetic acid/300 mL eosin	2.5 mL 12N HCl 500 mL 70% EtOH	500 mL 1x PBS 20 g PFA Stir and heat at 60°C for 30 minutes pH 7.4
10X PBS	**Mowiol Mounting medium**	**0.2 % Triton X-100**	
80 g NaCl 2.0 g KCl 14.4 g Na2HPO4 2.4 g KH2PO4 1L ddH_20, pH 7.4 Dlute to 1x PBS	6 g glycerol 2.4 g Mowiol (Polysciences 17951-500) 6 mL ddH20 12 mL 0.2 M Tris (pH 8.5)	0.1 mL 10% Triton 4.9 mL 1x PBS	

Immunoblotting

RIPA Lysis Buffer	**Laemmli buffer**	
50 mM Tris-Cl 1% NP-40 1 mM EDTA 50 mM NaCl, pH 7.5 1% proteinase inhibitor mix 0.5% sodium orthovanadate 0.1% NaF 10% sodium deoxycholate	781 µL 2M Tris-HCL pH6.5 0.5 g 10% SDS 0.0125 g 0.25% Bromophenol Blue 1.25 mL β-mercaptoethanol 2.5 mL Glycerol	